

國立交通大學

電子工程學系 電子研究所碩士班

碩 士 論 文

應用於數位電視廣播規格之同步化系統設計



**Synchronization System
for DVB-T/H Standard**

學生：李家豪

指導教授：李鎮宜 教授

中華民國九十五年七月

應用於數位電視廣播規格之同步化系統設計

**Synchronization System
for DVB-T/H Standard**

研究生：李家豪

Student : Chia-Hao Lee

指導教授：李鎮宜

Advisor : Chen-Yi Lee

國立交通大學
電子工程學系 電子研究所 碩士班
碩士論文



Submitted to Institute of Electronics
College of Electrical Engineering and Computer Science
National Chiao Tung University
in Partial Fulfillment of the Requirements
for the Degree of
Master of Science
in

Electronics Engineering

July 2006

Hsinchu, Taiwan, Republic of China

中華民國九十五年七月

應用於數位電視廣播規格之同步化系統設計


學生：李家豪

指導教授：李鎮宜 教授

國立交通大學

電子工程學系 電子研究所碩士班

摘要



在本論文中，我們提出了一個應用於數位電視廣播規格的同步化系統設計。此同步化系統設計由一組載波相位校準、取樣頻率漂移同步以及快速同步設計組成。我們團隊於 2006 年 ISSCC 期刊中發表的 DVB-T/H 基頻接收機設計為本篇論文的參考設計。我們提出的載波相位校準可以克服在 Rayleigh 衰減通道中，取樣頻率漂移 20ppm、都卜勒頻率 70Hz、載波頻率漂移 10.3 dB、訊雜比 34 分貝，其中，傳輸模式為 2K 模式，Viterbi 編碼率 2/3。第二部份，與傳統設計相比，取樣頻率漂移估計的正確度相比可達到 2~5 倍；取樣頻率漂移追蹤也可達到 3 倍的收斂速度。快速同步的設計也比傳統設計的同步速度快上 2~4.5 倍，而在 timing-slicing 的架構下，也使得我們的電路功率消耗節省約百分之 10，接收機記憶體減少 1~3Mbits。在不同的傳輸模式以及通道效應下，整體的系統效能只比完美同步系統損失 0~0.3 分貝。並且在硬體上我們整合了同步系統電路中重複的部分，與 ISSCC2006 的設計相比，同步化設計電路的部份可以節省百分之 46 的硬體。

Synchronization System for DVB-T/H Standard

Student : Chia-Hao Lee

Advisor : Dr. Chen-Yi Lee

**Institute of Electronics Engineering
National Chiao Tung University**

ABSTRACT

In this thesis, a synchronization system is proposed for Digital Video Broadcasting-Terrestrial/Handheld (DVB-T/H) standard. This synchronization system comprises 3 parts: carrier phase alignment, sampling clock synchronization, and fast synchronization schemes. In this paper, we take the DVB-T/H baseband receiver [1] proposed in ISSCC2006 as the reference design. First, the proposed carrier phase alignment can overcome sampling clock offset (SCO) 20ppm, Doppler frequency 70Hz, carrier frequency offset (CFO) 10.3 at Rayleigh fading channel with SNR 34dB in 2K mode and Viterbi coderate 2/3. Second, comparing with conventional design, the SCO estimation accuracy can reach 2~5 times; SCO tracking can obtain the convergent time 3 times fast. Then, the fast synchronization can increase the speed of synchronization 2~4.5 times. Under time-sling architecture, the saving of power consumption can improve about 10% and receiver buffer is decreased 1~3Mbits. The overall performances are only lose 0~0.3dB in different transmission modes. Finally, on the vision of hardware, we integrate the similar part of synchronization algorithms and compare with [1] in ISSCC2006. We can save the hardware 46%.

誌 謝

兩年的時光轉眼間就過去了，在 Si2 這個大家庭學習讓我感到相當充實。不但學到了許多專業知識，為人處事方面更是受益良多。

能完成這本論文，我要特別感謝 李鎮宜教授不厭其煩的指導與研究方向的指引。以及實驗室的所有學長姐、同學、學弟妹之間無私的指導與討論，每每讓我在研究時找到新的思路和方法。

在這裡，特別感謝 DVB group 的黎峰學長、昱偉學長、陳元學長、成偉學長、盧忠學長、英豪以及義閔學弟，感謝大家這兩年來的腦力激盪與相互討論，不但使我在相關的研究領域有所精進，更學習到團隊合作的可貴。還要感謝與我同屆的康正、毅宏、婉君、俊彥與志龍，在這兩年內，我們一起經歷過許多，有你們的陪伴，使我這兩年的碩士生涯充滿了多彩多姿的回憶。

最後，我要由衷的感謝我的父母及家人，感謝你們多年來的栽培及細心，讓我能順利完成碩士的學業。更要感謝我的女友瑞文，這幾年來有妳的一路相伴，使我的生活更豐富有趣，心裡有個寄託的地方。僅將此論文獻給你們，以表達我最深的感激。

Contents

CHAPTER 1. INTRODUCTION.....	1
1.1 MOTIVATION	1
1.2 INTRODUCTION TO DVB-T/H SYSTEM.....	2
1.3 INTRODUCTION TO TIME-SLICING TECHNOLOGY	11
1.4 ORGANIZATION OF THIS THESIS.....	13
CHAPTER 2. SYNCHRONIZATION ALGORITHMS.....	15
2.1 INTRODUCTION TO UNSYNCHRONOUS PROBLEMS	15
2.1.1 <i>Effect of Carrier Frequency Offset and Sampling Clock Offset</i>	16
2.1.2 <i>Effect of Symbol Timing Offset</i>	20
2.1.3 <i>Effect of Carrier Phase Mismatch</i>	2
2.2 CARRIER PHASE ALIGNMENT.....	27
2.3 FAST SYNCHRONIZATION SYSTEM	32
2.3.1 <i>TPS Decode</i>	34
2.3.2 <i>RS Packet Synchronization</i>	37
2.4 SAMPLING CLOCK OFFSET SYNCHRONIZATION	42
2.4.1 <i>Conventional SCO Estimation</i>	42
2.4.2 <i>Proposed SCO Estimation</i>	44
2.4.3 <i>Conventional Tracking Loop</i>	45
2.4.4 <i>Proposed Tracking Loop</i>	45
CHAPTER 3. SIMULATION AND PERFORMANCE ANALYSIS.....	49
3.1 SIMULATION PLATFORM.....	49
3.2 CHANNEL MODEL.....	54

3.2.1	<i>Multipath Fading Channel Model</i>	55
3.2.2	<i>Doppler Spread Model</i>	58
3.2.3	<i>Carrier Frequency Offset and Sampling Clock Offset model</i>	59
3.3	PERFORMANCE ANALYSIS.....	59
3.3.1	<i>Carrier Phase Alignment</i>	59
3.3.2	<i>Fast Synchronization</i>	63
3.3.3	<i>Sampling Clock Synchronization</i>	65
3.3.4	<i>Overall System Performance</i>	70
CHAPTER 4. HARDWARE INTEGRATION		74
4.1	ACQUISITION	75
4.2	TRACKING	79
4.3	INTEGRATION RESULT	80
CHAPTER 5. CONCLUSION AND FUTURE WORK		83
BIBLIOGRAPHY		84



List of Figures

FIG 1.1 FUNCTIONAL BLOCK DIAGRAM OF THE ADDITIONAL FEATURES.....	4
FIG 1.2 FRAME STRUCTURE.....	7
FIG 1.3 GENERATION OF PRBS SEQUENCE.....	8
FIG 1.4: TIMING-SLICING TECHNOLOGY IN DVB-H SYSTEM.....	11
FIG 1.5 THE TIME SLICING/MPE-FEC BUFFER IN THE RECEIVER.....	13
FIG 2.1 PHASE ROTATION IN TIME DOMAIN FOR LONG TIME RECEPTION WHEN $\epsilon=0.01$	18
FIG 2.2 SPECTRUM OF FIVE SUBCARRIERS IN CARRIER FREQUENCY OFFSET ENVIRONMENT	18
FIG 2.3 PHASE ROTATION DUE TO TIMING DRIFTS	20
FIG 2.4 ISI-FREE REGION	21
(A) SYMBOL TIMING OFFSET τ IN THE ISI-FREE REGION.....	22
FIG 2.5 PHASE ROTATION OF SYMBOL TIMING OFFSET $E=2$ AND $E=5$	22
FIG 2.6 MAPPING CONSTELLATION.....	2
FIG 2.7 THE INFLUENCE OF FRAME POSITION ERROR TO INTERPOLATIONS	24
FIG 2.8 RELATIVE CIR DUE TO INACCURATE FFT WINDOW.....	24
FIG 2.9 INTERPOLATION OF 2D CHANNEL ESTIMATION.....	25
FIG 2.10 THE PHASE ROTATION OF PILOTS' CFR CAUSED BY DIFFERENT SYMBOL TIMING OFFSET	26
FIG 2.11 RELATIVE CHANNEL IMPULSE RESPONSE WITH MULTI-PATH	27
FIG 2.12 LOCATION OF PHASE ALIGNMENT IN RECEIVER PLATFORM.....	28
FIG 2.13 COMPARISON OF PERFORMANCE BETWEEN 2-D CE AND 1-D CE.....	29
FIG 2.14 THE PHASE ROTATION OF PILOTS' CFR CAUSED BY DIFFERENT SYMBOL TIMING OFFSET	30
FIG 2.15 2-D CHANNEL INTERPOLATION	30

FIG 2.16 PROPOSED TIME AXIS PHASE ALIGNMENT ARCHITECTURE	32
FIG 2.17 COMPOSITION OF COMPLETED SYNCHRONIZATION TIME.....	33
FIG 2.18 LOCATION OF FAST SYNCHRONIZATION IN RECEIVER PLATFORM	34
FIG 2.19 THE OPERATION OF CONVENTIONAL TPS WORD	36
FIG 2.20 THE OPERATION OF PROPOSED TPS WORD.....	37
FIG 2.23 LOCATION OF FAST SYNCHRONIZATION IN RECEIVER PLATFORM	42
FIG 2.24 ARCHITECTURE OF SCO ESTIMATION [1].....	43
FIG 2.25 THE ARCHITECTURE OF PROPOSED SCO ESTIMATION	44
FIG 2.26 TIMING DIAGRAM OF CONVENTIONAL SCO TRACKING ARCHITECTURE	45
FIG 2.27 THE ARCHITECTURE OF PROPOSED SCO TRACKING LOOP.....	46
FIG 2.28 TIMING DIAGRAM OF PROPOSED SCO TRACKING LOOP ARCHITECTURE.....	47
FIG 2.29 THE ARCHITECTURE OF PROPOSED SCO TRACKING LOOP WITH SP METHOD	48
FIG 3.1 BLOCK DIAGRAM OF SIMULATION PLATFORM	49
FIG 3.2 OVERVIEW OF RECEIVER DESIGN	50
FIG 3.3 STRUCTURE OF INNER RECEIVER	51
FIG 3.4 ISI EFFECT ON CFO ACQUISITION	53
FIG 3.5 2-D INTERPOLATION IN CHANNEL ESTIMATION UNIT DESIGN.....	54
FIG 3.6 CHANNEL MODEL OF DVB-T/H SYSTEM	54
FIG 3.7 CHANNEL RESPONSE OF RAYLEIGH AND RICEAN (K=10DB) CHANNEL.....	57
FIG 3.8 DOPPLER FREQUENCY SPREAD MODEL.....	58
FIG 3.9 BER VS SNR AFTER VITERBI DECODER WITH ONE FINE TUNE EVERY 8 SYMBOL.....	60
FIG 3.10 BER VS SNR AFTER VITERBI DECODER WITH ONE FINE TUNE EVERY 64 SYMBOL.....	61
FIG 3.11 TOLERANCE RANGE OF SCO @ RAYLEIGH, SNR=34DB, AND DOPPLER 70HZ.....	62
FIG 3.12 BER AFTER VITERBI VS DOPPLER FREQUENCY.....	63
FIG 3.13 PERFORMANCE OF THE RESIDUAL SCO CONVERGENCE IN CP-LLS ALGORITHM BETWEEN WITH AND WITHOUT FEEDBACK FORWARD ARCHITECTURE.....	68

FIG 3.14 PERFORMANCE OF THE RESIDUAL SCO CONVERGENCE IN SP-LLS ALGORITHM BETWEEN WITH AND WITHOUT FEEDBACK FORWARD ARCHITECTURE.....	68
FIG 3.15 PERFORMANCE OF THE RESIDUAL SCO CONVERGENCE BETWEEN CP-LLS AND SP-LLS ALGORITHM WITH FEEDBACK FORWARD ARCHITECTURE.....	69
FIG 3.16 OVERALL SYSTEM PERFORMANCE IN STATIC GAUSSIAN CHANNEL.....	70
FIG 3.17 OVERALL SYSTEM PERFORMANCE IN STATIC RICEAN CHANNEL.....	71
FIG 3.18 OVERALL SYSTEM PERFORMANCE IN STATIC RAYLEIGH CHANNEL.....	71
FIG 3.19 OVERALL SYSTEM PERFORMANCE IN RAYLEIGH CHANNEL WITH DOPPLER FREQUENCY 70Hz	73
FIG 4.1 OVERALL SYNCHRONIZATION SCHEME	74
FIG 4.2 LOCATIONS OF INTEGRATION SYNCHRONIZATION SYSTEM IN RECEIVER PLATFORM.....	75
FIG 4.3 NORMAL MAXIMUM CORRELATION ALGORITHM FOR GI/MODE DETECTOR.....	76
FIG 4.5 THE PROPOSED GUARD BAND POWER DETECTION BASED APPROACH.....	79
FIG 4.6 THE ARCHITECTURE OF PROPOSED RESIDUAL CFO TRACKING LOOP WITH SP METHOD..	80
FIG 4.7 TIMING DIAGRAM OF PROPOSED RESIDUAL CFO TRACKING LOOP ARCHITECTURE WITH SP METHOD.....	80

List of Tables

TABLE 1-1 PARAMETERS FOR 8MHZ CHANNEL IN DVB-H STANDARD.....	5
TABLE 1-2 PARAMETERS FOR 7MHZ CHANNEL IN DVB-H STANDARD.....	6
TABLE 1-3 PARAMETERS FOR 6MHZ CHANNEL IN DVB-H STANDARD.....	6
TABLE 1-4 PARAMETERS FOR 5MHZ CHANNEL IN DVB-H STANDARD.....	6
TABLE 1-5 CARRIER INDICES FOR CONTINUAL PILOT CARRIERS FOR 8K MODE	9
TABLE 1-6 CARRIER INDICES FOR TPS CARRIERS FOR 8K MODE.....	10
TABLE 2-1 TPS SIGNALING INFORMATION AND CONTENT	35
TABLE 2-2 NUMBER OF RS 204 BYTES PACKETS PER OFDM SUPER-FRAME FOR ALL COMBINATIONS OF CODE RATES AND MODULATION FORMS.....	38
TABLE 2-3 THE PACKETS IN ONE CARRIER WITH VARIED CODE RATE IN QPSK MAPPING.....	39
TABLE 2-4 THE PACKETS IN ONE CARRIER WITH VARIED CODE RATE IN 16-QAM MAPPING	39
TABLE 2-5 THE PACKETS IN ONE CARRIER WITH VARIED CODE RATE IN 64-QAM MAPPING	39
TABLE 2-5 RESIDUAL CARRIERS FOR RS PACKET SYNCHRONIZATION FOR 2K MODE	40
TABLE 2-6 RESIDUAL CARRIERS FOR RS PACKET SYNCHRONIZATION FOR 4K MODE	40
TABLE 2-7 RESIDUAL CARRIERS FOR RS PACKET SYNCHRONIZATION FOR 8K MODE	41
TABLE 3-1 SYNCHRONIZATION TIME (MS) IN 8 MHZ CHANNEL	64
TABLE 3-2 SYNCHRONIZATION TIME (MS) IN 7 MHZ CHANNEL	64
TABLE 3-3 SYNCHRONIZATION TIME (MS) IN 6 MHZ CHANNEL	64
TABLE 3-4 SYNCHRONIZATION TIME (MS) IN 5 MHZ CHANNEL	64
TABLE 3-5 THE ESTIMATION ACCURACY OF THE SCO IN PPM	66
TABLE 3-6 CHANNEL MODEL OF THE SIMULATION IN SCO ESTIMATION ALGORITHM.....	66
TABLE 3-7 CHANNEL MODEL OF THE SIMULATION IN SCO TRACKING LOOP ARCHITECTURE	67
TABLE 3-8 SNR LOSS IN STATIC GAUSSIAN, RICEAN AND RAYLEIGH CHANNEL	72

TABLE 3-9 SYNCHRONIZATION LOSS AND TOTAL SNR LOSS IN MOBILE CHANNEL..... 73

TABLE 4-1 THE HARDWARE GATE COUNT OF SYNCHRONIZATION FUNCTION IN [1]..... 81

TABLE 4-2 THE HARDWARE GATE COUNT OF SYNCHRONIZATION FUNCTION FOR THE PROPOSED
DESIGN..... 81



Chapter 1 .

Introduction

1.1 Motivation

Coded Orthogonal Frequency Division Multiplexing (COFDM) technique has developed for a while time to resist mobile channel effect in wireless communication. As European Telecommunication Standard Institute (ETSI) Digital Video Broadcasting-Handheld (DVB-H) system [], the wireless channel environment, like fast frequency selective fading, time variant, Doppler effect, sampling clock offset (SCO) and carrier frequency offset (CFO) is concerned. Under such severe channel effect, the synchronization schemes are especially important in receiver design for COFDM system. In such severe channel, the synchronization is very difficult. However, future DVB-H terminals will most probably make intensive use of a TDM system called “Time-Slicing” [4] to cut power consumption to reasonable number for handheld environment.

In order to fully exploit the potential power reduction, synchronization times of DVB-H receiver must keep a minimum. In this paper, we propose fast synchronization architecture including fast TPS decoder, fast RS header decoder and fast SCO/CFO tracking in the integrated synchronization system.

And then in such severe channel environment, the phase mismatch would happen in post-FFT symbols. If we use the 2-D linear equalization, the problem will make performance degradation much. We need a phase alignment in time axis to solve it. Although the phase mismatch is not caused channel effect but it is the problem followed after synchronizers, fine symbol synchronizer and resampler. Proposed phase alignment in time axis can also be placed

in the proposed integrated synchronization system.

After we solve the synchronization problems in the system, the integrated synchronization will be introduced. The motivation of integration of synchronization system is from this problem that algorithm cores of different synchronization schemes are too similar. Integrating the whole synchronization system and obtaining the most hardware reuse can reduce cost and get the best solution. Fast synchronization architecture, phase alignment and integrated synchronization system can also be integrated into [1], the published paper in ISSCC 2006.

1.2 Introduction to DVB-T/H system

DTV (Digital TV) is popularly used as the next-generation video broadcasting transmission technology in recent years. DTV provides much higher A/V quality and less transmission noise than conventional analog TV. Nowadays, the developed DTV standards consist of DVB (Digital Video Broadcasting) in Europe, ATSC (Advanced Television Systems Committee) in U.S., ISDB (Integrated Services Digital Broadcasting) in Japan and DMB (Digital Multimedia Broadcasting) in China. The transmission modes of DTV include direct satellite broadcasting, cable and terrestrial broadcasting (over-the-air). In terrestrial broadcasting, particularly, video signal is transmitted against severer channel distortions such as multipath fading, co-channel interference and adjacent-channel interference. Since broadcasting transmission system is usually designed to operate within the UHF spectrum allocation for analogue transmissions, it has to provide sufficient protection against high levels of co/adjacent-channel interference emanating from existing PAL (Phase Alternative Line) / SECAM (SEquentiel Couleur Avec Memoire or sequential color with memory) services. Therefore, it is clearly that the terrestrial broadcasting has more challenges in research.

DVB-T standard, one kind of the most popular standards, has been produced by European Telecommunication Standard Institute (ETSI) in Aug, 1997. It has been applied in many countries in the world. In Taiwan, DVB-T standard is also applied as the broadcasting standard. In order to provide the high data rate required for video transmission and resist severe channel distortion in DVB-T, concatenated-coded Orthogonal Frequency Division Multiplexing (COFDM) has been adopted into DVB-T in particular. COFDM is a very popular technology today due to its high data rate transmission capability with high bandwidth efficiency and its robustness to multipath distortion. It has been also chosen as the transmission technique of other communication systems such as ADSL, VDSL, XDSL, DAB and IEEE802.11a/g.

For resisting all kinds of propagation conditions encountered in the wireless broadcasting channel, many parameters of COFDM for DVB-T can be dynamically changed according to channel conditions. The number of COFDM subcarriers can either be 2048 (2K) or 8192 (8K) so that the desired trade-off can be made between inter-symbol-interference (ISI) and Doppler spread. In 2K mode, wider subcarrier spacing can significantly reduce the distortion caused by Doppler frequency spread. In 8K mode, longer OFDM symbol duration can overcome larger multipath fading. Other parameters like guard interval length, constellation mapping mode and coding rate of Viterbi can be also properly decided up to the broadcasting channel condition of the local area. Like guard interval, longer ones have more powerful capability in severe multipath channel than shorter ones. QPSK can resist more noise distortion than 16-QAM and 64-QAM. Less coding rate can detect out more incorrect bit, it is suitable in the severe error channel.

Although the DVB-T reception can also be applied in mobile environment, the ability of reception for handheld terminals is still not good enough because of its high operation power. Therefore, Digital Video Broadcasting-Handheld (DVB-H) was also proposed based on the DVB-T technology to provide broadcast services for handheld devices such as PDAs or mobile phones [6].

DVB-H, the specification for bringing broadcast services to battery-powered handheld

receivers, was formally adopted as an ETSI standard in November 2004. This is the official DVB-H website maintained by the DVB Project Office. The DVB-H technology is a spin-off of the DVB-T standard. It is large extent compatible to DVB-T but takes into account the specific properties of the addressed terminals- small, lightweight, portable, battery-powered devices in mobile environment. Unlike the DVB-T transport stream adopted from the MPEG2 standard, the DVB-H system is IP (Internet Protocol)-based, therefore the outer DVB-H interface is the IP interface. The IP data are embedded into the transport stream by means of the MPE (Multi Protocol Encapsulation) frame, an adaptation protocol defined in the DVB Data Broadcasting Specification [4]. One MPE frame contains one or more IP datagrams and has a maximum number of 1024 rows and a constant number of 255 columns. The transmission system for DVB-T/H standard is shown in Fig 1.1. It contains the blocks for source coding, outer coding and interleaving, inner coding and interleaving, mapping and modulation, frame adaptation and COFDM transmission. The additional features of DVB-H are also shown in Fig 1.1.

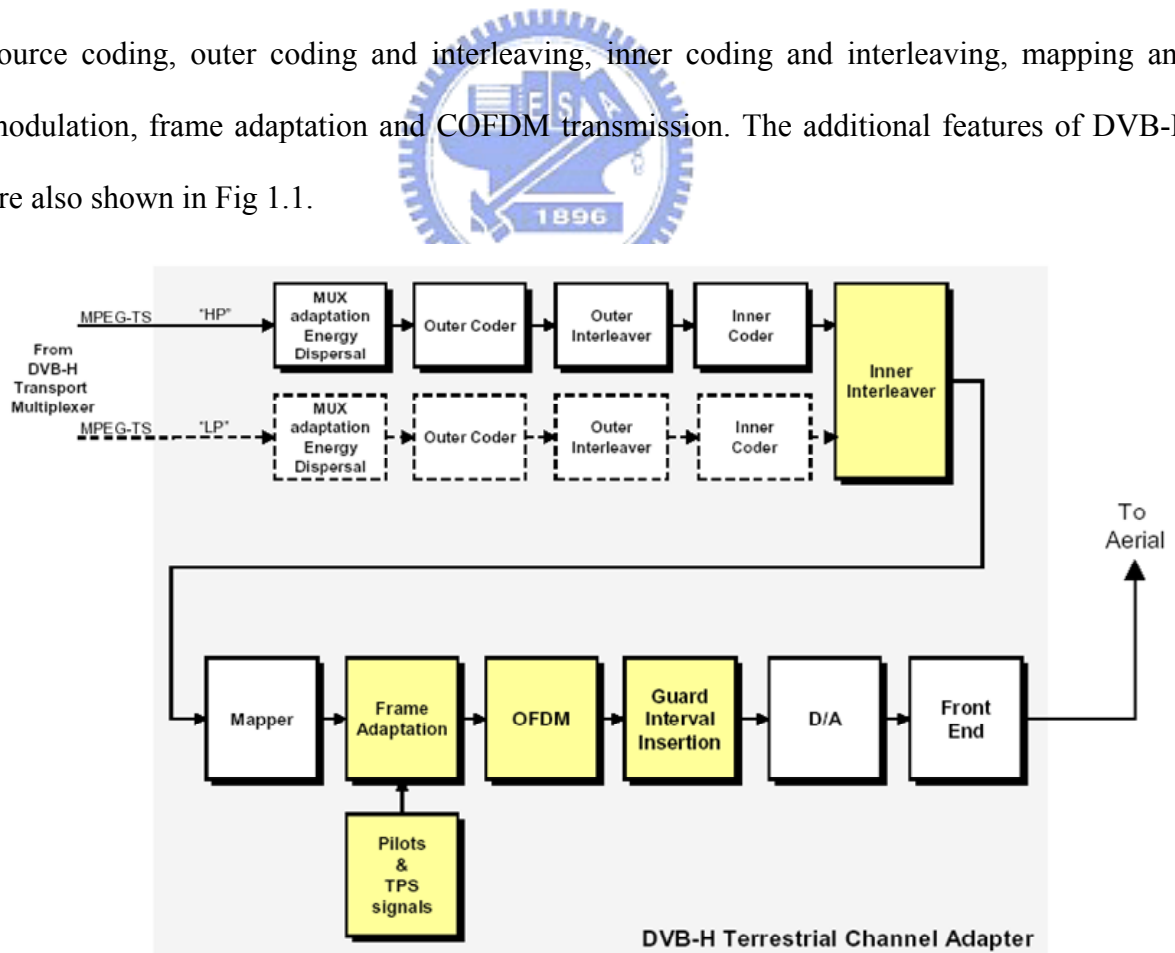


Fig 1.1 Functional block diagram of the additional features

As we can see the DVB-H codec is additional composed of the MPE, MPE-FEC, and time-slicing. Time-slicing architecture will be introduced in section 1.3. For mobile channels reception and long delay spread conditions, an enhanced error protection scheme on the link layer is needed. This scheme is called MPE-FEC and employs powerful channel coding and time interleaving. The MPE-FEC scheme consists of an RS code in conjunction with an extensive block interleaving. The RS (255, 191, 64) code is utilized to perform MPE-FEC error protection. Besides, a virtual block interleaving effect is also performed by reading from and writing to the MPE frame in column direction whereas coding is applied in row direction.

The parameters for 8MHz channel bandwidth in DVB-H standard are listed in Table 1-1.

Table 1-1 Parameters for 8MHz channel in DVB-H standard

Parameter	8k mode	4k mode	2k mode
Number of subcarriers K	6817	3409	1705
Value of carrier number K_{min}	0	0	0
Value of carrier number K_{max}	6816	3408	1704
FFT size N	8192	4096	2048
Symbol duration T_U	896 μ s	448 μ s	224 μ s
Subcarrier spacing $1/T_U$	1.116KHz	2.232KHz	4.464KHz
Spacing between K_{min} and K_{max}	7.61MHz	7.61MHz	7.61MHz
Guard interval N_g/N	1/4,1/8,1/16,1/32	1/4,1/8,1/16,1/32	1/4,1/8,1/16,1/32

Table 1-2, Table 1-3, and Table 1-4 shows the different parameters for 7MHz, 6MHz, and 5MHz channel in DVB-H standard. The DVB-H also supports 5MHz transmission channel bandwidth in addition.

Table 1-2 Parameters for 7MHz channel in DVB-H standard

Parameter	8k mode	4k mode	2k mode
Symbol duration T_U	1024 μ s	512 μ s	256 μ s
Subcarrier spacing $1/T_U$	0.977KHz	1.953KHz	3.906KHz
Spacing between K_{min} and K_{max}	6.66MHz	6.66MHz	6.66MHz

Table 1-3 Parameters for 6MHz channel in DVB-H standard

Parameter	8k mode	4k mode	2k mode
Symbol duration T_U	1194.67 μ s	597.33 μ s	298.67 μ s
Subcarrier spacing $1/T_U$	0.837KHz	1.674KHz	3.348KHz
Spacing between K_{min} and K_{max}	5.71MHz	5.71MHz	5.71MHz

Table 1-4 Parameters for 5MHz channel in DVB-H standard

Parameter	8k mode	4k mode	2k mode
Symbol duration T_U	1433.60 μ s	716.80 μ s	358.40 μ s
Subcarrier spacing $1/T_U$	0.697KHz	1.395KHz	2.790KHz
Spacing between K_{min} and K_{max}	4.75MHz	4.75MHz	4.75MHz

In the case of two-level hierarchy, the functional block diagram of the system must be expanded to include the modules shown in dashed in. The splitter separates the incoming data stream into the high-priority and the low-priority stream. These two bitstreams are mapped onto the signal constellation by the mapping and therefore the modulator has a corresponding. This system uses COFDM transmission. All data carriers in one COFDM symbol are mapped either as QPSK, 16-QAM, 64-QAM, non-uniform-16-QAM or non-uniform-64-QAM. In

addition to the transmitted data, a COFDM symbol contains scattered pilots, continual pilots and TPS (Transmission Parameter Signaling) pilots. These reference signals can be used for synchronization, channel estimation and transmission mode verification. The COFDM frame consists of 68 COFDM symbols and four frames constitute one super-frame. The frame structure involving distribution of scattered pilots is shown in Fig 1.2. Scattered pilots insert every 12 subcarriers and have an interval of 3 subcarriers in the next adjacent symbol.

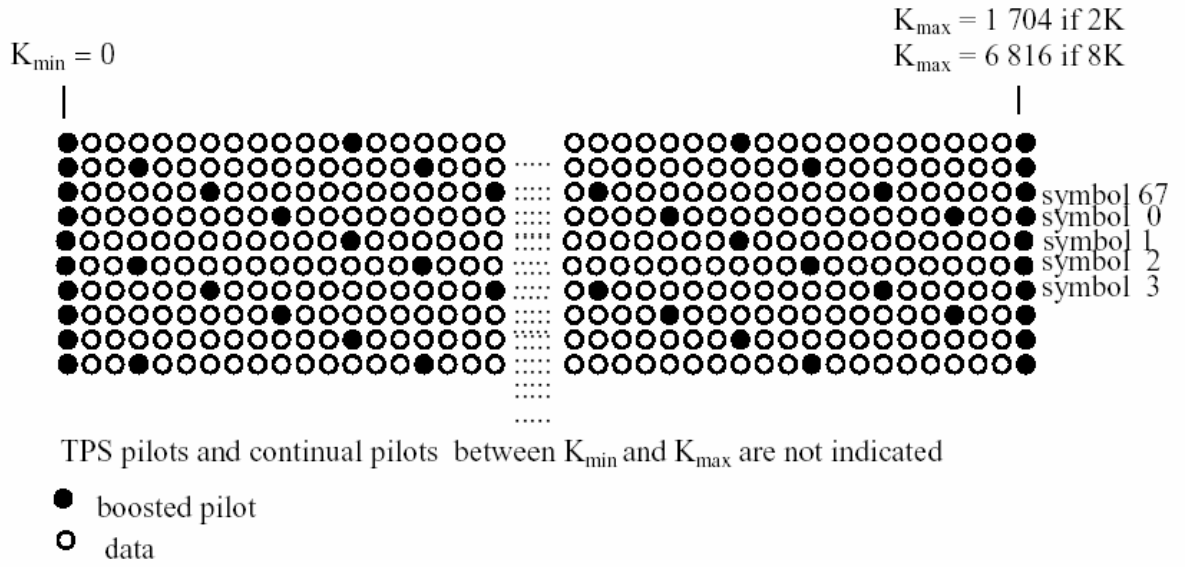


Fig 1.2 frame structure

The carrier indices of scatter pilots are shown as

$$SP = \{k = K_{\min} + 3 \times (l \bmod 4) + 12p \mid p \text{ integer}, p \geq 0, k \in [K_{\min}; K_{\max}]\} \quad (1-1)$$

The corresponding modulation of scattered pilots is expressed as

$$\begin{aligned} \text{Re}\{c_{m,l,k}\} &= 4/3 \times 2(1/2 - w_k) \\ \text{Im}\{c_{m,l,k}\} &= 0 \end{aligned} \quad (1-2)$$

where w_k means Pseudo Random Binary Sequence (PRBS), and $c_{m,l,k}$ means k -th subcarrier in l -th symbol in m -th frame. PRBS sequence $(X^{11}+X^2+1)$ determines the values of scattered pilots, continual pilots and TPS pilots. The PRBS generator is shown as in Fig 1.3.

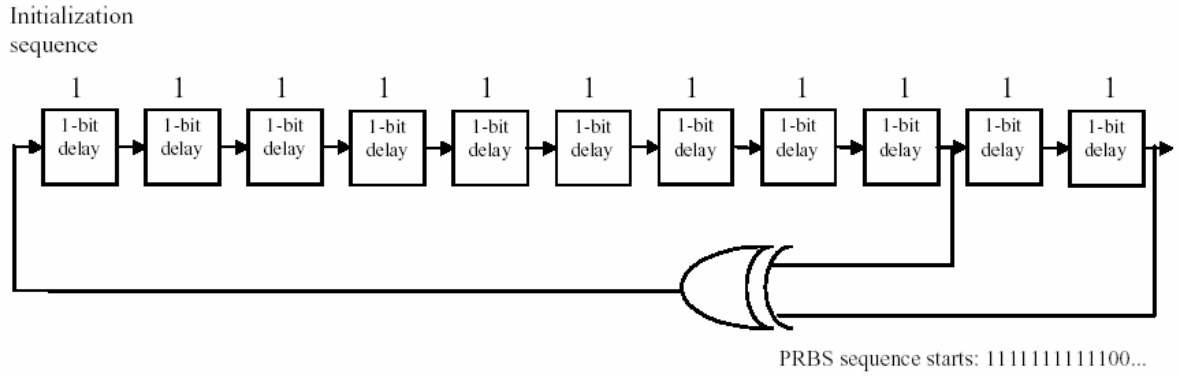


Fig 1.3 Generation of PRBS sequence

Continual pilots locate at fixed indices of subcarrier, which contains 177 pilots in 8K mode, 89 pilots in 4K mode, and 45 pilots in 2K mode. The corresponding modulation is expressed as

$$\begin{aligned} \text{Re}\{c_{m,l,k}\} &= 4 / 3 \times 2 (1/2 - w_k) \\ \text{Im}\{c_{m,l,k}\} &= 0 \end{aligned} \tag{1-3}$$

The subcarrier indices of continual pilots in 8K mode are shown in Table 1-5. The carrier indices of pilots in 2K mode are 0 to 1704 in Table 1-5, and that in 4K mode are 0 to 3408.

Table 1-5 carrier indices for continual pilot carriers for 8K mode

0	48	54	87	141	156	192	201	255	279	282	333	432	450	483	525	531	618	636	714	759	765	
780	804	873	888	918	939	942	969	984	1050	1101	1107	1110	1137	1140	1146	1206	1269					
1323	1377	1491	1683	1704	1752	1758	1791	1845	1860	1896	1905	1959	1983	1986	2037							
2136	2154	2187	2229	2235	2322	2340	2418	2463	2469	2484	2508	2577	2592	2622	2643							
2646	2673	2688	2754	2805	2811	2814	2841	2844	2850	2910	2973	3027	3081	3195	3387							
3408	3456	3462	3495	3549	3564	3600	3609	3663	3687	3690	3741	3840	3858	3891	3933							
3939	4026	4044	4122	4167	4173	4188	4212	4281	4296	4326	4347	4350	4377	4392	4458							
4509	4515	4518	4545	4548	4554	4614	4677	4731	4785	4899	5091	5112	5160	5166	5199							
5253	5268	5304	5313	5367	5391	5394	5445	5544	5562	5595	5637	5643	5730	5748	5826							
5871	5877	5892	5916	5985	6000	6030	6051	6054	6081	6096	6162	6213	6219	6222	6249							
6252	6258	6318	6381	6435	6489	6603	6795	6816														

Both scattered pilots and continual pilots are transmitted at a boosted power level of 16/9 whereas the power level of other symbols is normalized to 1.

The TPS carriers are used for the purpose of signaling parameters related to the transmission scheme, i.e. to channel coding and modulation. The TPS is defined over 68 consecutive OFDM symbol and transmitted in parallel on 17 TPS carriers for the 2K mode and on 68 carriers for the 8K mode. Each OFDM symbol conveys one TPS bit which is differentially encoded in every TPS carriers. The TPS information contains frame number, constellation, hierarchy, code rate, guard interval, transmission mode and BCH error protection code. There is 17-bit word as synchronization word in one frame. Unlike scattered and continual pilots, TPS pilots are transmitted at the normal power level of 1 with DBPSK modulation. The modulation is expressed as

$$\begin{aligned} \text{if } sl = 0, \text{ then } \operatorname{Re}\{c_{m,l,k}\} &= \operatorname{Re}\{c_{m,l-1,k}\}; \operatorname{Im}\{c_{m,l,k}\} = 0; \\ \text{if } sl = 1, \text{ then } \operatorname{Re}\{c_{m,l,k}\} &= -\operatorname{Re}\{c_{m,l-1,k}\}; \operatorname{Im}\{c_{m,l,k}\} = 0. \end{aligned} \quad (1-4)$$

The absolute modulation of the TPS carriers in the first symbol in a frame is derived from the reference sequence w_k as follows:

$$\begin{aligned} \operatorname{Re}\{c_{m,l,k}\} &= 2(1/2 - w_k) \\ \operatorname{Im}\{c_{m,l,k}\} &= 0 \end{aligned} \quad (1-5)$$

The carrier indices for TPS carriers in 8k mode are listed in Table 1-6, and that is in 2k mode and 4k mode are from 0 to 1687 and from 0 to 3048. It concludes 17, 34 and 68 TPS carriers in 2K, 4K and 8K mode respectively.

Table 1-6 Carrier indices for TPS carriers for 8K mode

34	50	209	346	413	569	595	688	790	901	1073	1219	1262	1286	1469	1594	1687	1738	1754
1913	2050	2117	2273	2299	2392	2494	2605	2777	2923	2966	2990	3173	3298	3391	3442			
3458	3617	3754	3821	3977	4003	4096	4198	4309	4481	4627	4670	4694	4877	5002	5095			
5146	5162	5321	5458	5525	5681	5707	5800	5902	6013	6185	6331	6374	6398	6581	6706			
6799																		

The guard interval may have four values, i.e. 1/4, 1/8, 1/16 and 1/32. Guard interval 1/4 would occupy 25% of the usable transmission capacity and hence only be used in case of SFN operation with long distances between transmitter sites. In the case of smaller transmitter distances (local SFN) or non-SFN operation the smaller values of guard interval can be selected. In conclusion, DVB-T/H system has good flexibility for various transmission conditions, so that it becomes a successful technology for video broadcasting.

1.3 Introduction to Time-Slicing Technology

In order to satisfy the low power issue in battery-powered terminals, a time-multiplexed transmission of different service is exploited. This technique, called time slicing, allows for selective access to desired data and results in a large battery power saving effect. The burst duration of time slicing is in the range of several hundred ms whereas the off-time may amount to several seconds. The lead time for power-on and resynchronization is assumed to be less than 250ms. Depending on the duty/turn-off ratio, the resulting power saving may be more than 90%. Timing-Slicing technology in DVB-H system [4], as Fig.1.4, provides a low power consumption methodology. The saving of power consumption depends on each kind of parameter in Time Slice identifier descriptor in DVB-H data [4]. The main spirit of Time-Slicing technology is to utilize the unused bandwidth. Because that the resolution of DVB-H system in handheld device is smaller than household system, the residual bandwidth is waste. Hence, stack the data in burst time can reduce the computing power and the bandwidth will not waste. And the cost of Time-Slicing architecture is to store the symbol data in buffers.

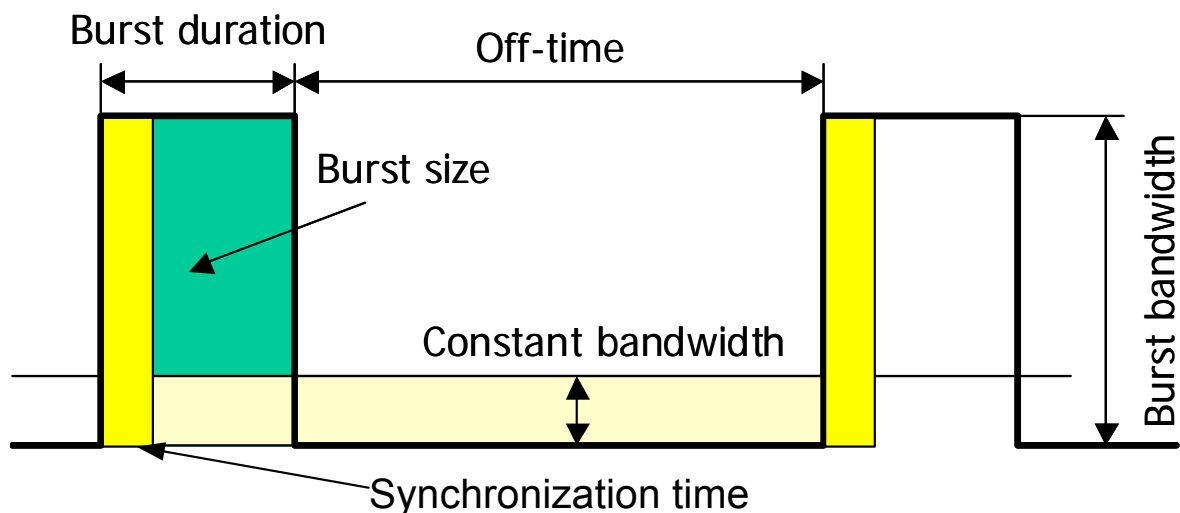


Fig 1.4: Timing-Slicing technology in DVB-H system

The related formulas of power saving are listed below.

- Bd Burst Duration (seconds)
- Bs Burst Size (bits)
- Bb Burst Bandwidth (bits per second)
- Cb Constant Bandwidth (bits per second)
- Ot Off-time (seconds)
- St Synchronization Time (seconds)
- Ps Power Saving (per cent)
- Dj Delta-t Jitter (seconds)

$$\begin{aligned}
 Bd &= \frac{Bs}{Bb \times 0.96} \\
 Ot &= \frac{Bs}{Cb \times 0.96} - Bd \\
 Ps &= \left(1 - \frac{(Bd + St + (3/4 \times Dj)) \times Cb \times 0.96}{Bs}\right) \times 100\%
 \end{aligned} \tag{1-6}$$

where most of burst parameters are shown in Fig. 1.3 and delta-t means the period of on-off (Bd+Ot). These parameters are decided from identifier descriptor in MAC layer in DVB-H system [4]. And we list several key parameters, identifier descriptors, relative to power consumption in Time-Slicing technology below.

$$\text{Burst Duration (variable of 8-bit number)} = (\text{8-bit number}) \times 20 \text{ (ms)} \tag{1-7}$$

Burst Size (fixed):

128kbits; 256kbits; 384kbits; 512kbits; 640kbits; 768kbits; 896kbits; 1024kbits; 1152kbits;
 1280kbits; 1408kbits; 1536kbits; 1664kbits; 1792kbits; 1920kbits; 2048kbits

Constant Bandwidth (fixed):

16 kbps; 32 kbps; 64 kbps; 128 kbps; 256 kbps; 512 kbps; 1024 kbps; 2048 kbps

Base on the above mentioned equations and identifier descriptors, we can attempt to calculate the saving ratio of power consumption. For instance, in 8k mode, guard interval 1/4, Bd=260ms, St=240ms, Dj=10ms, Cb=256kbps and Bs=1280kbits, the saving of power consumption reaches 90% than DVB-T system. Another example, in 2k mode guard interval 1/32, Bd=120ms, St=160ms, Dj=10ms, Cb=512kbps, Bs=1024kbits, the saving of power

consumption reaches 86% than DVB-T.

However, the cost of saving power is the buffers in receiver. In Fig 1.4, it illustrates a simplified model for the Time Slicing/MPE-FEC buffer which is used in the Receiver to store the time slicing burst and to offer constant bit stream for streaming services during off time. The data is received at the rate of B_b and the leakage rate, i.e. the rate at the output of the buffer, is R_{out} . The buffer has a certain size and when the data is written into the buffer, there is a certain processing delay (including, e.g. MPE-FEC decoding time) before the data can be read out. For each elementary stream, the maximum average bit rate over one time slicing cycle denoted by C_b is signalled in the `time_slice_fec_identifier` descriptor, and it is defined as:

$$C_b = \frac{B_s}{B_d + O_t} = \frac{B_s}{T_c} \quad (1-8)$$

where B_s and B_d are the size and the duration of the burst, respectively, O_t is the off-time between the bursts, and T_c is the cycle time for the burst ($B_d + O_t$). All parameters are here defined with respect to layer 3 datagrams. By knowing C_b and its own processing time, the Receiver can, for instance, check if the leakage rate R_{out} is high enough to successfully receive the particular elementary stream.

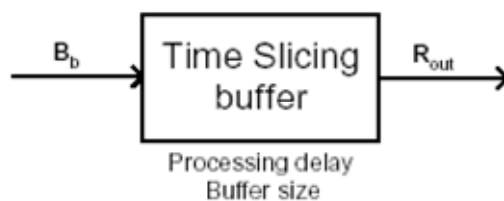


Fig 1.5 The Time Slicing/MPE-FEC buffer in the Receiver

1.4 Organization of This Thesis

This thesis is organized as follows. In chapter 2, the signal models and the detailed algorithms of the proposed CFO synchronization scheme will be introduced. The simulation

result and performance analysis will be discussed in chapter 3. Chapter 4 will introduce the design methodology, hardware architecture, and the chip summary of the proposed design. Conclusion and future work will be given in chapter 5.



Chapter 2 .

Synchronization Algorithms

2.1 Introduction to Unsynchronous Problems

In OFDM system, unsynchronous problems can be divided into two parts: timing and frequency. Timing unsynchronous problems concludes sampling clock offset (SCO) and symbol timing offset. The symbol timing offset occurs when symbol synchronization finds incorrect OFDM symbol boundary, and sampling clock offset is caused by the difference between the sampling frequencies of the digital-to-analog converter (DAC) and the one of the analog-to-digital converter (ADC). Sampling clock offset can also lead to symbol timing drift. Unlike other packet based communication system such as 802.11a, DVB-T system is a continuous-data transmission. Therefore, sampling clock offset is a critical problem to be solved.

Frequency unsynchronous problems are carrier frequency offset (CFO) and phase mismatch in time axis. Phase mismatch problem is happened when symbol timing offset changed in the system with 2-D linear interpolation in channel estimation. The phase rotation difference in the same carrier index between adjacent symbols causes interpolation error in time axis is called phase mismatch. And in OFDM system, the spectrum of the individual subcarrier mutually overlaps and exhibits orthogonality to achieve optimum spectrum efficiency. However, CFO would make inter carrier interference (ICI). CFO is also introduced by the mismatch of oscillator frequency between transmitter and receiver. Once CFO exists, the orthogonality between subcarriers will be destroyed and the degradation of the system performance will be serious. Compared with other OFDM based system such as IEEE 802.11a, the subcarrier space of DVB-T/H system is relatively narrower and the tolerance of carrier frequency offset is also worse [3][7]. Hence the CFO synchronization is a very critical

problem to be solved in DVB-T/H system.

2.1.1 Effect of Carrier Frequency Offset and Sampling Clock Offset

Consider an OFDM system using an inverse fast Fourier transform (IFFT) of size N for modulation. Each OFDM symbol is composed of K ($K < N$) data subcarriers $a_{l,k}$, where l denotes the OFDM symbol index and k ($0 \leq k < K$) denotes the subcarrier index. After IFFT, a cyclic prefix composed of N_g samples is inserted to avoid the influence of multipath channel delay spread. So a transmitted symbol has $N_s = N + N_g$ samples with sample period T . The transmitted complex baseband signal of the l -th symbol can be expressed as

$$s_l(t) = e^{j2\pi f_{c,tx} t} \left\{ \frac{1}{N} \sum_{k=0}^{K-1} a_{l,k} \cdot e^{\frac{j2\pi k'(t - (N_g + l \cdot N_s)T)}{NT}} \right\} \quad (2-1)$$

where $f_{c,tx}$ is the central frequency of the transmitter RF oscillator, and k' is the subcarrier index relative to the centre frequency, $k' = k - (K-1)/2$.

Since the CFO Δf ($\Delta f = f_{c,tx} - f_{c,rx}$) between transmitter and receiver RF oscillator can be expressed as a time-variant phase error, $e^{j2\pi\Delta f t}$, the l -th received symbol after sampling with period T' at time instants $t_n = (lN_s + N_g + n)T'$ and removing guard interval can be expressed as

$$\begin{aligned} r_l(n) &= e^{j2\pi\Delta f t_n} \cdot s_l(t_n) * h(t_n, \tau) + w_l(n) \\ &= e^{j2\pi\Delta f t_n} \cdot \frac{1}{N} \sum_{k=0}^{K-1} a_{l,k} \cdot e^{\frac{j2\pi k'(t_n - (N_g + l \cdot N_s)T)}{NT}} * h(t_n, \tau) + w_l(n) \end{aligned} \quad (2-2)$$

where $h(t_n, \tau)$ is the channel impulse response with delay spread τ , $w_l(n)$ is the complex-valued additive white Gaussian noise (AWGN).

After demodulation via a fast Fourier transform (FFT), the l -th OFDM symbol at subcarrier k , $R_{l,k}$ is as follows

$$\begin{aligned}
R_{l,k} &= \sum_{n=0}^{N-1} r_l(n) e^{-j2\pi k'n/N} \\
&= e^{j2\pi\varepsilon(IN_s+N_g)(1+\zeta)/N} e^{j\frac{2\pi k'}{N}(IN_s+N_g)\zeta} \cdot \alpha \cdot H_{l,k} \cdot a_{l,k} + ICI_{l,k} + W_{l,k}
\end{aligned} \tag{2-3}$$

where $\varepsilon = \Delta fNT$ is the CFO value normalized with the subcarrier space, ζ is the sampling clock offset (SCO) ($\zeta = (T' - T)/T$), α is an attenuation factor which is close to 1, and $ICI_{l,k}$ is the inter-carrier interference noise due to carrier frequency offset. Likewise, $H_{l,k}$ is the channel frequency response on the k -th subcarrier of the l -th OFDM symbol with the assumption that the channel is stationary within at last one symbol, $W_{l,k}$ is a zero-mean stationary complex process as well.

As previous section shows, CFO introduces various imperfect effects to the received signal. From the viewpoint of time domain, the CFO can be expressed as a time-variant phase error. The rotated phase error is in proportion to the received sample time instants t_n and can be expressed as

$$\theta_l(n) = 2\pi\Delta f t_n = 2\pi\varepsilon(IN_s + N_g + n)/N \tag{2-4}$$

where θ is the phase rotation caused by CFO. Unlike other packet-based communication systems such as IEEE 802.11a, DVB-T/H is a continuous-data transmission system and the receiving of data continues until the receiver is turned off. So the phase error will still be large even in very weak CFO environment when the receiver operates for a long time as shown in Fig 2.1.

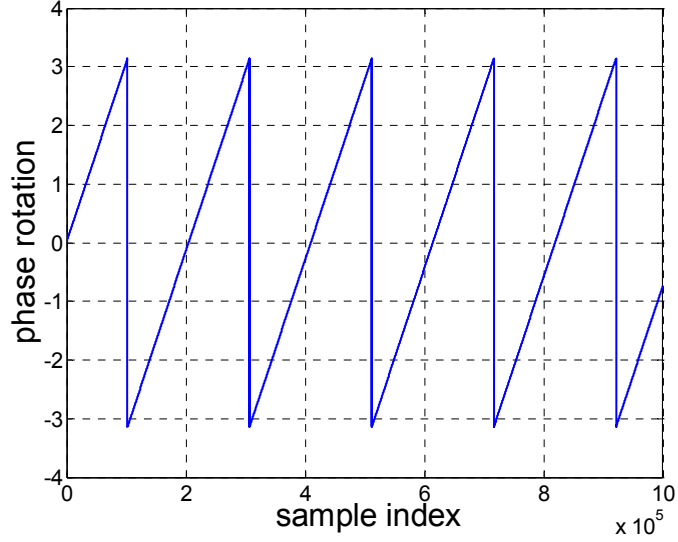


Fig 2.1 Phase rotation in time domain for long time reception when $\varepsilon=0.01$

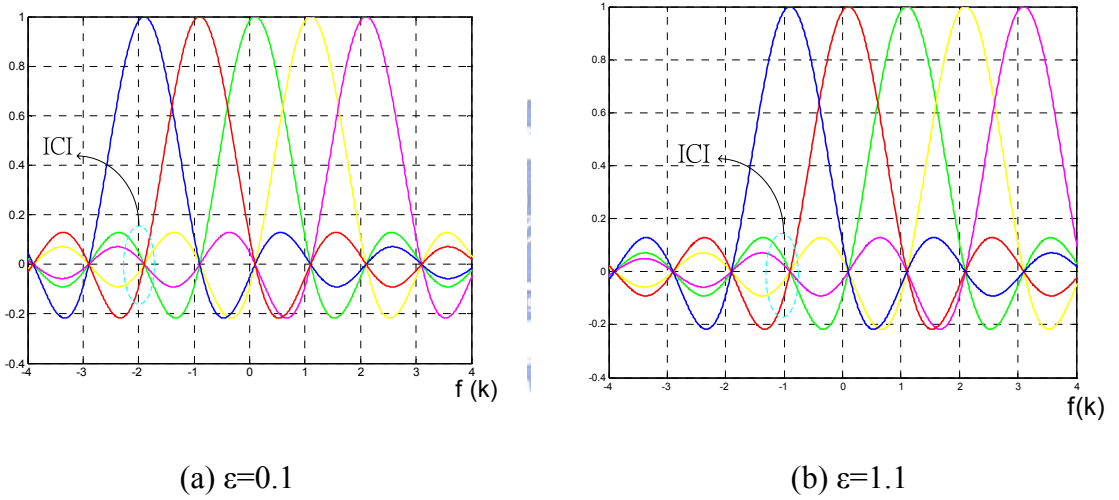


Fig 2.2 Spectrum of five subcarriers in carrier frequency offset environment

CFO results in different effects in frequency domain. It not only reduces the amplitude but also shifts the phase of the demodulated signal. Further more, the second term of (2-3) $ICI_{l,k}$ degrades the system performance strongly because it destroys the orthogonality within each subcarrier in OFDM symbols, and can be expressed as

$$ICI_{l,k} = \sum_{\substack{\tilde{k}=0 \\ \tilde{k} \neq k}}^{K-1} H_{l,k} a_{l,\tilde{k}} \frac{\sin(\pi\varepsilon)}{N \sin(\pi(\tilde{k}-k+\varepsilon)/N)} \cdot e^{j\pi\varepsilon(N-1)/N} e^{-j\pi(\tilde{k}-k)/N} \quad (2-5)$$

Because the subcarrier space of DVB-T/H system is very narrow (about 0.7~4.5 KHz), we can divide the normalized CFO value into integral part and fractional part, and can be

expressed as

$$\varepsilon = \varepsilon_I + \varepsilon_F \quad (2-6)$$

From Fig. 2.2, we can find that CFO causes inter-carrier interference noise within each subcarrier and makes the orthogonality of spectrum lost. Once the integral part of CFO ε_I is not zero, all of the subcarriers will shift circularly. The shift of subcarrier index will make the channel estimator receive wrong pilot sequence at the pre-defined pilot index and then the calculated channel frequency response will be not reliable. Also the TPS decoder can not receive correct TPS pattern to decode the correct system parameter. All of these imperfect effects in different domain should be corrected by the aid of CFO synchronization to obtain good receiving performance.

The difference of rotated phases between two adjacent symbols is represented as:

$$\begin{aligned} \varphi'_i(k) &= \varphi_i(k) - \varphi_{i-1}(k) \\ &= 2\pi\Delta f N_s T + 2\pi\Delta f N_s T \zeta + \frac{2\pi N_s k \zeta}{N} \\ &\approx 2\pi\Delta f N_s T + \frac{2\pi N_s k \zeta}{N} \end{aligned} \quad (2-7)$$

We can ignore the term $2\pi\Delta f N_s T \zeta$, since the SCO is usually less than 1.0×10^{-4} . As (2-7) indicates, CFO causes mean phase error as well as SCO causes linear phase error between two adjacent symbols.

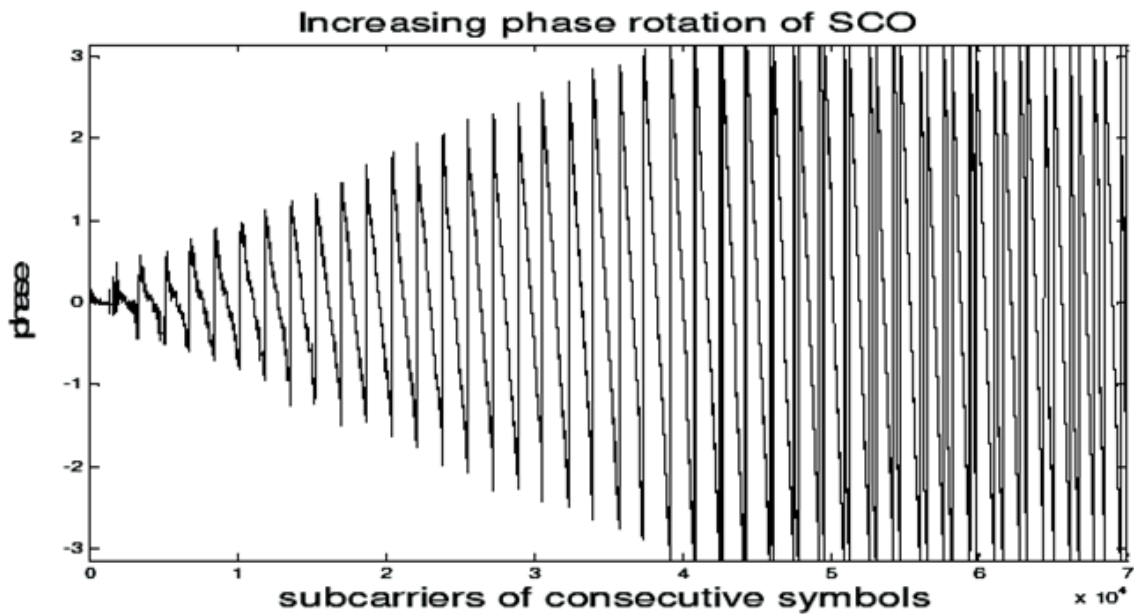


Fig 2.3 Phase rotation due to timing drifts

In Fig 2.3, it demonstrates the phase rotation of timing drift due to sampling clock offset. In the former symbols, the total amount of phase rotation is limited in 2π (rads) since the drift point is less than one sample. After symbol timing drift exceeding one sample, phase rotation becomes severer increasingly. Regardless of the case of symbol timing drifting into ISI region, the violent phase variation still reduce the performance of channel estimation. If symbol timing drifts out of ISI-free region, inter-symbol interference is produced and hence system performance degrades much.

2.1.2 Effect of Symbol Timing Offset

The symbol synchronization of the OFDM system is to find the start of OFDM symbol, i.e. the FFT window position. Just as what is shown in Fig 2.4, we call Δ the ISI-free region. If the estimated start position of OFDM symbol is located within the ISI-free region, data will not be affected by inter-symbol interference (ISI). The effect of phase rotation caused by symbol timing offset can be easily corrected after FFT.

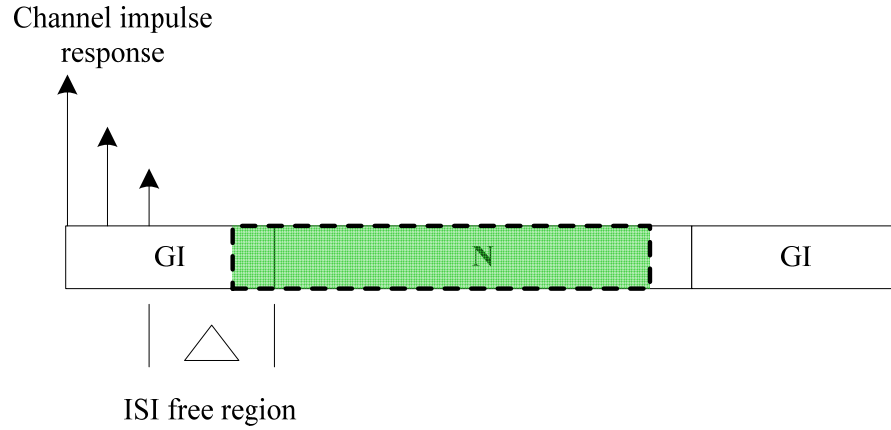


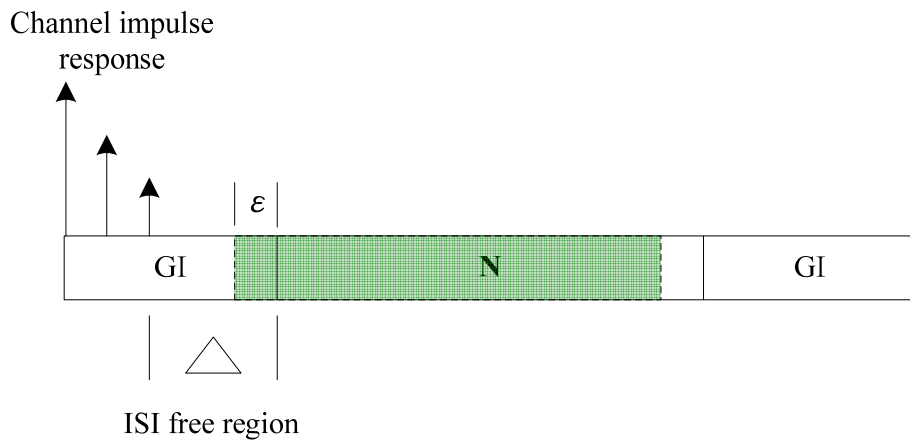
Fig 2.4 ISI-free region

Assume $x(n)$ represents received data in time domain, $X(k)$ is subcarrier after FFT operation for $x(n)$ with perfect symbol timing, and $\hat{X}(k)$ denotes subcarrier after FFT operation with symbol timing offset ε in the ISI-free region. The detail equations are demonstrated as follows.

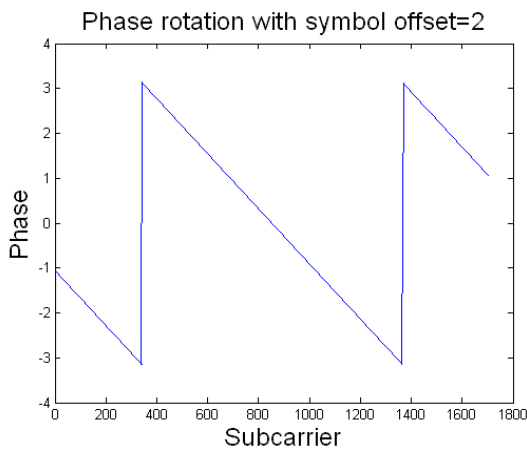
$$\begin{aligned}
 X(k) &= \sum_{n=0}^{N-1} x(n) e^{-i2\pi k \frac{n}{N}} \\
 \hat{X}(k) &= \sum_{n=0}^{N-1} x(n) e^{-i2\pi k \frac{n+\varepsilon}{N}} \\
 \hat{X}(k) &= \sum_{n=0}^{N-1} x(n) e^{-i2\pi k \frac{n}{N}} e^{-i2\pi k \frac{\varepsilon}{N}} \\
 \hat{X}(k) &= X(k) e^{i2\pi k \varepsilon / N}
 \end{aligned} \tag{2-8}$$

where k represents the subcarrier index, n denotes sample index in time domain, and N is the number of subcarriers in an OFDM symbol. Note the last term $e^{i2\pi k \varepsilon / N}$ in (2-8), which exhibits the phase rotation. Therefore, we can conclude that the effect of symbol timing offset in the ISI-free region is phase rotation and unchanged magnitude of subcarrier, which can be compensated by equalizer completely. The phase rotation effect is shown in Fig 2.5. Fig 2.5(b) depicts the condition of symbol timing offset $\varepsilon = 2$ while Fig 2.5(c) shows the condition of $\varepsilon = 5$. As symbol timing offset ε is larger, the phase variation is severer. The additional variance of channel response due to timing error will increase the difficulty of channel estimation. In order to

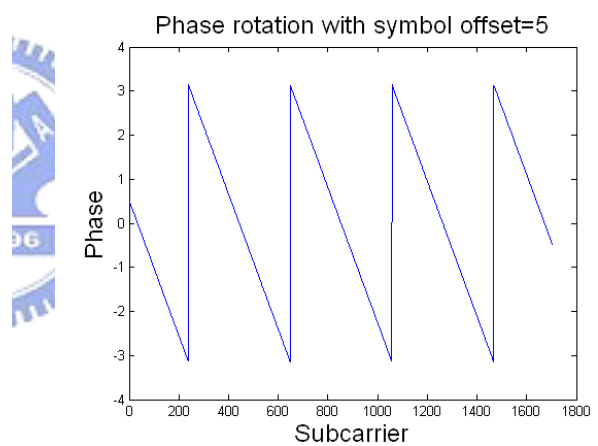
ease the load of channel estimation unit, the symbol timing effect should be as small as possible even the phase rotate effect can be completely corrected in theory.



(a) Symbol timing offset ϵ in the ISI-free region



(b) Phase rotation due to symbol timing offset=2

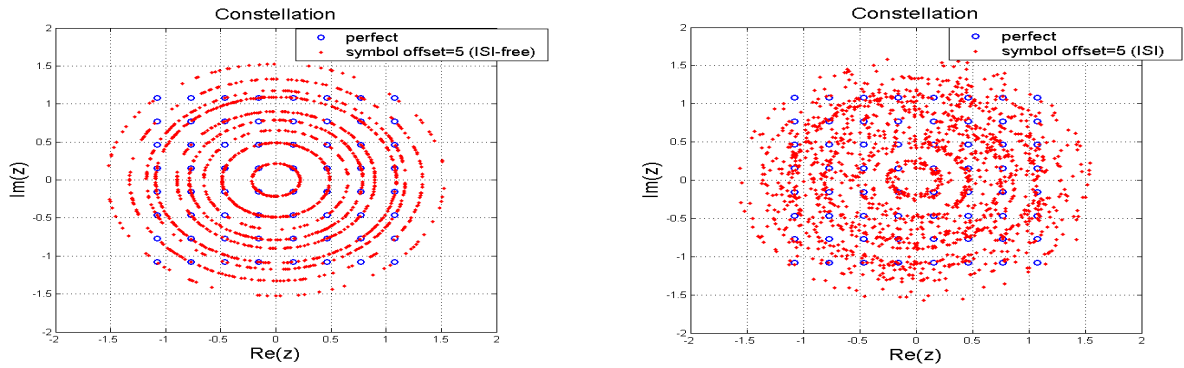


(c) Phase rotation due to symbol timing offset=5

Fig 2.5 Phase rotation of symbol timing offset $\epsilon = 2$ and $\epsilon = 5$

On the other hand, if the estimated start position locates out of ISI-free region, the sampled OFDM symbol will contain some samples that belong to previous symbol or following symbol, which leads to the dispersion of signal constellation (ISI) and reduce system performance much. Therefore, the objective of symbol synchronization, first of all, is to avoid the estimated symbol boundary lying in ISI region and subsequently reduce the

symbol timing offset as far as possible. The relative mapping constellations are depicted in Fig 2.6. Fig 2.6(a) shows the phase rotation effect due to symbol timing offset of 5 samples while Fig 2.6(b) shows the ISI effect which destroys the signal constellation heavily.



(a) Symbol offset 5 samples in the ISI-free region

(b) Symbol offset 5 samples in the ISI region

Fig 2.6 Mapping constellation

2.1.3 Effect of Carrier Phase Mismatch

The problem of carrier phase mismatch comes from the different phase rotation of post-FFT symbols by using 2-D channel equalization (2-D CE). To observe the carrier phase mismatch problem, we should discuss from fine symbol synchronization, SCO tracking and 2-D channel interpolation.

First, we discuss fine symbol synchronization. Fine symbol synchronization scheme in DVB-T/H system is the function of precisely monitoring the time symbol boundary to prevent ISI occurring in serious frequency selective fading channel. If we don't use fine symbol synchronization, the carrier phase rotation would be too large and the phase between pilots to pilots would make the interpolation error, as shown in Fig 2.7. The performance would decrease very seriously.

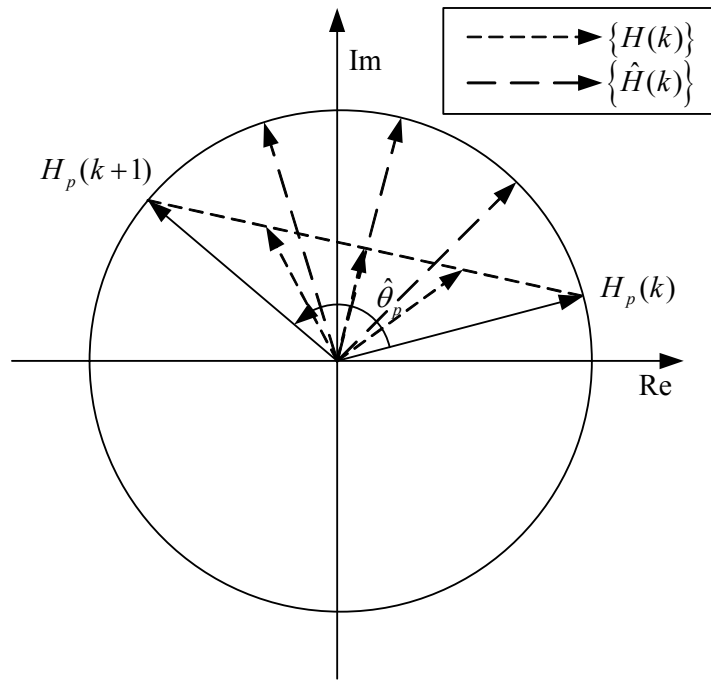


Fig 2.7 the influence of frame position error to interpolations

In our simulation, we choose IFFT method to be the algorithm of fine symbol synchronization. IFFT based method is the most popular algorithm in DVB-T/H system as shown in [1], [2]. Observing the channel impulse response (CIR) in time domain we can obtain the residual symbol timing offset information as shown in Fig 2.8.

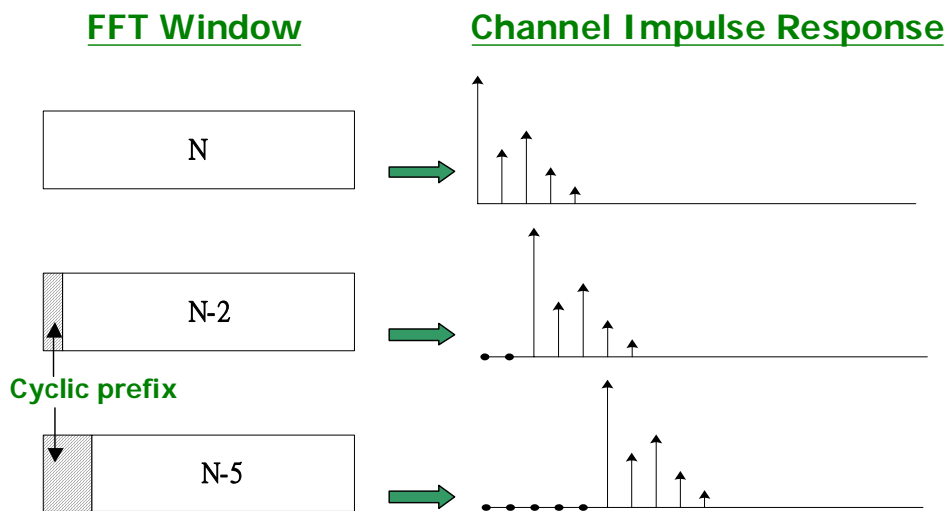


Fig 2.8 Relative CIR due to inaccurate FFT window

As we know, fine symbol synchronization of IFFT based method uses the channel frequency response (CFR) of pilots in frequency domain. It goes through IFFT operation and then gets CIR. The source of CFR is calculated from 2-D linear interpolation as shown in Fig 2.9.

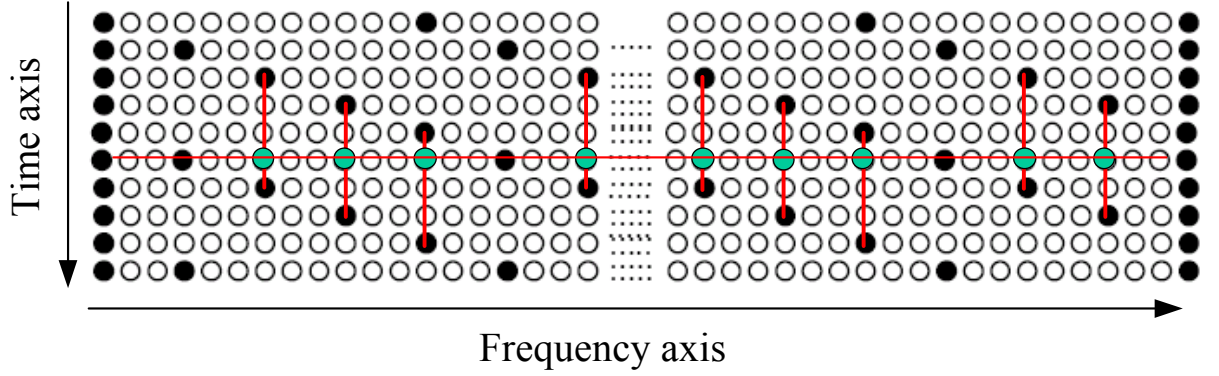


Fig 2.9 Interpolation of 2D channel estimation

2-D channel interpolation [8], usually used to resist severe multi-path and mobile environment, includes time and frequency axis interpolations. The first step is to store the previous 3 post-FFT symbols and use the pilot information producing the time axis interpolation. Then, in frequency axis it interpolates the total CFR $H_{l,k}$ of previous 3-th post-FFT symbol. Before the frequency axis interpolation and after time axis interpolation, we take the interpolated $(K/3)$ pilots to IFFT for obtaining CIR. And we must pad zeros to $(N/2)$. The decision equation express as

$$\hat{\delta} = \frac{2}{3} \min \{n \mid \hat{S}_x > \hat{S}_{\max} / 16, x = 0, \dots, (K-1)/3-1\} \quad (2-9)$$

$$\hat{S}_x = |h_x|^2$$

where h_x is CIR of pilots, x is its index and M is $K/3$.

After fine symbol updating, it remains phase rotation between pilots' CFR, as shown in Fig 2.10. And the previous and current post-FFT symbols have different phase rotation. In 2-D linear interpolation algorithm, the previous symbols and pilots are stored in memory in order to time axis interpolation. At the same subcarrier index between previous and current

symbols, the different phase rotation makes phase mismatch. It would cause the performance degradation. The carrier phase mismatch is shown as

$$\begin{aligned}\hat{H}_{p-pre}(k) &= H_p(k)e^{i2\pi k\varepsilon_{pre}/N} \\ \hat{H}_{p-cur}(k) &= H_p(k)e^{i2\pi k\varepsilon_{cur}/N} \\ \hat{H}(k) &= H(k)e^{i2\pi k(\varepsilon_{cur}-\varepsilon_{pre})/N} = H(k)e^{i2\pi k\Delta\varepsilon/N}\end{aligned}\quad (2-10)$$

where $H_{p-pre}(k)$ and $H_{p-cur}(k)$ respectively means CFR of k -th pilot in previous symbols and current symbol in f-domain. $H(k)$ means CFR of k -th subcarrier in f-domain symbol. $\hat{H}(k)$ means the estimated value.

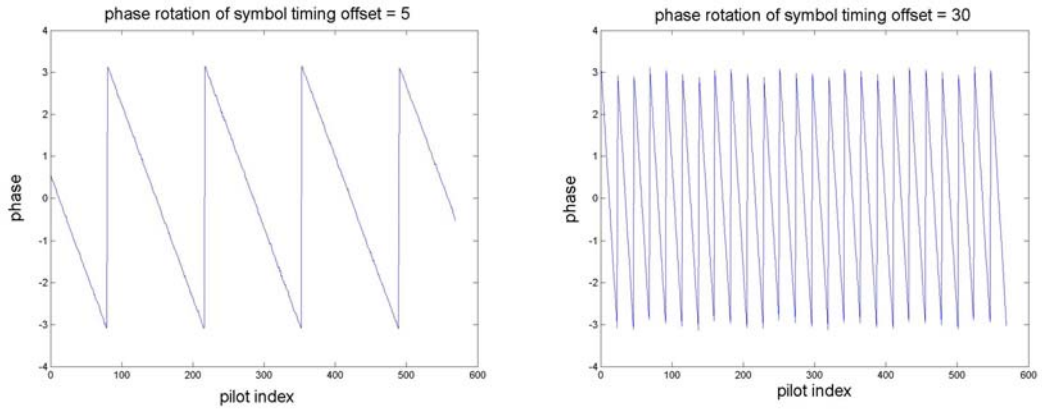


Fig 2.10 the phase rotation of pilots' CFR caused by different symbol timing offset

When the multi-path fading spread changes seriously, the channel impulse response would also changes, as shown in Fig 2.11. This situation is obvious in SCO effect in mobile environment. In order to simulate the influence of SCO in carrier phase mismatch, we plus one term to modify the equation and is expressed as

$$\hat{H}(k) = H(k)e^{i2\pi k(\varepsilon_{cur}-\varepsilon_{pre}-\varepsilon_{\Delta\delta})/N} = H(k)e^{i2\pi k\Delta\varepsilon/N}\quad (2-11)$$

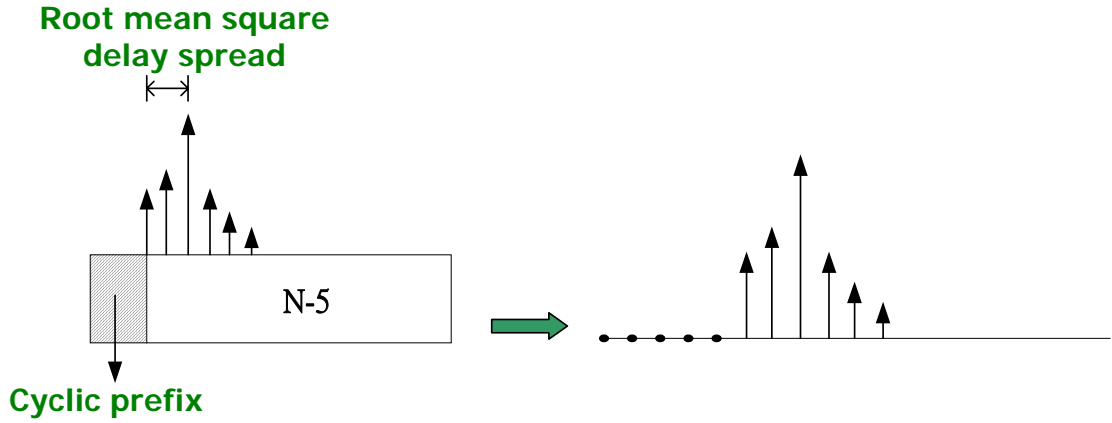
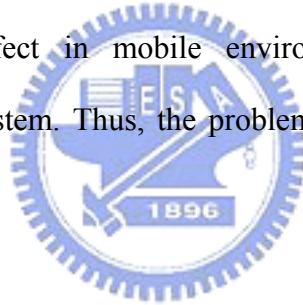


Fig 2.11 Relative channel impulse response with multi-path

Summary of this section, we understand the carrier phase mismatch in time axis is happened in a specific situation. It is in mobile environment with SCO effect and 2-D CE must be used in receiver platform. However, 2-D CE is the most common architecture in state-of-the-art and SCO effect in mobile environment is the significant issue for synchronization in DVB-H system. Thus, the problem of carrier phase mismatch has to be solved.



2.2 Carrier Phase Alignment

Phase alignment locates after fine symbol synchronization scheme and passes information to channel estimator and equalizer, as shown in Fig 2.12. In recent research, carrier phase rotation problem caused by residual symbol timing offset is brought up to discuss. Large phase rotation will produce significant errors in linear channel interpolation, as mentioned in Section 2.1.4. To solve this problem, in [5], it provides a phase compensation method. It can deal with the interpolation error by compensating the phase rotation of pilots and symbols. And the compensating equation is expressed as

$$\hat{H}_p(k) = H_p(k) \cdot e^{j\hat{\theta}_p k} \quad (2-12)$$

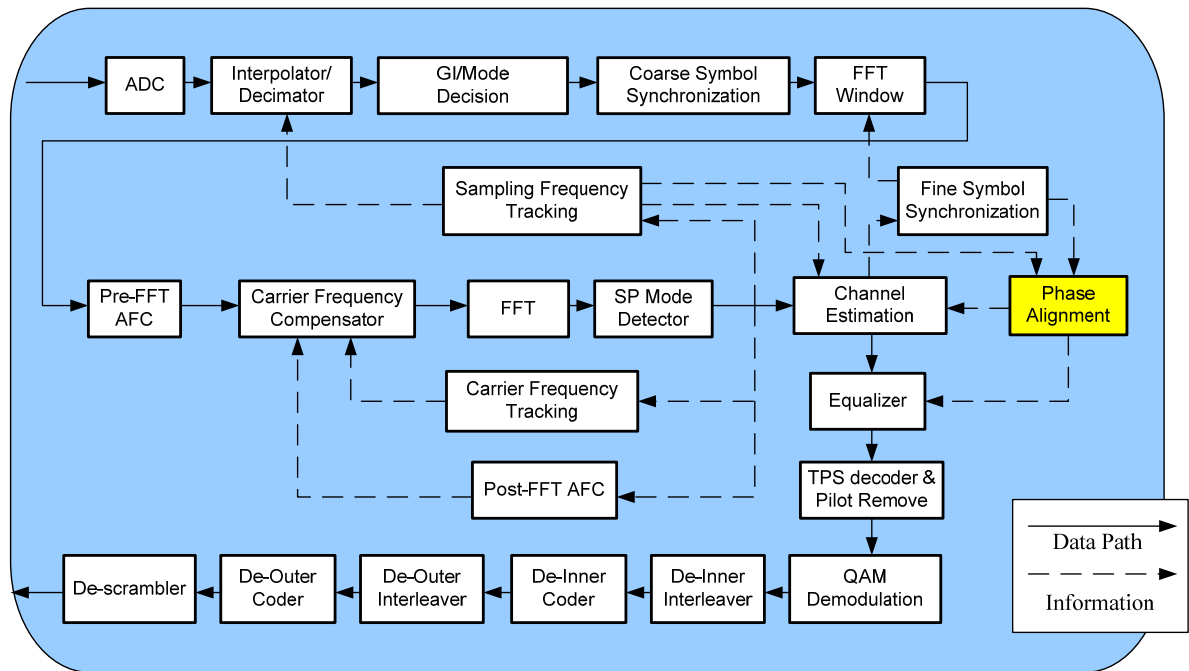


Fig 2.12 Location of phase alignment in receiver platform

where $\hat{\theta}_p$ is detected out from channel frequency response of post-FFT symbols. Note that it doesn't move the symbol boundary and it uses phase compensator to replace fine symbol scheme. It will cause a problem in fast frequency selective channel when the system is without fine symbol synchronization, the samples drift. Also, we show the comparison of performance between 2-D CE and 1-D CE in Fig 2.13.

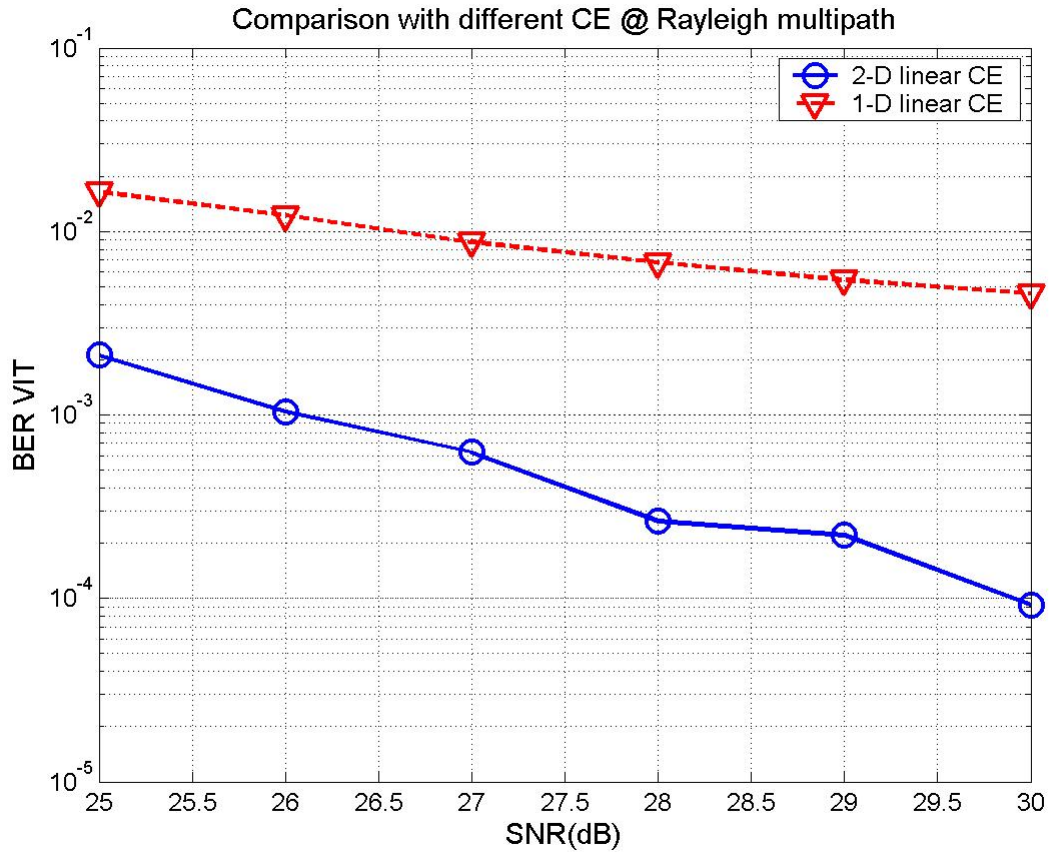


Fig 2.13 Comparison of performance between 2-D CE and 1-D CE



However, two problems remain in [5]. The system of [5] is not scattered pilot based. 2-D CE is not discussed in [5] but the carrier phase mismatch is happened with 2-D CE. Moreover, in [5], the influence of SCO with Doppler effects is not considered. However, these two conditions are significant issues for synchronization in DVB-H system.

The proposed carrier phase alignment in time axis is to align the phase rotation of previous post-FFT symbols in 2-D interpolator buffers. The block diagram is shown in Fig 2.14.

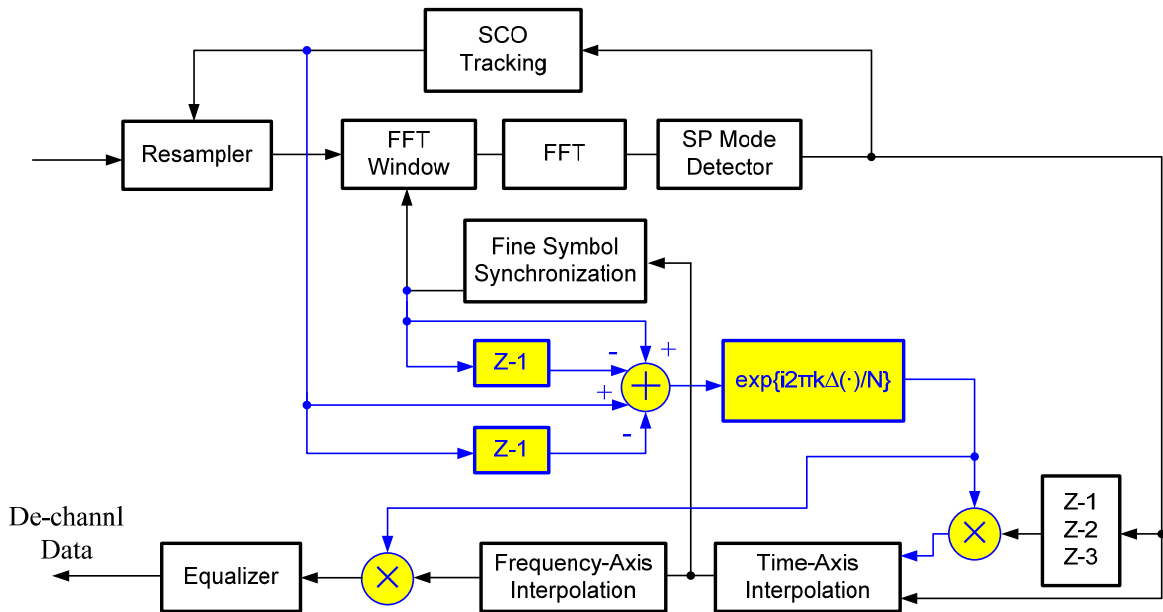


Fig 2.14 the phase rotation of pilots' CFR caused by different symbol timing offset

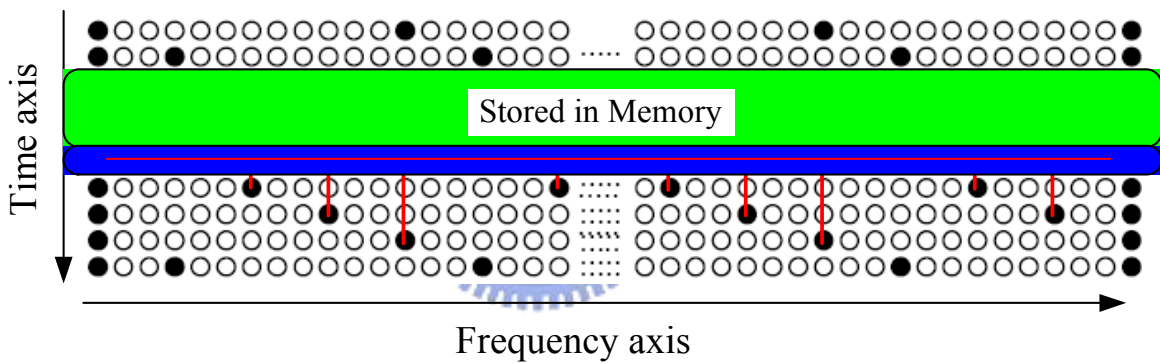


Fig 2.15 2-D channel interpolation

In Fig 2.15, it shows 2-D CE. Interpolation in time axis acts before in frequency axis. The proposed phase alignment in time axis is to align the phase rotation of previous post-FFT symbols in 2-D interpolator buffers.

First step of carrier phase alignment, we take out the CFR of post-FFT symbol pilots by interpolation in time axis. Then, CFR is passed through fine symbol synchronization and we get the updating symbol bound. When the symbol boundary updated, the current symbol is passed to frequency domain and cause the phase mismatch to previous symbols in buffers. Then, residual SCO drifted point is considered in the system. Carrier phase alignment in time

axis will multiply the alignment factor in 3 parts, one is pilots before 3 previous symbols and the other parts are the estimated pilots and the symbol data before divider. Here the equations are expressed as

$$\begin{aligned}\hat{H}_{p-align}(k) &= H_p(k)e^{i2\pi k\epsilon_{pre}/N} \times e^{i2\pi k\Delta\epsilon/N} \\ &= H_p(k)e^{i2\pi k\epsilon_{cur}/N}\end{aligned}\quad (2-13)$$

where $\Delta\epsilon$ means the difference timing symbol offset $\epsilon_{cur} - \epsilon_{pre} - \epsilon_{\Delta\delta}$. $\epsilon_{\Delta\delta}$ means the error terms at resampler out. After aligning the pilots in time axis, we interpolate the CFR of pilots in every 3 subcarriers in time axis, it can be expressed as

$$\hat{H}_{p-align,l}(k) = \left(1 - \frac{i}{4}\right) \times \hat{H}_{p-align,l-i}(k) + \frac{i}{4} \times \hat{H}_{p-align,l+i}(k), \quad i = 1, 2, 3 \quad (2-14)$$

Then interpolating the frequency axis subcarrier CFR to get total CFR in each subcarrier, it is expressed as

$$\hat{H}_{align}(k) = \left(1 - \frac{j}{4}\right) \times \hat{H}_{p-align,l}(k-j) + \frac{j}{4} \times \hat{H}_{p-align,l}(k+j), \quad K_{min} \leq k \leq K_{max}, \quad i = 1, 2, 3, \quad (2-15)$$

Before subcarrier data are sent into divider, we align the phase as CFR of carriers. And the equations are expressed as

$$\begin{aligned}\hat{R}_{align}(k) &= R(k)e^{i2\pi k\epsilon_{pre}/N} \times e^{i2\pi k\Delta\epsilon/N} \\ &= R(k)e^{i2\pi k\epsilon_{cur}/N}\end{aligned}\quad (2-16)$$

$$\hat{Y}_{align}(k) = \frac{\hat{R}_{align}(k)}{\hat{H}_{align}(k)} = \frac{R(k)}{H(k)} \quad (2-17)$$

Architecture of the proposed phase alignment in time axis is shown in Fig 2.16.

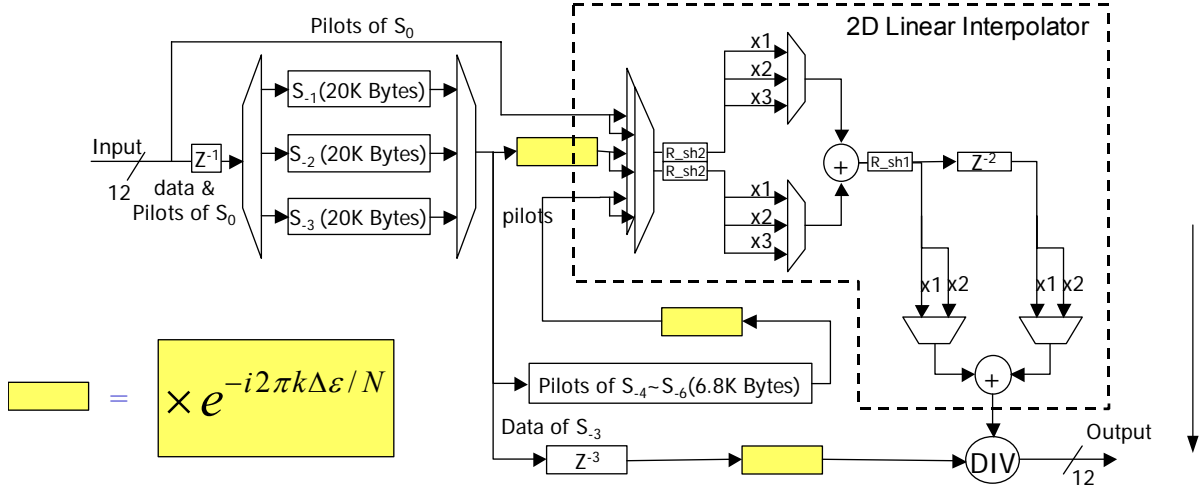


Fig 2.16 Proposed time axis phase alignment architecture

After multiplying phase alignment factor $e^{-i2\pi k \Delta \epsilon / N}$, the CFR of pilots and symbol data are both on the same phase criterion. And the phase alignment is completed.

2.3 Fast Synchronization System

For the reason of power saving, Time-Slicing methodology in DVB-H system is used. The saving of power consumption is in (1-6), where B_d means burst duration, S_t means synchronization time, D_j means delta-t jitter C_b means constant bandwidth, B_s means burst size and P_s means power saving. In this equation, B_d , C_b and B_s are defined in the DVB-H data, [4]. Hence, note that the synchronization time dominates the saving of power consumption in fixed mode. In Fig 2.17, it shows the composition of completed synchronization time. According to Fig 2.17, we can get the information as

$$S_t = \max \{ (T_a + T_{tps} + T_{rs}); (T_a + T_t) \} \quad (2-18)$$

where S_t means synchronization time, T_a means acquisition time, T_{tps} means transmission parameter signaling (TPS) decode time, T_{rs} is Reed-Solomon (RS) packet synchronization time and T_t means the SCO/CFO tracking time.

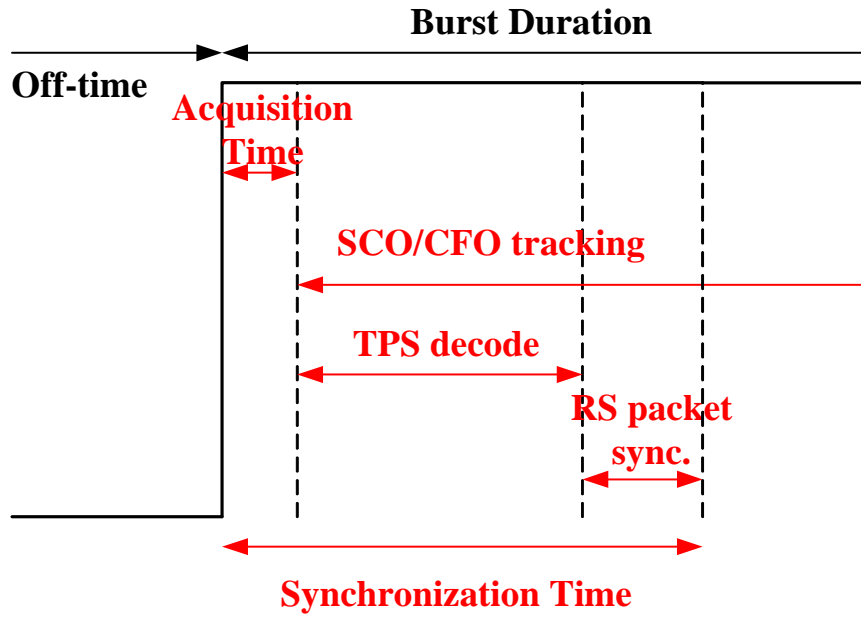


Fig 2.17 composition of completed synchronization time

The determination of synchronization time depends on SCO/CFO tracking is longer or the summation of TPS decoded time and RS packet synchronization time is longer. SCO/CFO tracking time depends on channel effects. However, the TPS decoder and RS packet synchronization needs a fixed time to receive enough symbols. Hence, in this section, we discuss the TPS decoded and RS packet synchronization. In Fig 2.18, it shows the location of these two designs in the receiver platform.

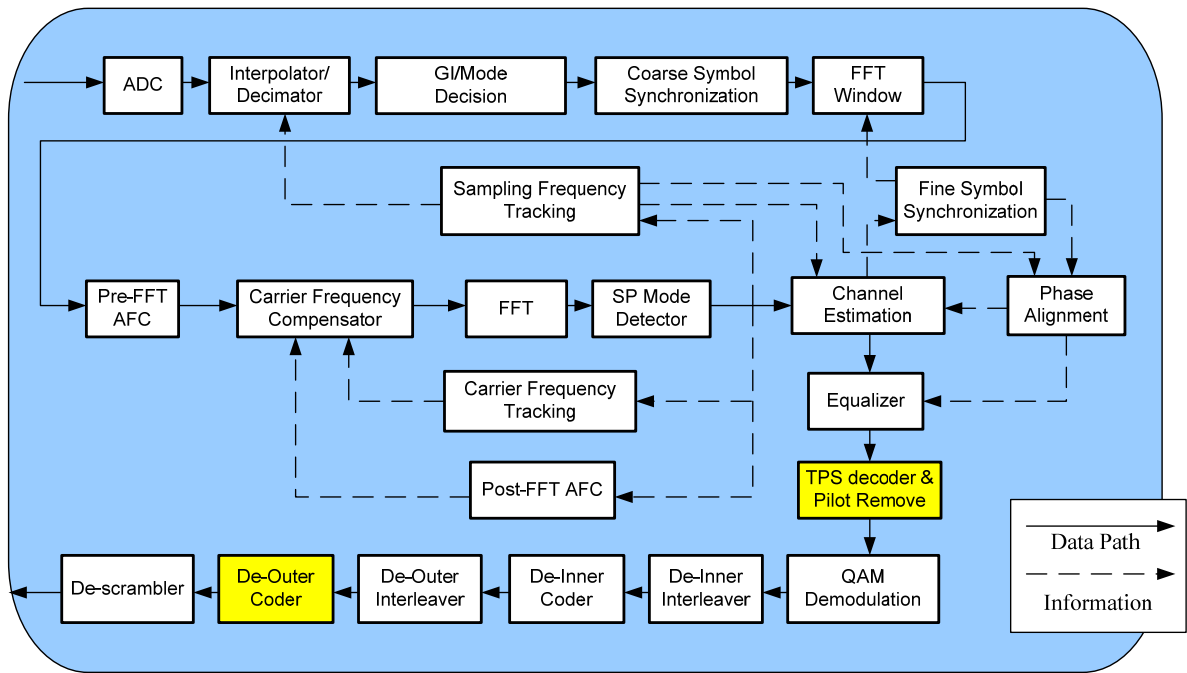


Fig 2.18 Location of fast synchronization in receiver platform

Acquisition time is about 10 symbols, TPS decoded time is about 2 frames (136 symbols), RS sync. Time is about 4/2/1 frames (272/136/68 symbols) and the total synchronization time in costs 417/281/213 symbols in 8k/4k/2k mode in conventional method. And we can see the symbol duration time in this equation:

$$\text{symbol duration} = N \times T \times (1 + GI) \quad (2-19)$$

where N is 2k/4k/8k, T is elementary period 7/64, 1/8, 7/84 and 7/40 μs in 8MHz, 7MHz, 6MHz and 5MHz channel and GI is 1/4, 1/8, 1/16 and 1/32.

2.3.1 TPS Decode

The structure of TPS listed in DVB-T/H standard [3] is composite of 68-bit word (one frame) and concludes 16-bit synchronization word and 1 initialization bit. The transmission parameter information shall be transmitted as shown in table 2-1. Here, one symbol includes one bit TPS and one frame includes 68 bits TPS information.

The mapping of each of the transmission parameters: constellation characteristics, α value, code rate(s), super-frame indicator and guard interval onto the bit combinations is performed according to clauses appendix A. The left most bit is sent first.

Table 2-1 TPS signaling information and content

Bit number	Purpose/Content
S ₀	Initialization
S ₁ to S ₁₆	Synchronization word
S ₁₇ to S ₂₂	Length indicator
S ₂₃ , S ₂₄	Frame number
S ₂₅ , S ₂₆	Constellation
S ₂₇ , S ₂₈ , S ₂₉	Hierarchy information
S ₃₀ , S ₃₁ , S ₃₂	Code rate, HP stream
S ₃₃ , S ₃₄ , S ₃₅	Code rate, LP stream
S ₃₆ , S ₃₇	Guard interval
S ₃₈ , S ₃₉	Transmission mode
S ₄₀ to S ₄₇	Cell identifier
S ₄₈ , S ₄₉	DVB-H signaling
S ₅₀ to S ₅₃	Reserved for future use
S ₅₄ to S ₆₇	Error protection

The first bit, s₀, is an initialization bit for the differential 2-PSK modulation. The modulation of the TPS initialization bit is derived from the PRBS sequence defined in [3]. Bit 1 to 16 of the TPS is a synchronization word. The first and third TPS block in each super-frame has the following synchronization word:

$$s_1 - s_{16} = 0011010111101110.$$

The second and fourth TPS blocks have the following synchronization word:

$$s_1 - s_{16} = 1100101000010001.$$

The conventional design [1] of TPS decoded costs 135 (68 + 67) symbols time in the worst situation to receive the completed TPS word and then synchronizes the header. This is the primitive method, that it uses more than one frame to find the synchronization word and initialization bit and then decodes TPS. The conventional operation of TPS word distributes in Fig 2.19.

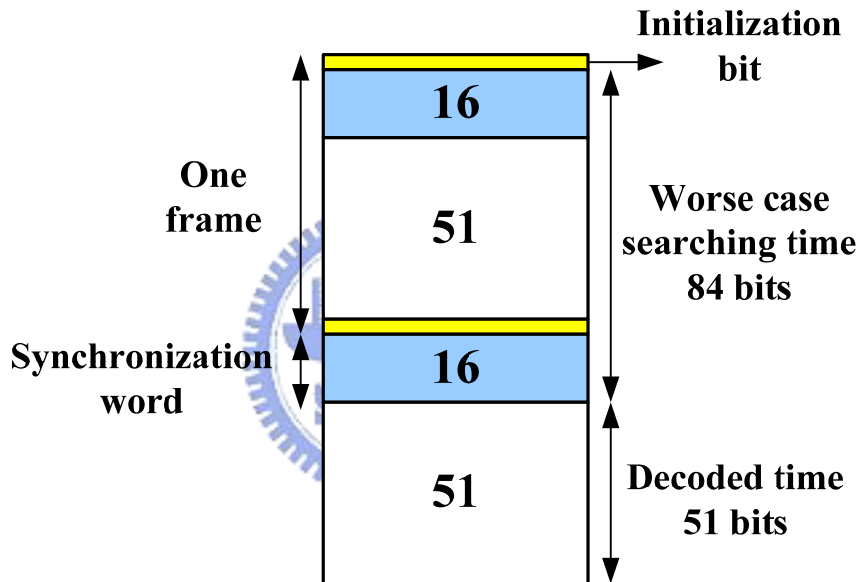


Fig 2.19 the operation of conventional TPS word

The proposed method can decode out TPS faster than conventional method. The proposed method is to buffer the previous 68-bit TPS word. When finding the 16-bit synchronization word and initialization bit, we read the previous 51 words information as TPS decoded word. Hence, we can advance the time of 51 symbols. The worst case of the decoded time is 84 (67+17) symbols. We can see the operation of proposed TPS word distribution in Fig 2.20.

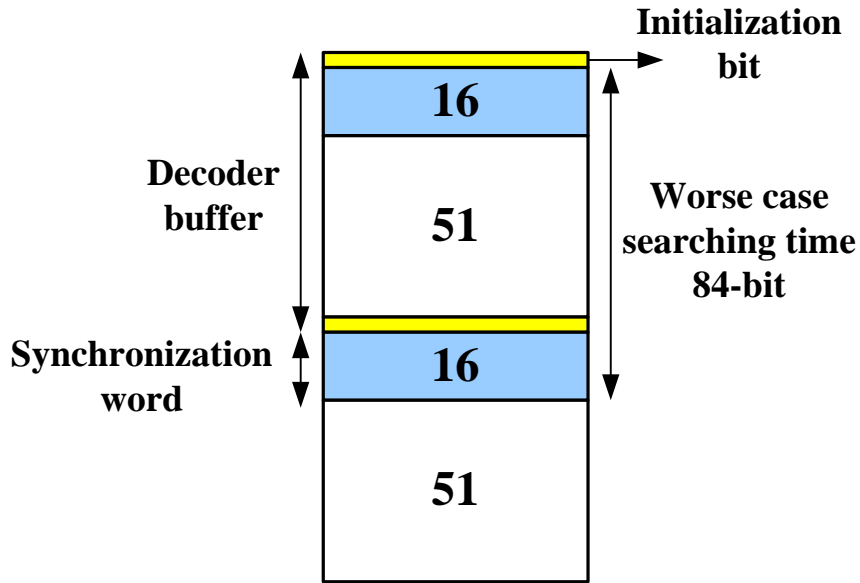


Fig 2.20 the operation of proposed TPS word

2.3.2 RS Packet Synchronization

As Fig 2.21 shown, we know the outer decoder is RS decoder. Because that the input of RS decoder must be a completed packet. In other word, we must synchronize the header of the RS packet. The impact of RS packet is shown as Fig. 8. If we don't consider the header and the completed packet for the RS decoder input, the decoder must waste a lot of time for waiting synchronization word.



Fig 2.21 RS packet structure

The worst condition of RS packet synchronization time in conventional method is 4/2/1 frame (272/136/68 symbols) in 2k/4k/8k mode. The conventional method is to synchronize the packet in completed frames, but the proposed method just needs to calculate the carrier index to synchronize the packet in the completed carriers. The proposed method will help us to reduce the synchronization time a lot. We can reduce the synchronization time to 5/3/2

symbols in 2k/4k/8k modes.

To introduce the conventional design, we discuss how many RS packets in one super-frame (4 frames). It shows the RS packets in one super-frame in Table. 2. It is accomplished by the formula:

$$(\text{packets/super-frame}) = \frac{(\text{mapping bits}) \times (\text{data carriers}) \times (\text{symbols}) \times (\text{code rate})}{204 \times 8} \quad (2-20)$$

For instance, in QPSK mapping, 2k mode and code rate 7/8, we can calculate the RS packets in a super-frame as $\frac{2 \times 1512 \times 68 \times 4 \times 7/8}{204 \times 8} = 441 \text{ packets}$. According to Table 2-2 we can

know one super-frame concludes how many packets in all kinds of transmission mode, mappings and code rates. The conventional design of RS packet of synchronization in [1] directly synchronizes in 4/2/1 frame (272/136/68 symbols) in 2k/4k/8k mode. Because that the RS packets in 4k/8k mode can be divided by 2/4 with no remainder in all kinds of mappings and code rates. Hence, RS packets synchronization in 4k/8k mode can be synchronized in 2/1 frame. The worst RS packet synchronization time is 272/136/68 symbols in 2k/4k/8k mode in conventional method.

Table 2-2 number of RS 204 bytes packets per OFDM super-frame for all combinations of code rates and modulation forms

Code rate	QPSK			16-QAM			64-QAM		
	2k	4k	8k	2k	4k	8k	2k	4k	8k
1/2	252	504	1008	504	1008	2016	756	1512	3024
2/3	336	672	1344	672	1344	2688	1108	2016	4032
3/4	378	756	1512	768	1512	3024	1134	2268	4536
5/6	420	840	1680	840	1680	3360	1260	2520	5040
7/8	441	882	1764	882	1764	3528	1323	2646	5292

The following discussion is the proposed design. The proposed design is based on subcarrier

including packets. Before finding how many subcarriers constituting with completed packets, we calculate the how many packets in a subcarrier. There is a formula to calculate that how many packets are included in a subcarrier:

$$(\text{packets/subcarrier}) = \frac{(\text{code rate}) \times (\text{mapping})}{(204 \times 8)} \quad (2-21)$$

The solution of this equation is listed in Table 2-3, Table 2-4, and Table 2-5. The denominator of packets/subcarrier is the answer of synchronization subcarriers.

Table 2-3 the packets in one carrier with varied code rate in QPSK mapping

Code rate	1/2	2/3	3/4	5/6	7/8
Packets/carrier	1/1632	1/1224	1/1088	5/4896	7/6528
Sync carrier	1632	1224	1088	4896	6528
Sync packet	1	1	1	5	7

Table 2-4 the packets in one carrier with varied code rate in 16-QAM mapping

Code rate	1/2	2/3	3/4	5/6	7/8
Packets/carrier	1/816	1/612	1/544	5/2448	7/3264
Sync carrier	816	612	544	2448	3264
Sync packet	1	1	1	5	7

Table 2-5 the packets in one carrier with varied code rate in 64-QAM mapping

Code rate	1/2	2/3	3/4	5/6	7/8
Packets/carrier	1/544	1/408	3/1088	5/1632	7/2176
Sync carrier	544	408	1088	1632	2176
Sync packet	1	1	3	5	7

The RS packet synchronization starts after TPS decoding the synchronization word. Hence, the synchronization carriers can be calculated after 17 symbols in 1st-4th frame. The

synchronization carriers are fixed in Table 2-5, Table 2-6 and Table 2-7. The equation is shown as:

$$\text{residual carriers} = (\text{sync carriers}) - \text{remainder}\{[(\text{frame_idx}-1) \times 68 + 17] / (\text{sync carriers})\} \quad (2-22)$$

Table 2-5 residual carriers for RS packet synchronization for 2K mode

Code rate	1/2	2/3	3/4	6/5	7/8
QPSK 1st frame	408	0	408	3672	408
QPSK 2nd frame	408	0	952	3672	2040
QPSK 3rd frame	408	0	408	3672	3672
QPSK 4th frame	408	0	952	3672	5304
16-QAM 1st frame	408	0	408	1224	408
16-QAM 2nd frame	408	0	408	1224	2040
16-QAM 3rd frame	408	0	408	1224	408
16-QAM 4th frame	408	0	408	1224	2040
64-QAM 1st frame	408	0	408	408	408
64-QAM 2nd frame	408	0	952	408	2040
64-QAM 3rd frame	408	0	408	408	1496
64-QAM 4th frame	408	0	952	408	952

Table 2-6 residual carriers for RS packet synchronization for 4K mode

Code rate	1/2	2/3	3/4	6/5	7/8
QPSK 1st frame	816	0	816	2448	816
QPSK 2nd frame	816	0	816	2448	4080
QPSK 3rd frame	816	0	816	2448	816
QPSK 4th frame	816	0	816	2448	4080

16-QAM 1st frame	0	0	272	0	816
16-QAM 2nd frame	0	0	272	0	816
16-QAM 3rd frame	0	0	272	0	816
16-QAM 4th frame	0	0	272	0	816
64-QAM 1st frame	272	0	816	816	816
64-QAM 2nd frame	272	0	816	816	1904
64-QAM 3rd frame	272	0	816	816	816
64-QAM 4th frame	272	0	816	816	1904

Table 2-7 residual carriers for RS packet synchronization for 8K mode

Code rate	1/2	2/3	3/4	6/5	7/8
QPSK 1st frame	0	0	544	0	1632
QPSK 2nd frame	0	0	544	0	1632
QPSK 3rd frame	0	0	544	0	1632
QPSK 4th frame	0	0	544	0	1632
16-QAM 1st frame	0	0	0	0	1632
16-QAM 2nd frame	0	0	0	0	1632
16-QAM 3rd frame	0	0	0	0	1632
16-QAM 4th frame	0	0	0	0	1632
64-QAM 1st frame	0	0	544	0	1632
64-QAM 2nd frame	0	0	544	0	1632
64-QAM 3rd frame	0	0	544	0	1632
64-QAM 4th frame	0	0	544	0	1632

We can use a counter to calculate the carrier index and then get completed packets and find the packet synchronization header. The additional complexity to complete this design is one

13-bit counter (>5304, the biggest number is 5304). In Table 2-5, Table 2-6 and Table 2-7, it shows the needed amount of subcarriers for RS packet synchronization.

2.4 Sampling Clock Offset Synchronization

This section introduces proposed SCO estimation algorithm and proposed SCO tracking loop architecture both. The proposed estimation algorithm and tracking loop architecture provide different improvements. The proposed estimation algorithm improves the estimation accuracy and the proposed tracking loop architecture reduces the time tracking. The blocks location is shown in Fig 2.23.

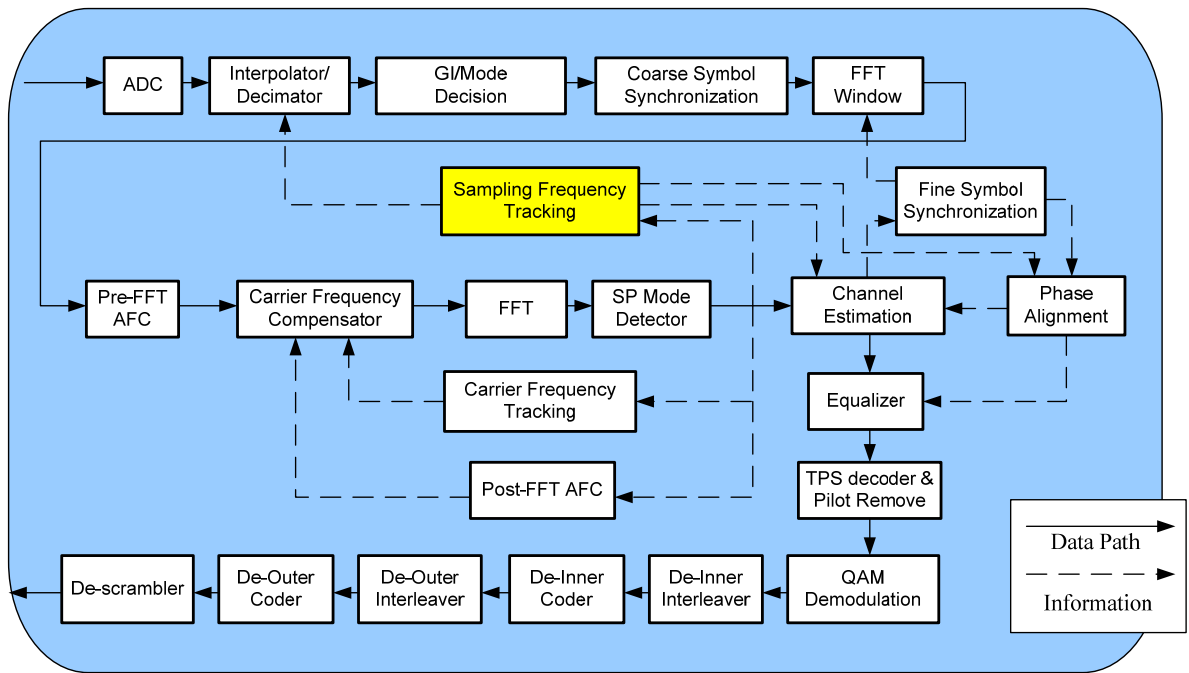


Fig 2.23 Location of fast synchronization in receiver platform

2.4.1 Conventional SCO Estimation

The first conventional SCO estimation algorithm is mentioned in [1] and [2], and it is a method of jointed SCO and CFO estimation (CFD/SFD) by calculating the phase difference between continual pilots of two consecutive symbols and then do average to the left part and

right part and calculate. The method has low mean error but unavoidable variance of SCO estimation. Then the linear least square is published [9]. Combine these two different methods, we obtain a jointed SCO and CFO LLS estimation method [10] implemented in [1]. The principle of the method is to calculate the phase difference between continual pilots of two consecutive symbols and then multiply a linear weight. Finally, calculate the slope of the line. The equations are listed as:

$$\hat{\zeta} = \frac{1}{2\pi(1+N_g/N)} \cdot \sum_{k=-M/2}^{M/2-1} B_{2,k} \cdot y_{l,k} \quad (2-23)$$

$$y_{l,k} = \text{Arg} [z_{l,k} \cdot z_{l-1,k}^*]$$

$$B = (A^T A)^{-1} A^T$$

$$A = \begin{bmatrix} 1 & k_1 \\ 1 & k_2 \\ \vdots & \vdots \\ 1 & k_M \end{bmatrix} \quad | \quad k_i \in CP$$

where $\hat{\zeta}$ is estimated SCO, N_g means guard interval length, N means $2/4/8k$, $z_{l,k}$ is carrier data, l is symbol index, k is continual pilot index, M is numerous of continual pilots in a symbol, $y_{l,k}$ is the phase difference between continual pilots of two consecutive symbols, and B is the linearization matrix. The architecture of jointed SCO/CFO LLS estimation is shown in Fig 2.24.

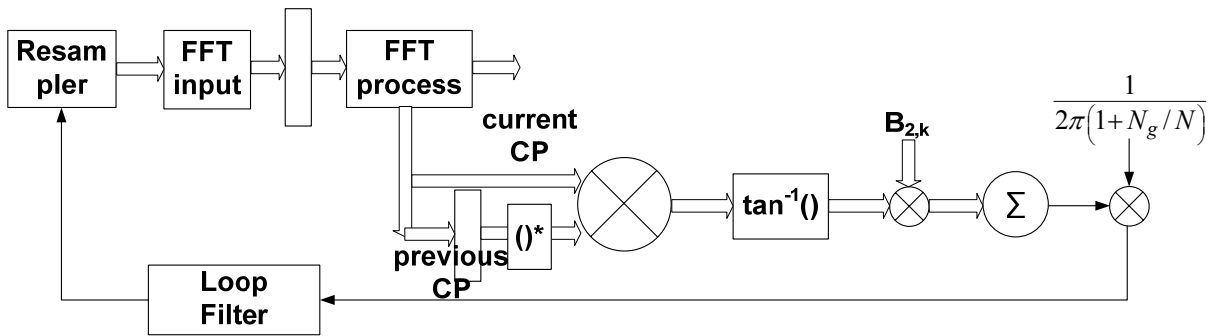


Fig 2.24 Architecture of SCO estimation [1]

And we will introduce a method that it has a better performance in chapter 3.

2.4.2 Proposed SCO Estimation

The proposed SCO estimation method has a key difference between the conventional designs: using the scatter pilots to replace the continual pilots. The equations become:

$$\hat{\zeta} = \frac{1}{2\pi(1 + N_g / N) \cdot 4} \cdot \sum_{k=-N/2}^{N/2-1} D_{2,x} \cdot y_{w,x} \quad (2-24)$$

$$y_{w,x} = \text{Arg} [z_{w,x} \cdot z_{w-1,x}^*]$$

$$D = (C^T C)^{-1} C^T$$

$$C = \begin{bmatrix} 1 & x_1 \\ 1 & x_2 \\ \vdots & \vdots \\ 1 & x_N \end{bmatrix} \mid x_i \in SP$$

Where z is carrier data, w is symbol index, x is scatter pilot index, N is numerous of scatter pilots in a symbol, y is the phase difference between scatter pilots of 4 symbol distance location, and D is the linearization matrix. The advantage is obvious, because the numerous of scatter pilots is 142/284/568 in 2/4/8k mode but the numerous of continual pilots is 45/89/177 in 2/4/8k mode. The architecture of proposed SCO estimation is shown in Fig 2.25.

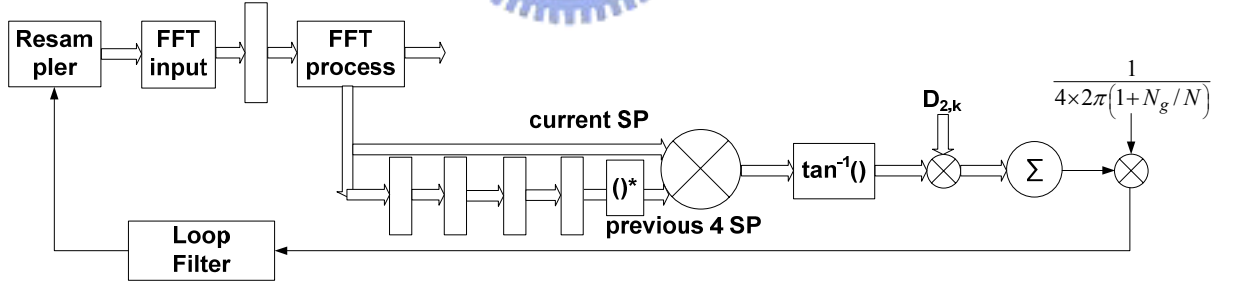


Fig 2.25 the architecture of proposed SCO estimation

Hence the proposed scatter pilot method is more accurate than continual pilot method. And the disadvantage of proposed method is the additional 4 buffers and throughput of estimation outcome up to 5 symbols. The buffers have already existed in 2-D channel estimation methodology [8] and the problem of throughput of estimation outcome will be solved in followed contents. We can also see the simulation results in chapter 3.

2.4.3 Conventional Tracking Loop

To compare these differences between different architecture, we choose the same algorithms: the linear least square method [3]. And the selection of algorithm will not affect the comparison of difference architecture. According to Fig 2.24, we can plot the timing diagram in Fig 2.26. In which d means the estimation outcome after loop filter and the number in timing diagrams means symbol index. And the same color means the same resample-modified symbol, in other words, the same color means the same effect of SCO.

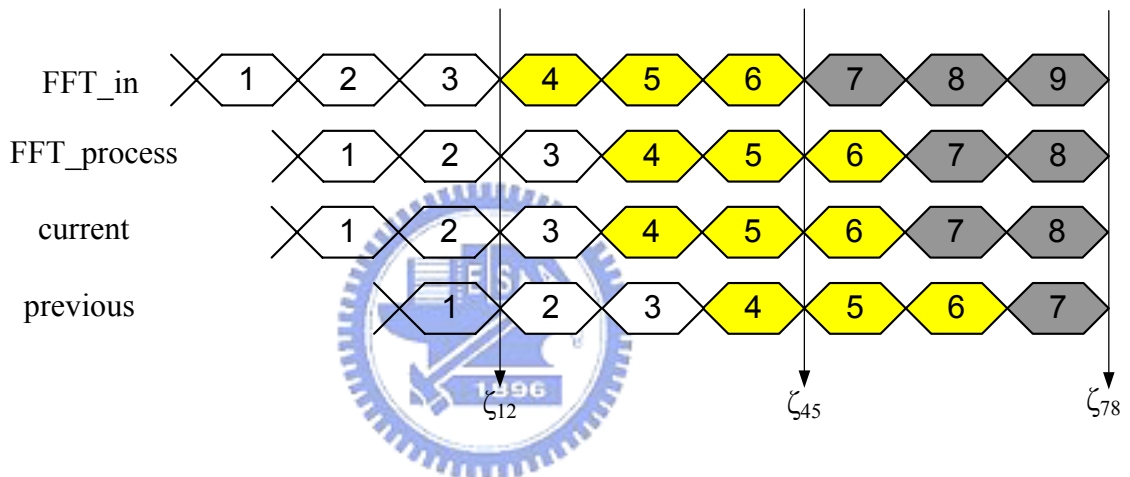


Fig 2.26 Timing diagram of conventional SCO tracking architecture

Because of the FFT process latency, after calculating the phase difference between continual pilots of consecutive symbols, the feedback outcomes are passed to time domain and then it waits two symbols time and calculates next SCO in third symbol. Thus, the throughput is three symbols.

2.4.4 Proposed Tracking Loop

The principle of proposed SCO tracking architecture is to add a feedback forward path in the SCO estimation loop. It is shown as Fig 2.27. The feedback forward architecture is to extract the previous two SCO estimation values after loop filter and then through some simple

transformation execution, the estimation values would change to become the phase information. Finally, do the phase compensation to the phase difference between continual pilots of two f-domain symbols that were not resample-modified at t-domain. As we compensate the phase forward, we would not wait for the FFT process latency, and we will improve the throughput of SCO tracking outcome. The timing diagram is shown in Fig. 2.28. Like the conventional design, the same color means the same resample-modified symbol, in other words, the same color means the same effect of SCO. We can obviously see the f-domain symbol is modified. The throughput becomes one symbol. The phase compensated equation is:

$$\varphi(k) = 2\pi(1 + N_g / N)k \times \zeta \quad (2-25)$$

where \hat{d} means the estimated outcome of SCO after loop filter, $\varphi(k)$ means the phase compensation, and k means continual pilot index.

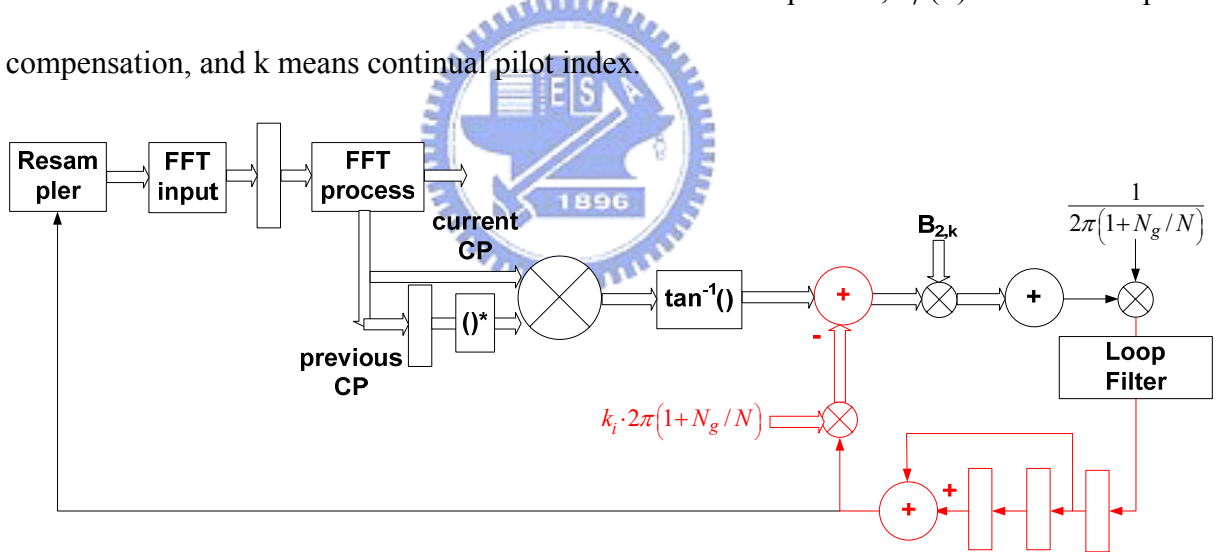


Fig 2.27 the architecture of proposed SCO tracking loop

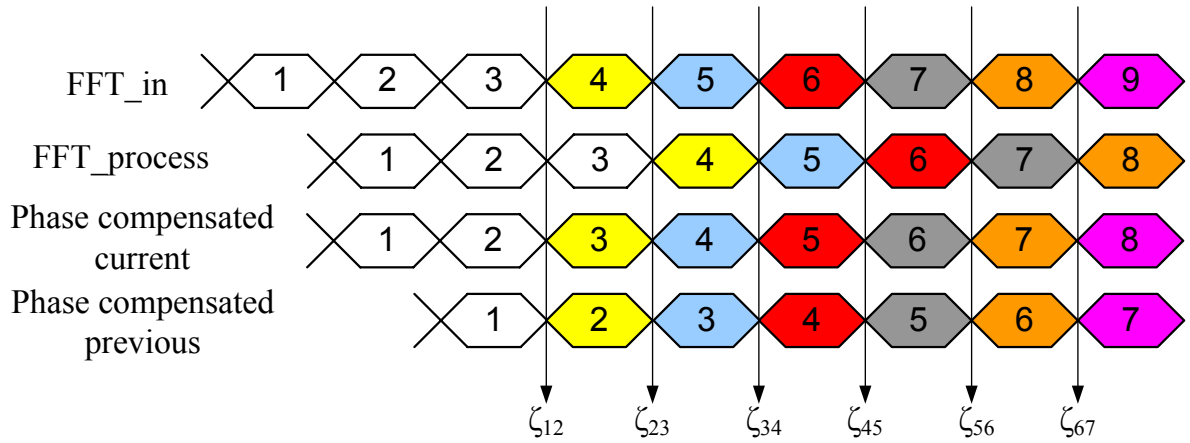


Fig 2.28 timing diagram of proposed SCO tracking loop architecture

Now, we choose proposed SCO estimation algorithm, scatter pilot method, to replace the conventional algorithm. The architecture is shown in Fig 2.29, and the timing diagram is shown in Fig 2.30. The phase compensation equation is:

$$\varphi(k) = 2\pi(1 + N_g / N) \cdot 4k \times \zeta \quad (2-30)$$

Where d means the estimated outcome of SCO after loop filter, $\varphi(k)$ means the phase compensation, and k means scatter pilot index. In section 2.4.1, we mentioned about the problem of the throughput of SP method. The throughput of the estimation outcome is high to six symbols, and five symbols for waiting for the scatter pilot location and one symbol for FFT process. In this section we will no longer see the problem because of the feedback forward path. The feedback forward path can add in any kind of algorithm and also can solve some problem like low throughput. Hence, this proposed architecture can combine with all other estimation algorithms.

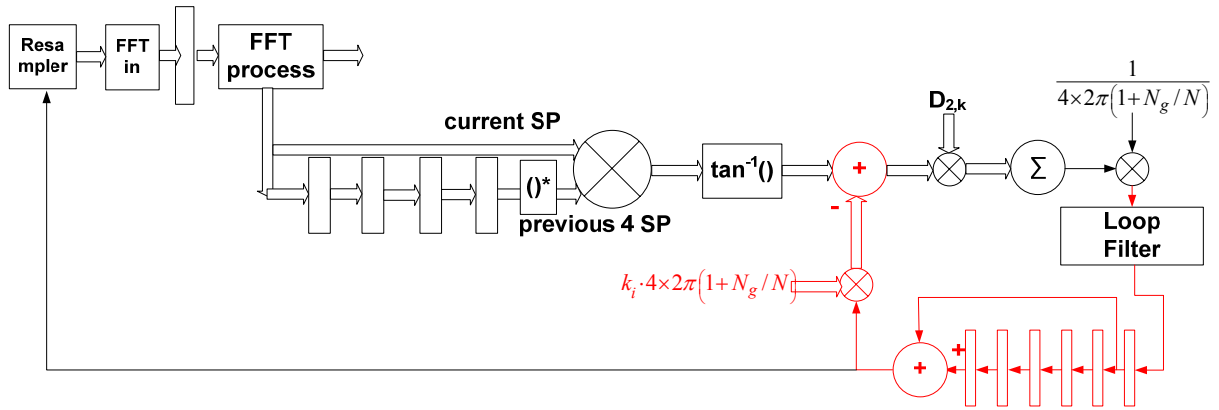


Fig 2.29 the architecture of proposed SCO tracking loop with SP method

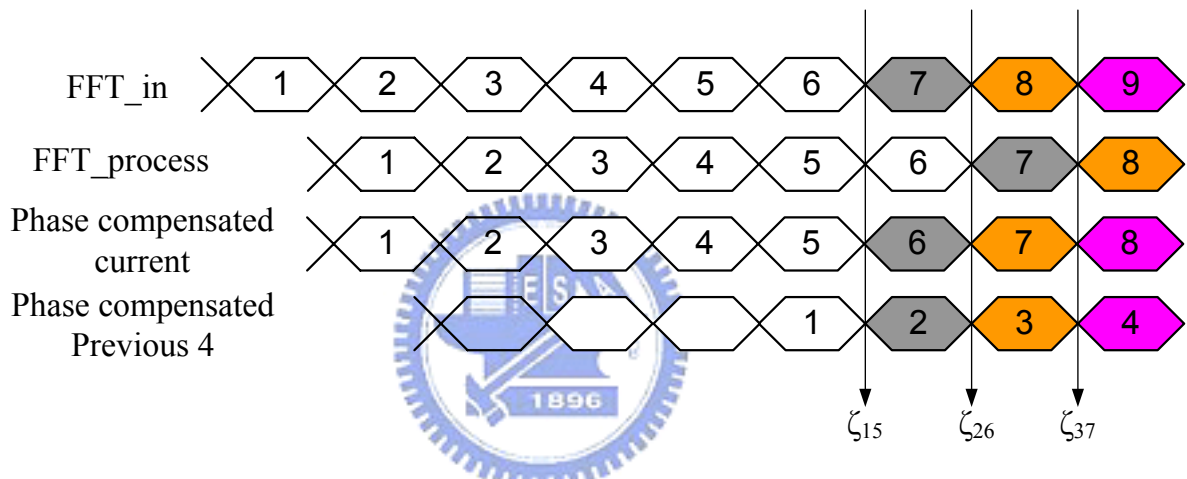


Fig 2.30 timing diagram of proposed SCO tracking loop architecture with SP method

In the comparison and results, first, we will show the estimation accuracy of proposed estimation algorithm and then we will show the improving throughput in proposed tracking loop architecture.

Chapter 3 .

Simulation and Performance Analysis

3.1 Simulation Platform

In order to verify the performance of proposed algorithm, a complete DVB-T baseband simulation platform is developed in Matlab. The block diagram of DVB-T simulation platform is depicted in Fig 3.1.

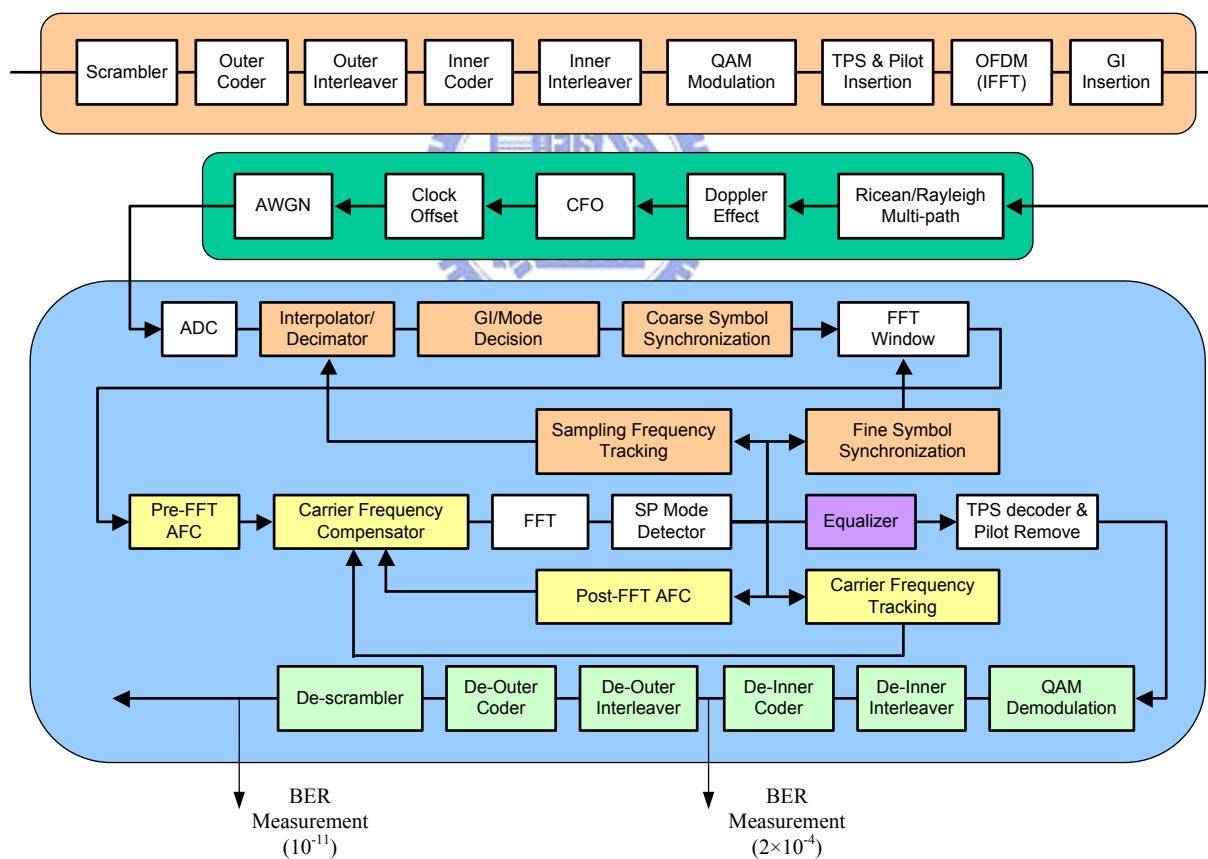


Fig 3.1 Block diagram of simulation platform

The platform consists of transmitter, channel and receiver. A typical transmitter receiving video data from MPEG2 encoder is fully established. Besides FEC blocks, constellation mapping, pilot insertion, IFFT modulation and GI insertion are built in order. The 2K and 8K with all other transmission modes are able to being selected as simulation parameters. In order to simulate discrete signal as far as continuously, upsampling and pulse shaping filter are adopted prior to entering channel. The upsampling rate is flexible and depends on the required simulation accuracy. The roll-off factor of pulse-shaping filter is not defined in ETSI DVB-T/H standard so that a normal value of $\alpha=0.15$ is used. In the channel model, various channel distortions are introduced for simulating real mobile wireless environment, which contains multipath fading, Doppler frequency spread, AWGN, CFO and SCO. In fact, there are some other distortions such as co-channel interference, adjacent-channel interference and common phase error due to defective front-end receiving. However, these distortions are relatively small compared to effective time-variant channel response caused by Doppler spread, CFO and SCO, so that we can neglect those channel effects.

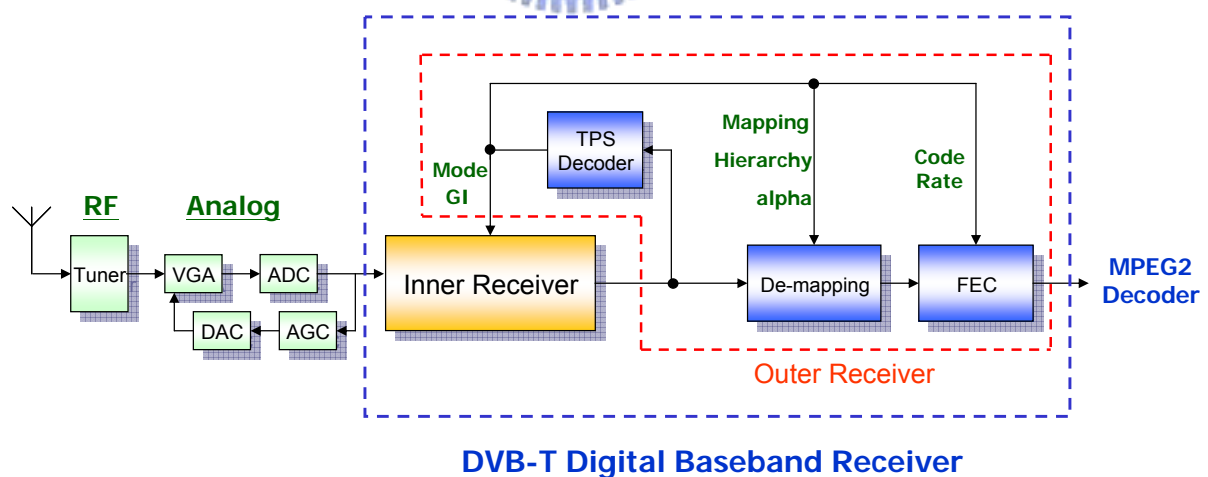


Fig 3.2 Overview of receiver design

In the receiver design, we focus on the baseband demodulation part between ADC and MPEG-2 decoder. The receiver can be divided into two portions, inner and outer receiver as

depicted in Fig 3.2. Inner receiver copes with pre-FFT synchronization, FFT, post-FFT frequency synchronization, channel estimation and pilot removal. Then TPS check, de-mapping, inner de-interleaver, Viterbi decoder, outer de-interleaver, RS decoder and de-scrambler are done in outer receiver. The transmission parameters computed by TPS decoder such as constellation mapping and code rate of Viterbi send to downstream blocks in outer receiver. Afterwards, the bitwise output of FEC blocks enters to source decoding block, MPEG-2 decoder. Note the TPS check should operate all the time to prevent transmission interruption. If TPS check error occurs, the inner receiver ought to reset and hence all blocks in acquisition mode restart. As for BER measurement, the quasi error-free condition is defined in ETSI standard [3] which means less than one uncorrected error event per hour, corresponding 10^{-11} after Reed-Solomon decoder and 2×10^{-4} after Viterbi decoder. Therefore, the BER should be measured both in the outputs of Viterbi and RS. In particular, the SER (symbol error rate) is usually applied as another performance measurement in several papers. As a result, we should exploit hard-decision demapping to measure SER in addition.

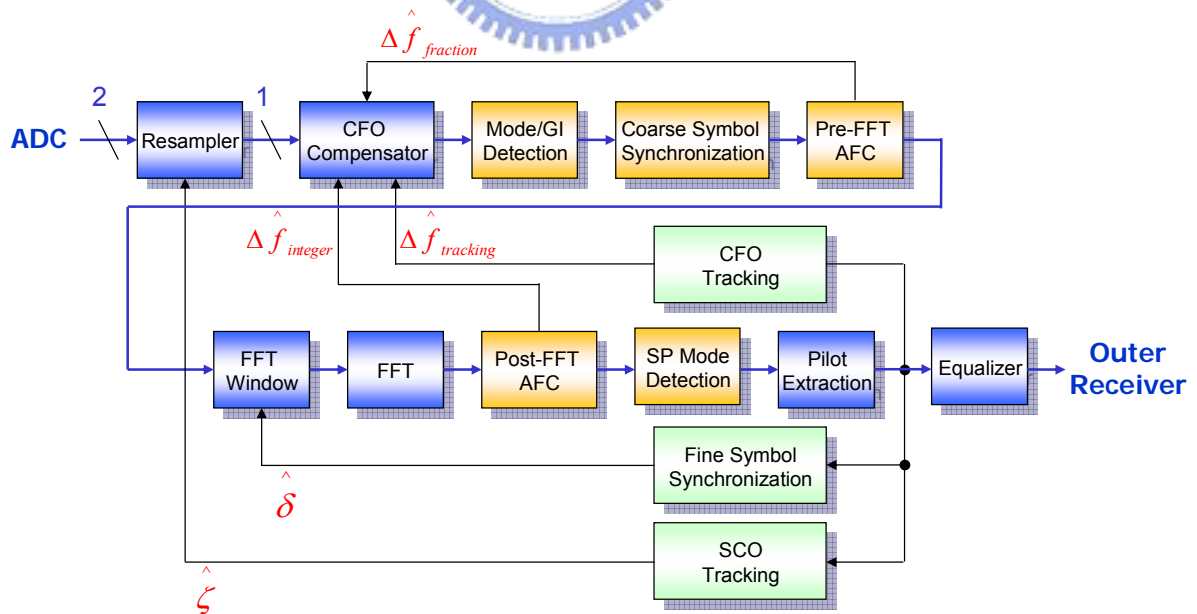


Fig 3.3 Structure of inner receiver

In Fig 3.3, it shows the detail structure of inner receiver. As mentioned in Chapter 2, synchronization task consists of symbol synchronization, frequency synchronization and sampling clock synchronization. Acquisition blocks operate in the initial synchronization period and turn off in tracking mode, and tracking blocks act all the while. Our frequency synchronization design consults reference [1]. Like coarse symbol synchronization, pre-FFT frequency acquisition is based on guard interval correlation. Disregarding ISI and sampling timing error, the tail received sample and its cyclic prefix show the same property except for a phase rotation between guard and tail segments being proportional to the fractional carrier frequency offset. Guard interval correlation samples thus become

$$x_n = r_n \times r_{n-N}^* \propto e^{j2\pi\Delta f} + noise \quad (3-1)$$

Given the coarse estimated symbol window \hat{n} , the ML frequency estimate [11] becomes

$$\Delta \hat{f} = \frac{1}{2\pi} \cdot \arg \left[\sum_{i=\hat{n}-N_g-1+x}^{\hat{n}} r(i) \cdot r^*(i-N) \right] \quad (3-2)$$

where x denote the forsaken samples distorted by ISI in multipath channel. Since the perfect coarse symbol window is impossible, we have to consider the ISI samples. In severe multipath fading channel as Rayleigh channel in DVB-T standard, long time delay profile raises the ISI effect which is illustrated in Fig 3.4. As a result, we must give up several beginning samples to reduce the ISI distortion. However, discarding too many samples will also degrade the averaging performance. The optimal value of x can be decided by simulation result.

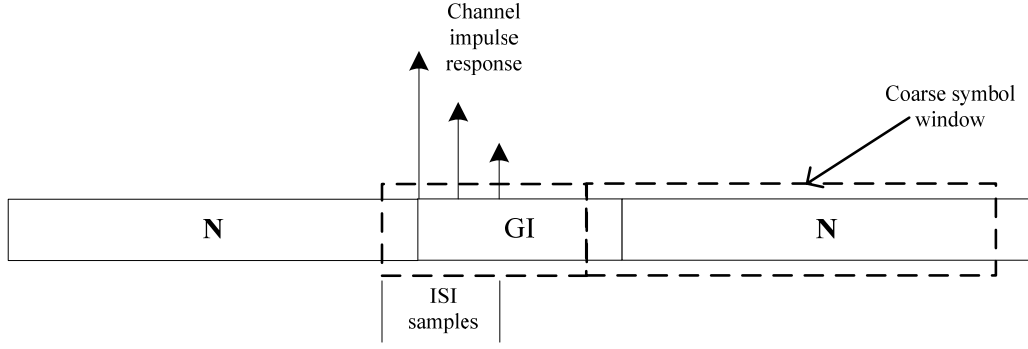


Fig 3.4 ISI effect on CFO acquisition

Post-FFT integer carrier frequency acquisition refers to [1]. Because of pre-FFT acquisition, the residual fractional offset Δf is small so that the *ICI* noise in this stage is also small. We assume the integer carrier frequency offset n_l (subcarrier spacing), which causes spectrum shift in frequency domain. The integer CFO must now be detected using continual pilots which are all boosted in power. Correlating FFT output samples of two consecutive OFDM symbols $l-1$, l and a particular set $k \in C+m$ are accumulated. The maximum absolute value of accumulation result then yields the estimated integer carrier frequency offset

$$\hat{n}_l = \arg \max_{m \in I} \left| \sum_{k \in C+m} z_{l,k} \cdot z_{l-1,k}^* \right| \quad (3-3)$$

where C denotes the positions of continual pilots and I represents the search range which is typical given by $[-n_{l,\max}, n_{l,\max}]$. Considering small offset Δf and ζ , the probability of false detection ($\hat{n}_l \neq n_l$) is very small. The channel estimation unit must estimate both the channel response and any residual phase errors caused by imperfect synchronization. In the channel estimation design of DVB-T system, it is common to use two-dimensional interpolation method such as [1] in order to estimate the mobile time-variant channel. The channel response is generated by interpolation in time and frequency dimension respectively. In time direction, channel gain estimates at scattered pilot are first interpolated so that channel gain estimates are available at every third subcarrier in every OFDM symbol as depicted in Fig 3.5. Subsequently, channel response estimates at all other subcarriers are obtained by interpolating

the resulting time-interpolated channel gain in frequency direction. In time-dimension interpolation, four complete OFDM symbols have to be stored for each noncausal tap. Considering the memory requirement, interpolation in time dimension exploits linear interpolation so that only the storage of three additional OFDM symbols is needed. As for frequency-dimension interpolation, it is general to adopt Wiener filter approach. In general, the high-complexity frequency direction interpolation deserves since the system performance is usually dominated in channel estimation unit.

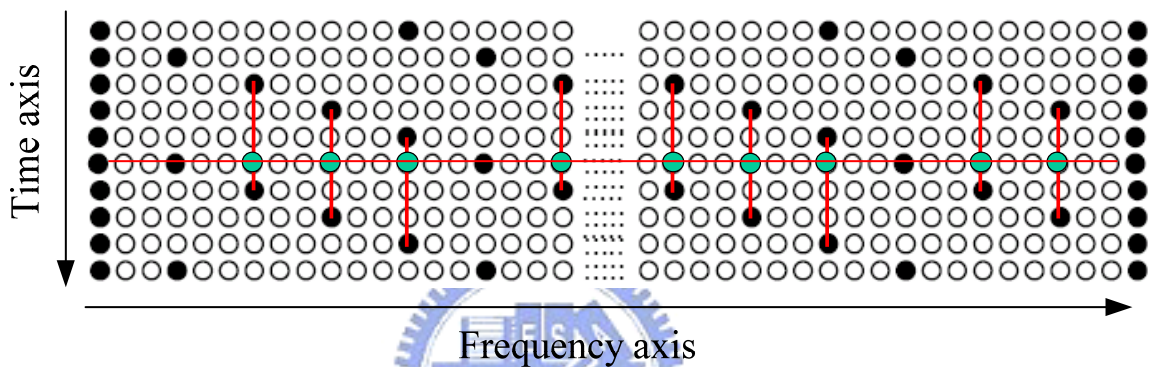


Fig 3.5 2-D interpolation in channel estimation unit design

3.2 Channel Model

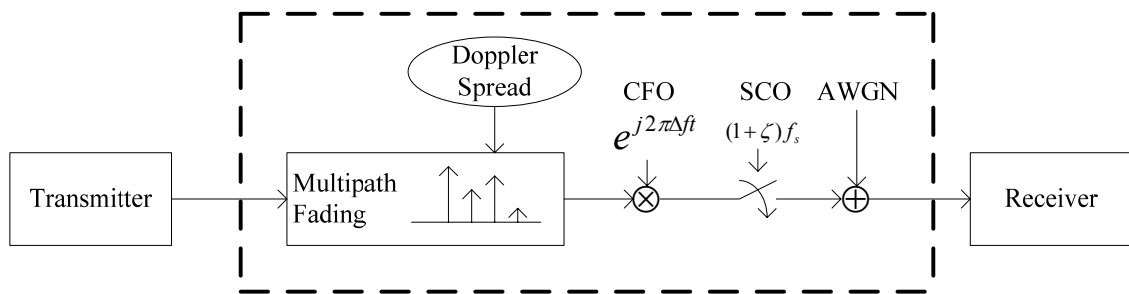


Fig 3.6 Channel model of DVB-T/H system

Fig 3.6 shows the typical baseband equivalent channel model of DVB-T system. The transmitted data passes through multipath fading, Doppler spread, AWGN, RF lowpass filter,

carrier frequency offset and sampling clock offset. The effects of inter-channel interference (co- and adjacent-channel interference) and common phase error are neglected in our simulation. In fact, the overall system performance represented as “BER versus SNR” shows nearly no difference. The detail illustration of each channel distortions will be shown in the following sections.

3.2.1 Multipath Fading Channel Model

In the wireless transmission, transmitted data is received through several paths with different time delay and power decay. This is so-called multipath fading. Two types of channel are specified by ETSI DVB-T standard. Fixed reception condition is modeled by Ricean channel (Ricean factor = 10db) while portable reception is modeled by Rayleigh channel. The full 20-tap Ricean and Rayleigh channel was used with floating point tap magnitude and phase values and with tap delay accuracies rounded to within 1/2 of duration (7/64 $\mu\text{s}/2$) for practical discrete simulation.

The major difference between Rayleigh and Ricean channel is the main path (The line of sight ray). In a Rayleigh fading channel, the received signals consist of several reflected signals with similar powers because there is no main path in Rayleigh channel. The rms delay of Rayleigh channel is about 12 sample time. This characteristic will cause serious synchronization error. A time delay and subcarrier distortion of frequency domain both occur in a Rayleigh fading channel. The frequency response and impulse response for each subcarrier are shown in Fig 3.7. The frequency response is not flat over the entire frequency region and some parts are severely distorted. The Ricean channel model defines Ricean factor K (the ration of the power of the direct path to the reflected paths) is given as

$$K = \frac{\rho_0^2}{\sum_{i=1}^N \rho_i^2} \quad (3-4)$$

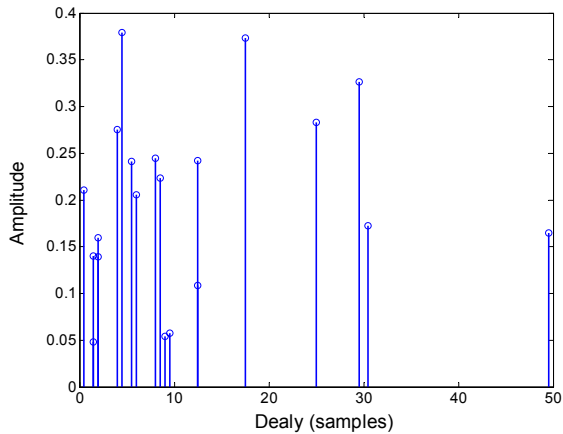
where ρ_i is the attenuation of the i 'th path. The channel models can be generated from the

following equation where $x(t)$ and $y(t)$ are input and output signals respectively

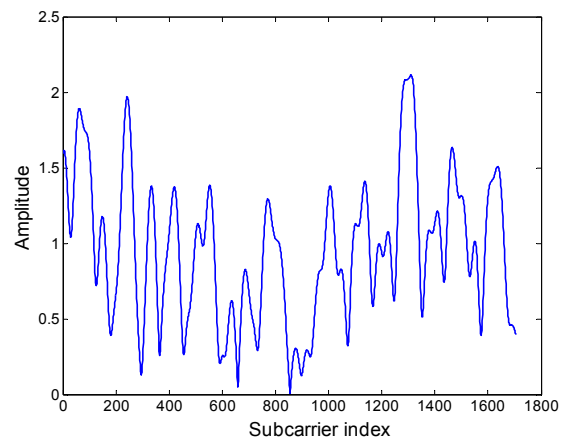
Rayleigh:
$$y(t) = k \sum_{i=1}^N \rho_i e^{-j\theta_i} x(t - \tau_i) \quad k = \frac{1}{\sqrt{\sum_{i=1}^N \rho_i^2}} \quad (3-5)$$

Ricean;
$$y(t) = \frac{\rho_0 x(t) + \sum_{i=1}^N \rho_i e^{-j\theta_i} x(t - \tau_i)}{\sqrt{\sum_{i=1}^N \rho_i^2}} \quad (3-6)$$

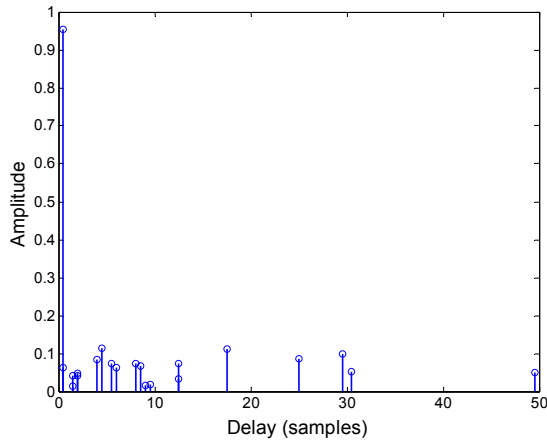
where N is the number of echoes equals to 20, θ_i is the phase shift from scattering of the i 'th path and τ_i is the relative delay of the i -th path. The detail value of above parameters is listed in table B.1 of [1]. The rms delay of Ricean channel ($k=10\text{db}$) and Rayleigh channel is respectively $0.4491 \mu\text{s}$ (about 4 samples) and $1.4426 \mu\text{s}$ (about 13 samples). The channel impulse response and channel frequency response of Ricean channel ($K=10\text{db}$) and Rayleigh channel are shown in Fig 3.7 respectively.



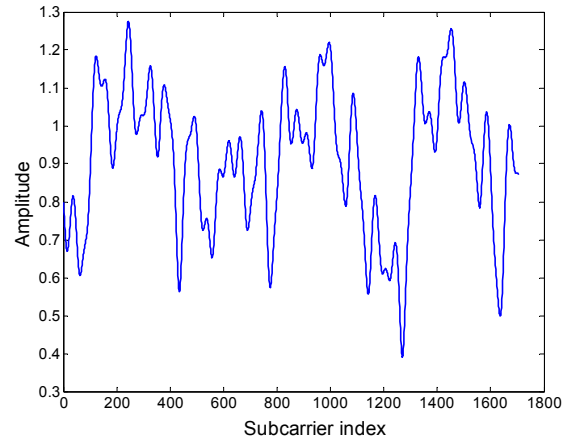
(a) Impulse response of Rayleigh channel



(b) Frequency response of Rayleigh channel



(c) Impulse response of Ricean channel



(d) Frequency response of Ricean channel

Fig 3.7 Channel response of Rayleigh and Ricean ($K=10\text{dB}$) channel

In addition to Rayleigh and Ricean channel, a statistical channel model WSSUS (Wide Sense Stationary Uncorrelated Scattering) [12] is adopted in our simulation. The power delay profile is measured in two different areas in Germany (Berlin and Darmstadt) with a system bandwidth of 8 MHz and at carrier frequencies of 714 and 920 MHz. We can regard this channel model as a real case of transmission environment. WSSUS channel model provides several type of channel model which contains *Non Line Of Sight (NLOS)* –models and *Type K (TypK)*-models. NLOS models have a very small Rice factor ($K \leq -20 \text{ db}$) and TypK models have a Rice factor around the 50% of its model category. The detail descriptions of each channel model have been discussed in [12].

3.2.2 Doppler Spread Model

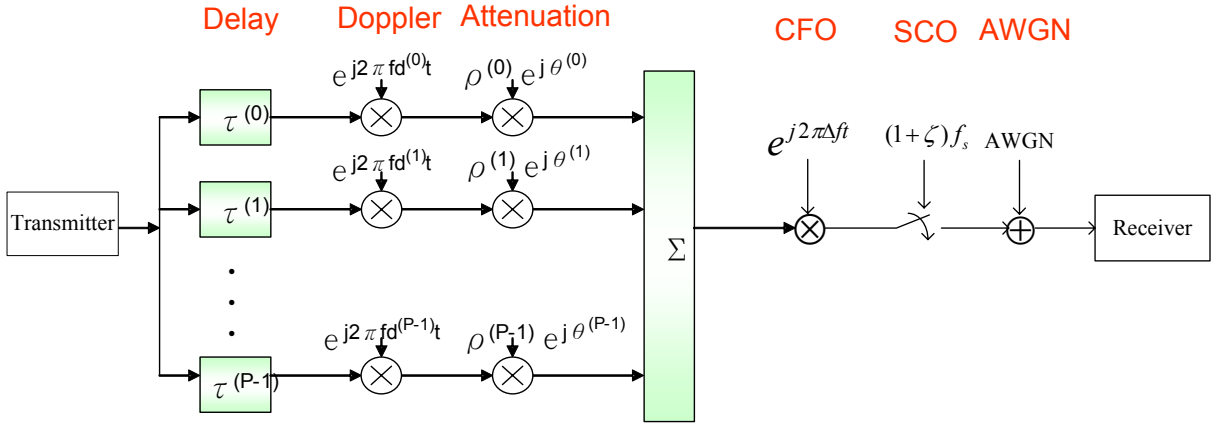


Fig 3.8 Doppler frequency spread model

It's well known that Doppler spread causes the loss of orthogonality in OFDM system. In DVB-T system, a mobile radio channel including Doppler spread must be considered. A simplified Doppler frequency spread model [13] is depicted in Fig 3.8. First, we initially assume a channel with a known and fixed number of paths P such as Ricean, Rayleigh or WSSUS with a Doppler frequency $f_d^{(k)}$, attenuation $\rho^{(k)} e^{j\theta^{(k)}}$, and time delay $\tau^{(k)}$. Every path has different amplitude, Doppler frequency, and time delay. Since each path has its own Doppler frequency, how to decide the statistical distribution for f_d is important. There are two commonly used Doppler frequency PDFs, uniform and classical. Obviously uniform case uses uniform distribution to model Doppler spread, and classical case uses Jakes' Doppler spectrum.

In some papers, a worst case of two-side Doppler spectrum is exploited, which shifts in frequency each even-indexed channel tap by $+f_d$, and each odd-indexed channel tap by $-f_d$. When we compare the performance with other papers, we should pay attention to the definition of Doppler Spectrum. The PDF of Jakes' Doppler spectrum [18] is derived as below.

$$p(f_d) = \frac{1}{\pi \cdot f_{d\max} \cdot \sqrt{1 - \left(\frac{f_d}{f_{d\max}}\right)^2}} \quad |f_d| < f_{d\max} \quad (3-7)$$

After transformation of random variable, we can obtain each f_d by the following equation.

$$f_d = \cos(2\pi \cdot rand(1)) \cdot f_{d\max} \quad (3-8)$$

The type of Doppler spread (uniform or Jakes') affects the performance very much. Because each path gets different f_d in each simulation case, the amount of the lost orthogonality will be not the same. Therefore, we should fix each f_d in each simulation and comparison.

3.2.3 Carrier Frequency Offset and Sampling Clock Offset model

The detailed signal model of CFO is already described in chapter 2 and will not be discussed repeatedly in this section. The model of SCO is built based on the concept of sinc interpolation. The input digital signals can be exploited to interpolate the intermediate value between two successive samples by using the shifted value of sic function. Assume that the sampling period is T_s and SCO is ζ . Then the sampling phase can be represented as $nT_s + n\zeta$. The resulting signal after ADC can be expressed as

$$\begin{aligned} r_{ADC}(nT_s) &= r(nT_s) * \text{sinc}\left(\frac{nT_s + n\zeta}{T_s}\right) \\ &= \sum_{k=-N}^N r(nT_s - kT_s) \cdot \text{sinc}\left(k + \frac{n\zeta}{T_s}\right) \end{aligned} \quad (3-9)$$

where $2N+1$ is the taps of the FIR interpolator, k is the sampling point index, $r(\cdot)$ is the received signal with perfect sampling, $r_{ADC}(\cdot)$ is the received signal while SCO is ζ , respectively.

3.3 Performance Analysis

3.3.1 Carrier Phase Alignment

In the analysis of carrier phase alignment, we divide into three parts: BER after Viterbi versus SNR in different frequencies of fine symbol synchronization, BER after Viterbi versus the tolerance of different SCO in the same channel model and BER after Viterbi versus different Doppler frequency with other channel parameter fixed.

In the first analysis, BER after Viterbi versus SNR in different frequencies of fine symbol synchronization is discussed. First, we introduce the simulation environment. The transmission mode is 2k mode, GI 1/4, 64-QAM mapping, code rate 2/3, sampling rate 2, alpha 1 and hierarchical false. The channel model is AWGN, Rayleigh multi-path, Doppler 70Hz and SCO 20ppm. Transmission mode and channel model are reference from [3], the ETSI-DVB-T/H standard. In the receiver, we choose channel equalizer in 2-D linear interpolation [8], fine symbol synchronization in IFFT based method [2], SCO tracking in LLS algorithm [9] with loop filter [14] and resampler [15]. In Fig 3.9 and Fig 3.10, it shows the BER after Viterbi versus SNR between with and without proposed architecture. It shows one fine tune in every 8 symbols and 64 symbols in Fig 3.9 and Fig 3.10, respectively.

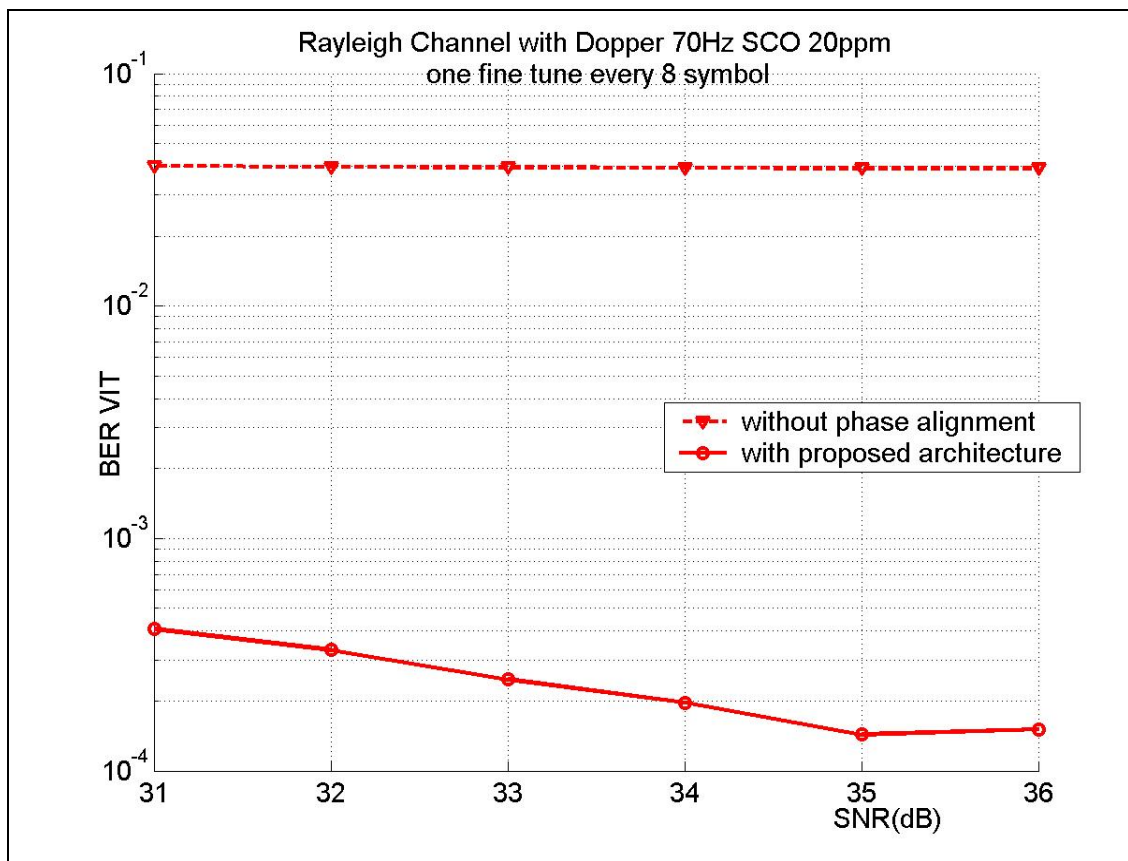


Fig 3.9 BER vs SNR after Viterbi decoder with one fine tune every 8 symbol

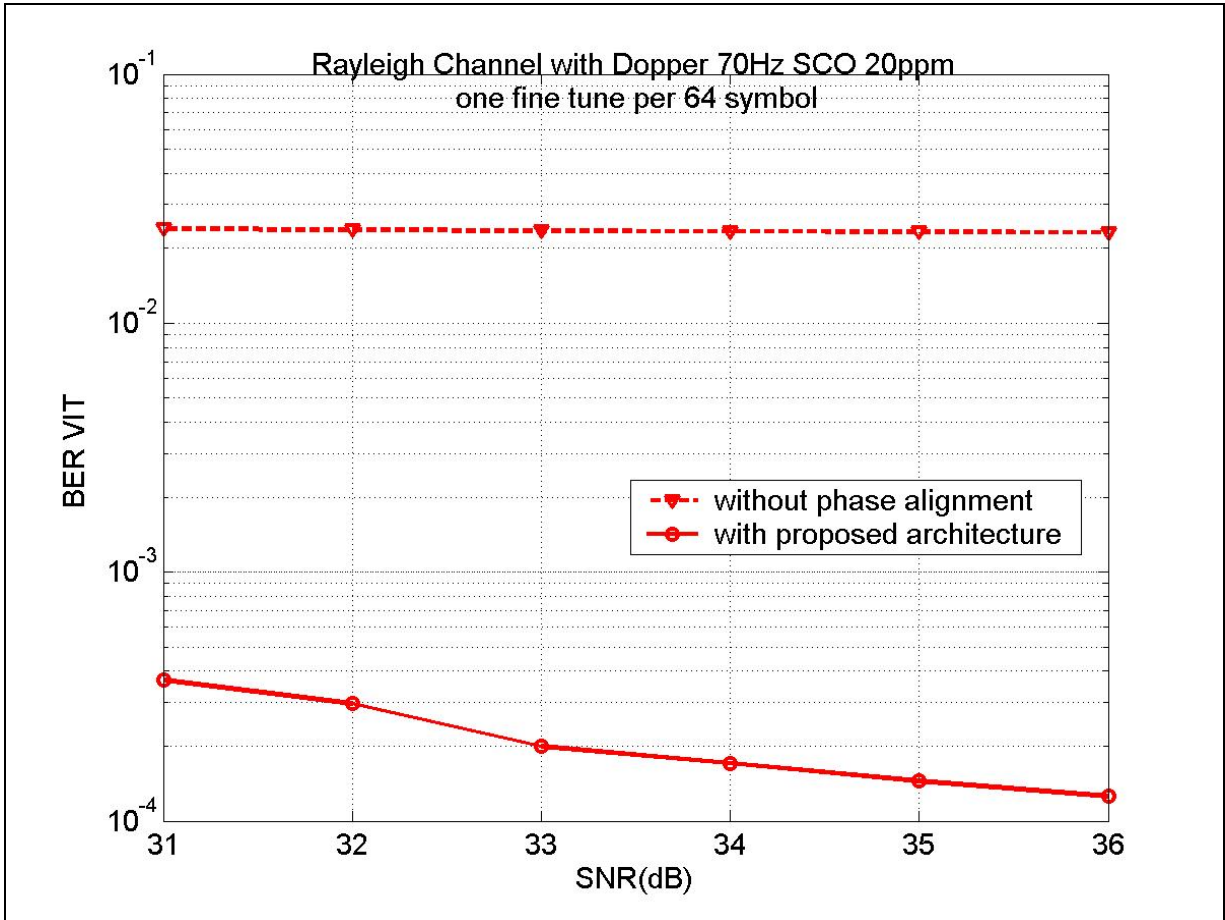


Fig 3.10 BER vs SNR after Viterbi decoder with one fine tune every 64 symbol

In Fig 3.9 and Fig 3.10, we can observe that with proposed design, the performance is much better than without proposed design. And no matter how many symbol cycles with the fine symbol synchronization. In Fig.11, BER after Viterbi versus the tolerance of different SCO in the same channel model is shown. The channel model is 2k mode, GI 1/4, 64-QAM mapping, code rate 2/3, sampling rate 2, alpha 1 and hierarchical false. The channel model is AWGN, Rayleigh multi-path, Doppler 70Hz and SNR 34dB.

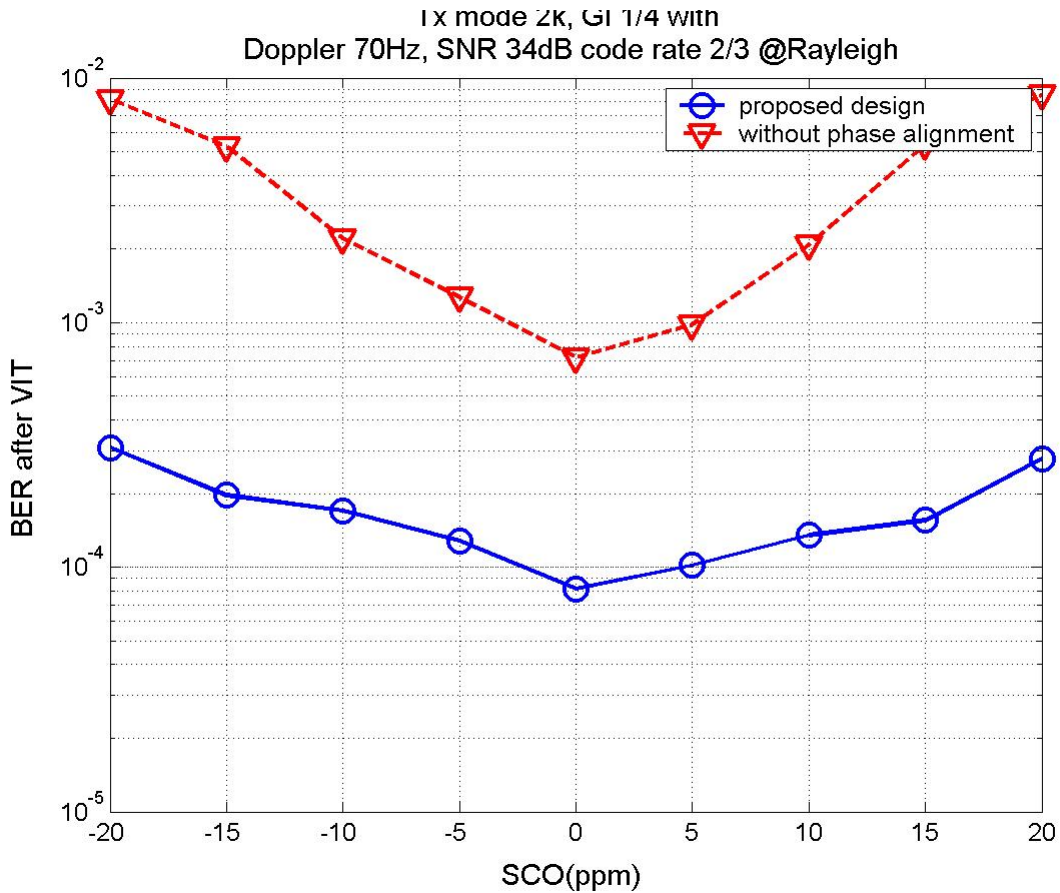


Fig 3.11 Tolerance range of SCO @ Rayleigh, SNR=34dB, and Doppler 70Hz

In Fig 3.11 it shows the tolerance of SCO. The required performance, Quasi Error Free (QEF) criterion, is $BER = 2 \times 10^{-4}$ after Viterbi decoder. And we can observe only our proposed design can reach QEF in worst channel.

BER after Viterbi versus different Doppler frequency with other channel parameter fixed is shown in Fig 3.12. The transmission is 2k mode, GI 1/4, 64-QAM mapping, code rate 2/3, sampling rate 2, alpha 1 and hierarchical false. The channel model is AWGN, Rayleigh multi-path, SNR 34dB and SCO 20ppm. Transmission mode and channel model are reference from [3], the ETSI-DVB-T/H standard. In the receiver, we choose channel equalizer in 2-D linear interpolation [8], fine symbol synchronization in IFFT based method [2], SCO tracking in LLS algorithm [9] with loop filter [14] and resampler [15].

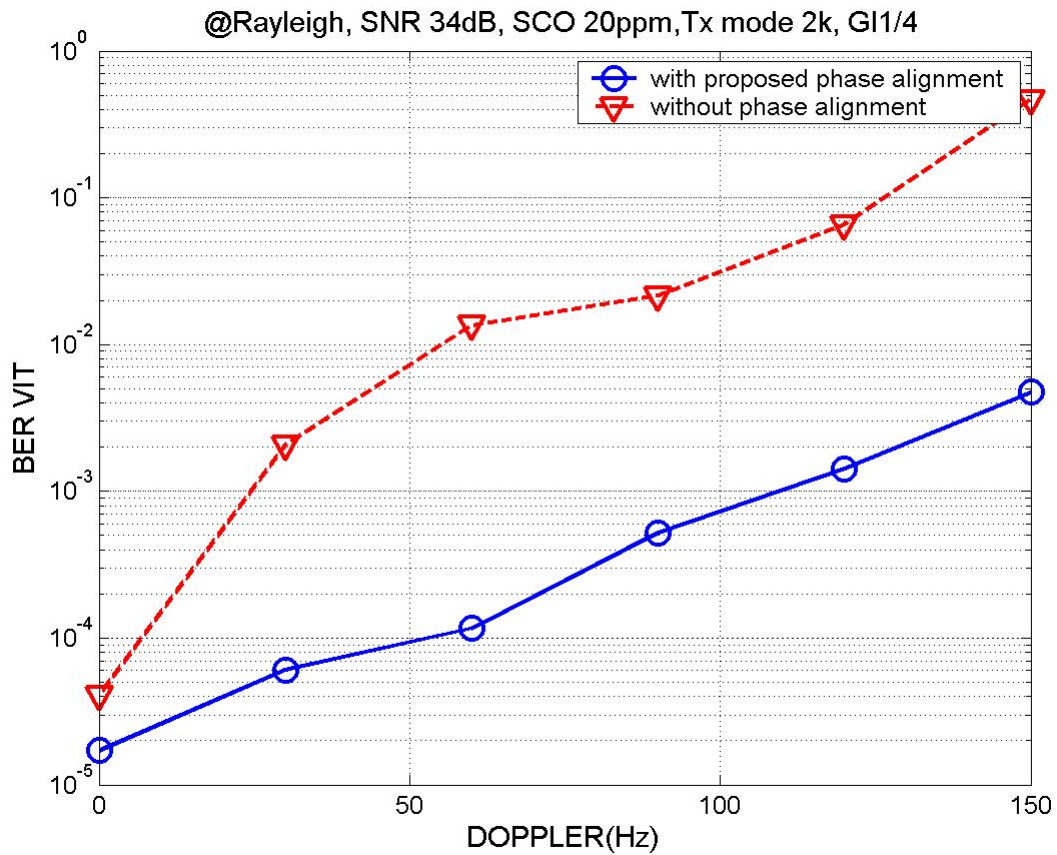


Fig 3.12 BER after Viterbi vs Doppler frequency



3.3.2 Fast Synchronization

The proposed method would not improve the accuracy of synchronization but the synchronization time could definitely be reduced. TPS decoder costs from 135 to 85 symbols time for synchronization. RS packet synchronization time is from 272/136/68 symbols to 5/3/2 symbols in 2k/4k/8k mode. One solution of the synchronization time is (acquisition time + TPS decoded time + RS packet synchronization time). The total results of this proposed system design reduce the synchronization time from 417/281/213 symbols to 100/98/97 symbols. Table 3-1, Table 3-2, Table 3-3 and Table 3-4 shows the synchronization time (ms) in 8MHz, 7MHz, 6MHz and 5MHz channel respectively.

Table 3-1 Synchronization time (ms) in 8 MHz channel

	2k mode				4k mode				8k mode			
GI	1/4	1/8	1/16	1/32	1/4	1/8	1/16	1/32	1/4	1/8	1/16	1/32
Conventional	116.8	105.1	99.2	96.3	157.4	141.6	133.8	129.8	238.6	214.7	202.8	196.8
Proposed	28	25.2	23.8	23.1	54.9	49.4	46.7	45.3	108.8	99.8	92.3	89.6

Table 3-2 Synchronization time (ms) in 7 MHz channel

	2k mode				4k mode				8k mode			
GI	1/4	1/8	1/16	1/32	1/4	1/8	1/16	1/32	1/4	1/8	1/16	1/32
Conventional	133.4	120.1	113.4	110.1	179.8	161.9	152.9	148.4	272.6	245.4	231.7	224.9
Proposed	32	28.8	27.2	26.4	62.7	56.5	53.3	51.7	124.2	111.7	105.5	102.4

Table 3-3 Synchronization time (ms) in 6 MHz channel

	2k mode				4k mode				8k mode			
GI	1/4	1/8	1/16	1/32	1/4	1/8	1/16	1/32	1/4	1/8	1/16	1/32
Conventional	155.7	140.1	132.3	128.4	209.8	188.8	178.3	173.1	318.1	286.3	270.3	262.4
Proposed	37.3	33.6	31.7	30.8	73.2	65.7	62.2	60.4	144.8	130.4	123.1	119.5

Table 3-4 Synchronization time (ms) in 5 MHz channel

	2k mode				4k mode				8k mode			
GI	1/4	1/8	1/16	1/32	1/4	1/8	1/16	1/32	1/4	1/8	1/16	1/32
Conventional	186.8	168.1	158.8	154.1	251.8	226.6	214	207.7	381.7	343.5	324.4	314.9
Proposed	44.8	40.3	38.1	36.9	87.8	79	74.7	72.4	173.8	156.4	147.8	143.4

We can see the different synchronization times in different transmission modes, and then we can choose one couple of them to calculate the saving of power consumption from (1-6). We can obtain different power savings in different modes. For instance, in 5MHz channel, 4k mode and GI 1/4, the conventional method costs 251.8ms and proposed method costs 87.8ms. According to chapter 1, let Burst Duration be 200ms, Delta-t Jitter be 10ms Constant Bandwidth be 512kbps and Burst Size be 1024kbits. Thus, we can obtain the conventional saving of power consumption is 78%, and the proposed method obtains 86% power saving. In this example, the saving power is up to 8%. The proposed method of fast synchronization in DVB- H system saves 65% to 95% power consumption than in DVB-T system. And the proposed design averagely reduces 10% power consumption than conventional design.

3.3.3 Sampling Clock Synchronization

In this section, we will show two kinds of simulation result. One is the SCO estimation algorithm, and the other is SCO tracking loop architecture. These two topics show different results respectively. SCO estimation shows the estimation accuracy and the SCO tracking loop architecture shows the tracking throughput.

(1) SCO estimation

We show the comparisons between different estimation algorithms. As mentioned in chapter 2, reference [2] proposed a “CP-LLS algorithm” to use the linear least square method between continual pilots of consecutive symbols. Reference [16] mentioned “CP-CFD/SFD algorithm” to joint CFO and SCO tracking, and “CP” means continual pilots too. Table 3-5 lists the estimation accuracy of the above two algorithm and proposed “SP-LLS algorithm” mentioned in chapter 2. And the channel model is listed in table 3-6.

Table 3-5 the estimation accuracy of the SCO in ppm

	Gaussian		Ricean + Doppler spread 70 Hz		Rayleigh + Doppler spread 70 Hz	
	Mean Error	Standard deviation	Mean Error	Standard deviation	Mean Error	Standard deviation
CP-CFD/SFD [5]	0.0694	5.9905	1.3678	7.2908	-2.0967	8.2107
CP-LLS [3]	-0.1567	5.4948	-0.0450	6.3277	-4.0990	8.6082
Proposed SP-LLS	0.0475	1.0645	0.1032	1.3617	-3.5122	4.8212

Table 3-6 channel model of the simulation in SCO estimation algorithm

Mode	2k
GI	1/4
Mapping	64QAM
Initial SCO	20ppm
AWGN	15dB

Thus, we can obviously see the proposed estimation algorithm with best standard deviation and the mean error of proposed SP-LLS is about the same with others.

(2) SCO tracking loop

The other simulation result is to show the throughput improvement of the proposed tracking loop architecture. We compare four different tracking loop architecture and estimation algorithm collections. First, “CP-LLS with conventional tracking loop architecture” is the conventional tracking loop architecture that the throughput is 3 symbols time. Second, “CP-LLS with proposed feedback forward loop architecture” is the continual

pilot based estimation method with proposed feedback forward tracking loop architecture. And then, third and fourth, “SP-LLS with conventional tracking loop architecture” and “SP-LLS with proposed feedback forward tracking loop architecture”. The simulation environment is the same in 2k mode, GI 1/4, and adding 20ppm SCO initial value in the Ricean channel with AWGN SNR 15dB. The loop filter is the function as:

$$K_p + K_I \frac{Z^{-1}}{1 - Z^{-1}} \quad (3-10)$$

where $K_I \approx K_p$ and we take $K_p = 1/8$ in those different conditions. And we also listed the channel model in Table 3-7.

Table 3-7 Channel Model of the simulation in SCO tracking loop architecture

Mode	2k
GI	1/4
Mapping	64QAM
Initial SCO	20ppm
AWGN	15dB
Kp	1/8
Multipath	Ricean

We can see the residual SCO (ppm) in Fig 3.13, Fig 3.14 and Fig 3.15. Fig 3.13 shows the comparison between “CP-LLS with feedback forward” and “CP-LLS”. Fig 3.14 shows the comparison between “SP-LLS with feedback forward” and “SP-LLS”. Fig 3.15 shows the comparison between “CP-LLS with feedback forward” and “SP-LLS with feedback forward”.

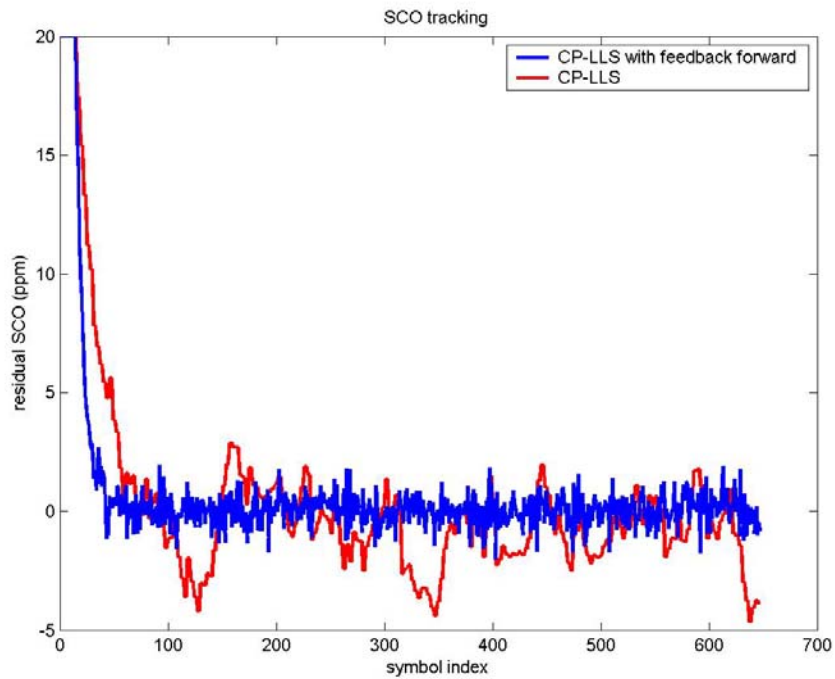


Fig 3.13 performance of the residual SCO convergence in CP-LLS algorithm between with and without feedback forward architecture

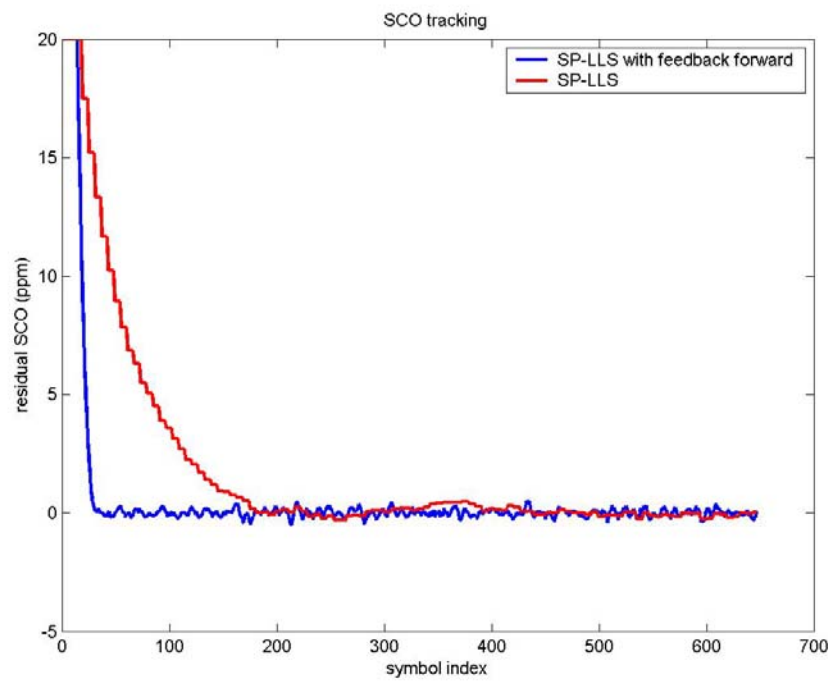


Fig 3.14 performance of the residual SCO convergence in SP-LLS algorithm between with and without feedback forward architecture

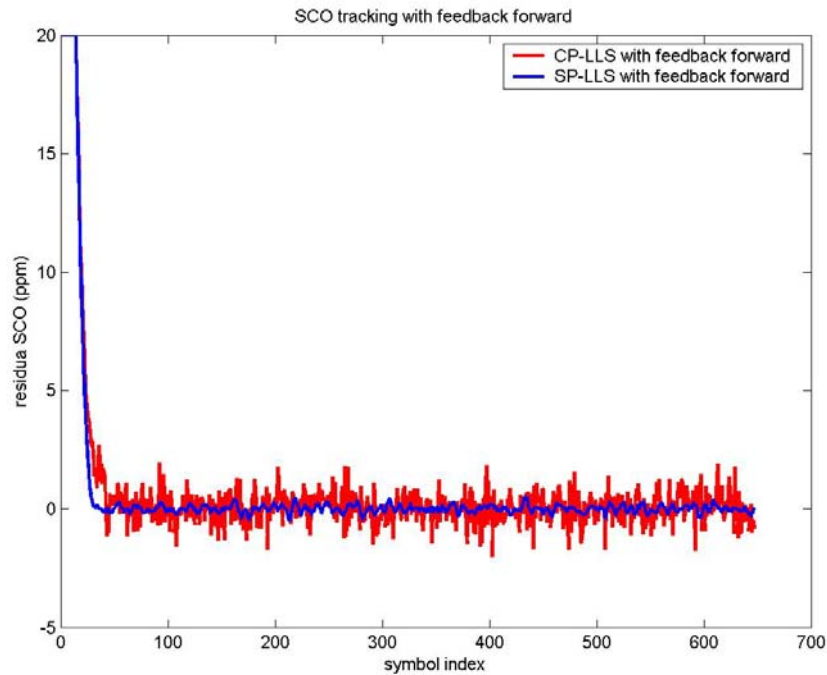


Fig 3.15 performance of the residual SCO convergence between CP-LLS and SP-LLS algorithm with feedback forward architecture

The numerous of scatter pilots is more than continual pilots, hence the estimation accuracy of SP method is better than CP method and the proposed feedback forward architecture has higher throughput to let the residual SCO nearby 0 ppm faster, it means to be convergent earlier and also means synchronization time to be reduced. The feedback forward tracking loop architecture has an additional advantage of estimation, that it is a phase compensation method and will also let the phase error compensating to the mean phase regression more closely. We calculate the standard deviation of “SP-LLS feedback forward”, “SP-LLS”, “CP-LLS feedback forward” and “CP-LLS” from 200th to 648th symbol, it means the steady state condition, and they are 0.16468, 0.18906, 0.65816 and 1.37996. We can see the “SP-LLS feedback forward” has the least standard deviation and performs best in the four conditions in steady state. Also we can see the convergent symbol of feedback forward tracking loop architecture is earlier than conventional tracking loop architecture at least 125

symbols in SP-LLS method and 50 symbols in CP-LLS method.

3.3.4 Overall System Performance

The overall system performance will be shown in this section. For separating fixed reception from portable reception, we divide the overall system performance into two parts: static channel and mobile channel.

(1) Static channel

The overall system performance in static Gaussian channel, Ricean channel and Rayleigh channel are depicted in Fig 3.16, Fig 3.17 and Fig 3.18 respectively. The transmission works in 2k mode, GI=1/4, code rate=2/3, SCO 20ppm, CFO 10.3.

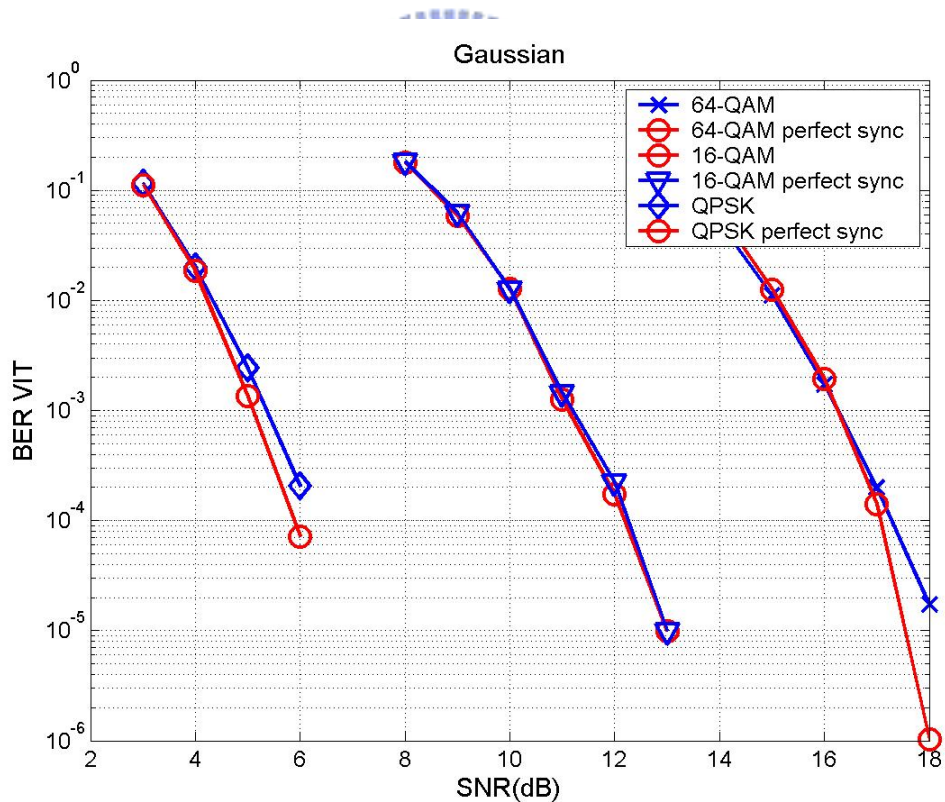


Fig 3.16 Overall system performance in static Gaussian channel

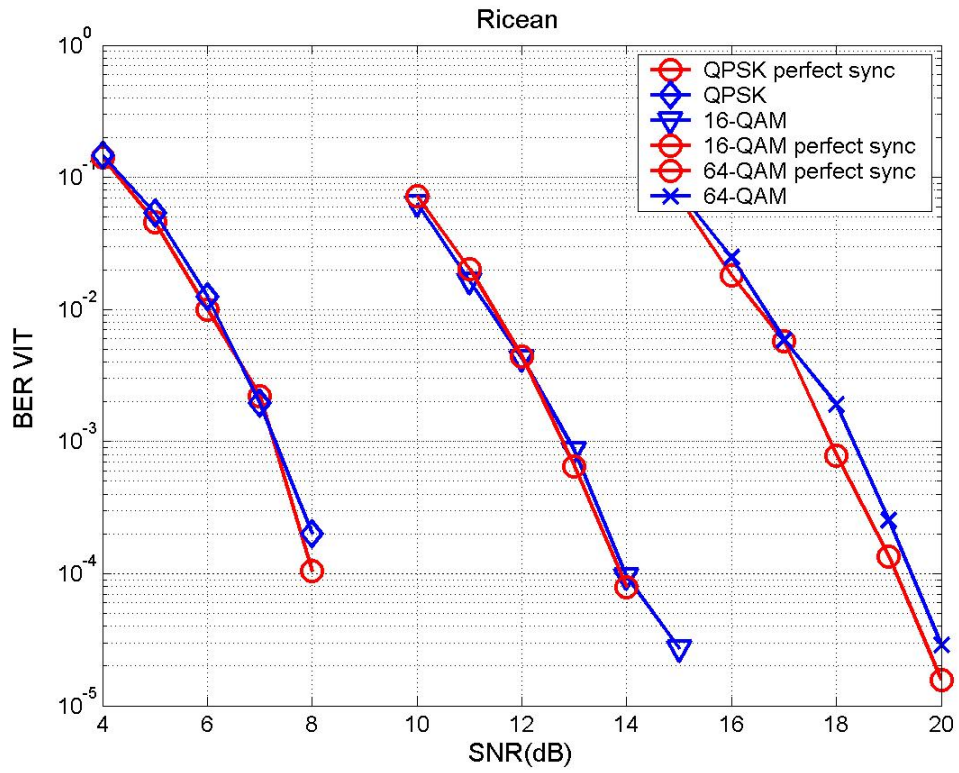


Fig 3.17 Overall system performance in static Ricean channel

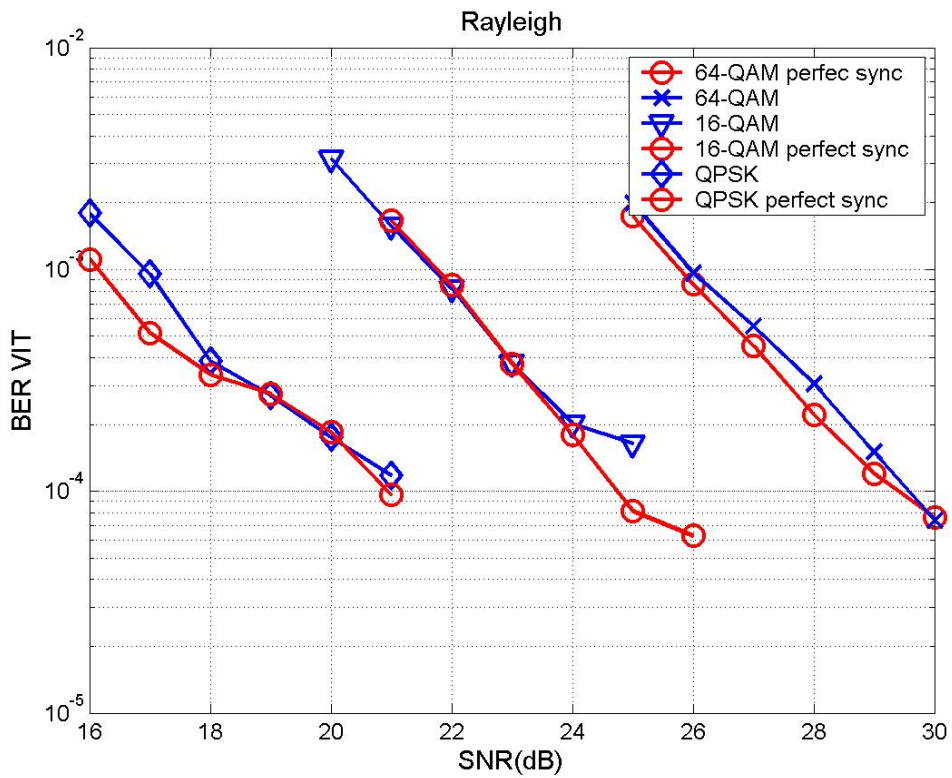


Fig 3.18 Overall system performance in static Rayleigh channel

It's clear that the frequency selective channel leads to an unavoidable degradation of several decibels with respect to nonselective AWGN channel. Severe frequency selectivity caused by very long channel delay profiles means the OFDM spectrum exhibits many notches which degrades the channel estimation gain and causes the noise enhancement. In the Rayleigh channel, the ideal system performance has SNR degradation of about 8dB compared with AWGN channel. The SNR loss of each case is listed in Table 3-8.

Table 3-8 SNR loss in static Gaussian, Ricean and Rayleigh channel

	Gaussian	Ricean	Rayleigh
QPSK	0.21	0.15	~0
16-QAM	~0	0.11	0.12
64-QAM	~0	0.28	0.31

(2) Mobile channel

In the case of mobile reception condition, the Doppler spread has to be considered. For providing practical environment simulation, we assume the maximum Doppler frequency as 70 Hz which is corresponding to velocity of 150 km/h. The overall system performance in Rayleigh channel with Doppler spread 70Hz is shown in Fig 3.19. The simulation performs in 2k mode, GI=1/4 and code rate=2/3, SCO 20ppm, CFO 10.3.

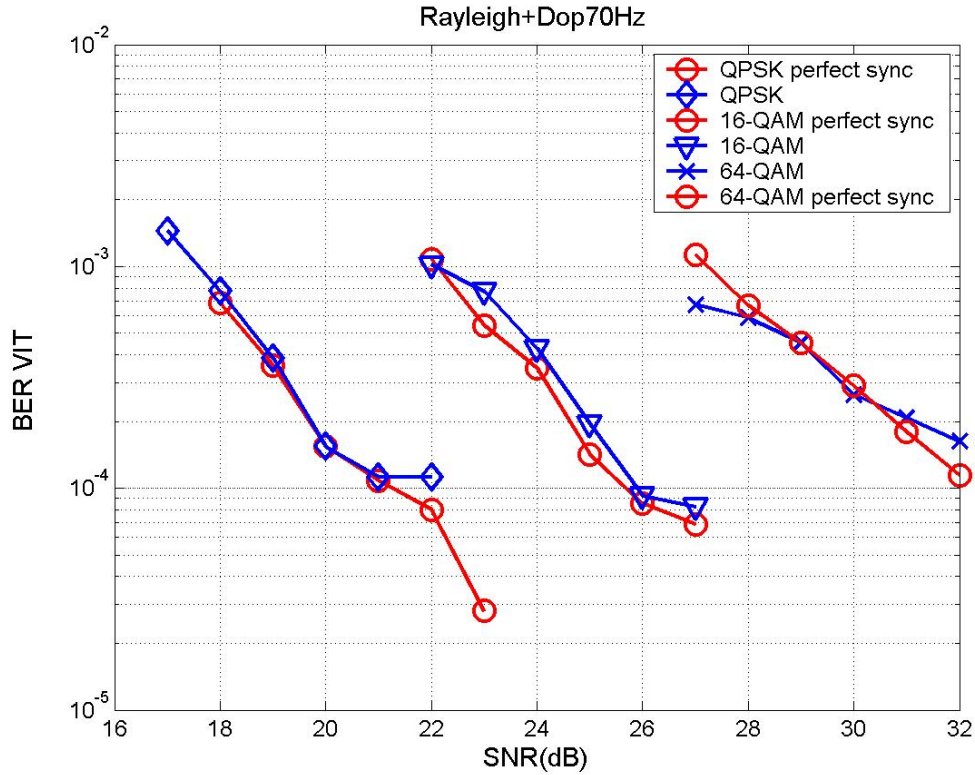


Fig 3.19 Overall system performance in Rayleigh channel with Doppler frequency 70Hz

The Doppler tolerance varies with transmission mode and constellation mapping. The synchronization loss is less than 0.2dB in every transmission mode. The detail values of synchronization loss are listed in Table 3-9.

Table 3-9 Synchronization loss and total SNR loss in mobile channel

	QPSK	16-QAM	64-QAM
Synchronization Loss	~0	0.20	0.13

Chapter 4 .

Hardware Integration

For overall synchronization system, it concludes 4 parts: acquisition, tracking, TPS decode and RS header synchronization. In section 2.4, we have already discussed the TPS decode and RS header synchronization. In this section, two parts of synchronization schemes for integration is brought out: the acquisition part and tracking part. The acquisition part concludes GI/Mode detector, coarse symbol synchronizer, fractional/integer CFO synchronizer and scattered pilot mode detector. Tracking part concludes fine symbol synchronization, SCO and residual CFO tracking. The overall synchronization scheme is shown in Fig 4.1. The block diagram of integration synchronization scheme is shown in Fig 4.2.

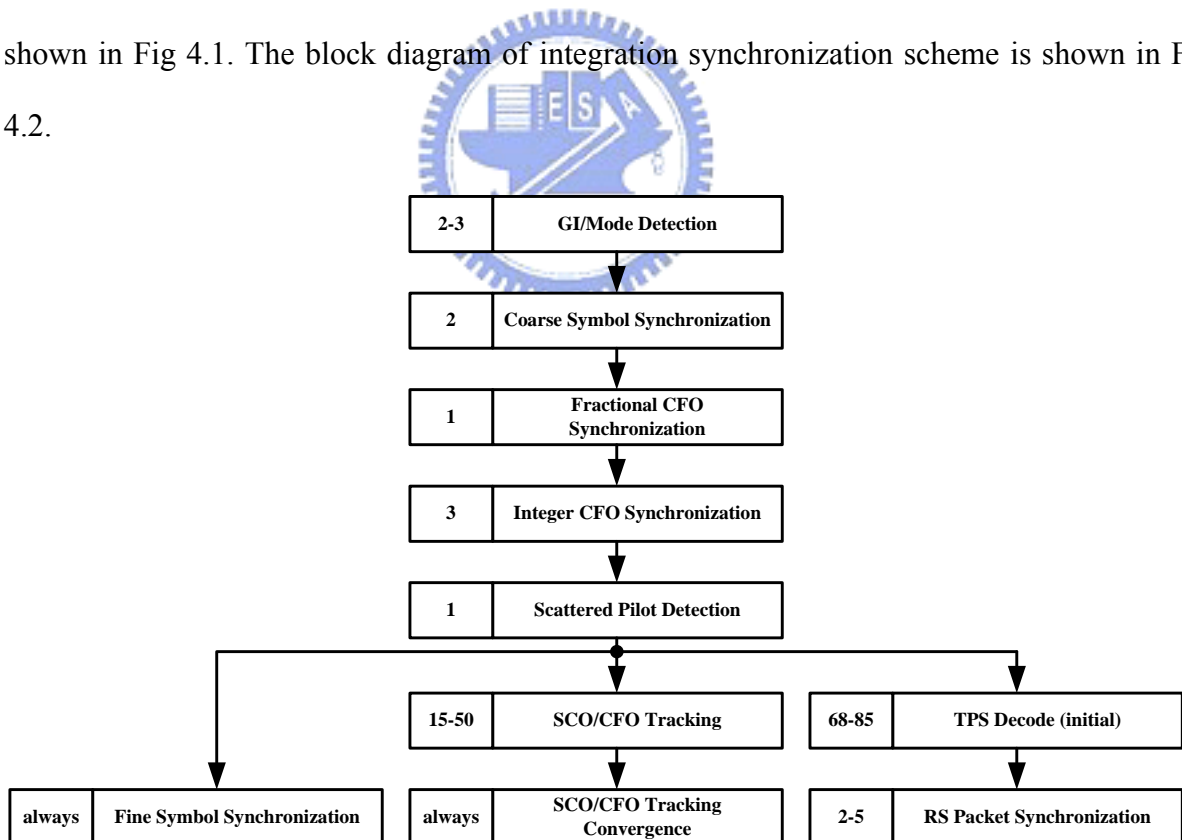


Fig 4.1 overall synchronization scheme

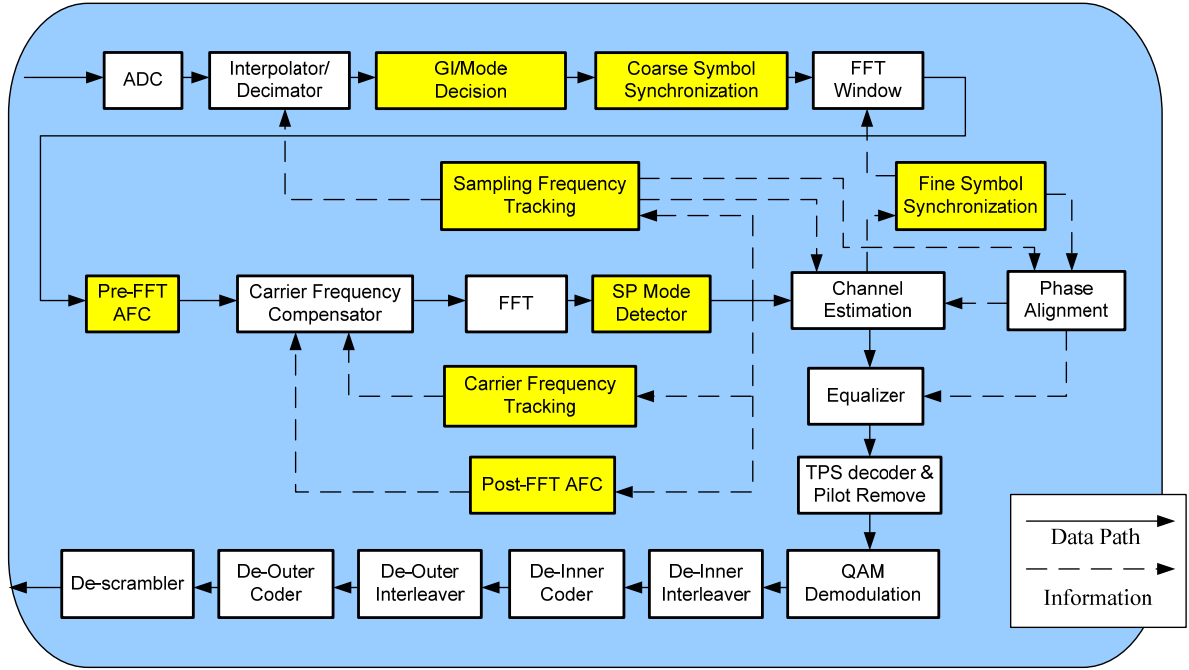


Fig 4.2 locations of integration synchronization system in receiver platform



4.1 Acquisition

(1) GI/Mode Detector

The Blind Detection of guard interval length and transmission mode must be done prior to timing synchronization and channel estimation. Mode/GI detection can exploit the cyclic prefix property of guard interval and use correlation method with normalization (NMC), as shown in Fig 4.3. The equation is expressed as:

$$Moving\ sum(GI/Mode) = \frac{\left| \sum_{i=0}^{N_1-1} r(k-i) \cdot r^*(k-i-N) \right|}{\left| \sum_{i=0}^{N_1-1} r(k-i) \cdot r^*(k-i) \right|} \quad (4-1)$$

where we choose moving length as 1/32 symbol length, it is the shortest guard interval length. And then correlating and normalizing the received data. According to cyclic prefix property we can obtain a moving sum curve and a fixed threshold. If we do not normalize the

correlation, the threshold is dynamic with guard interval length. Besides, first we check 2k mode and then check 8k mode.

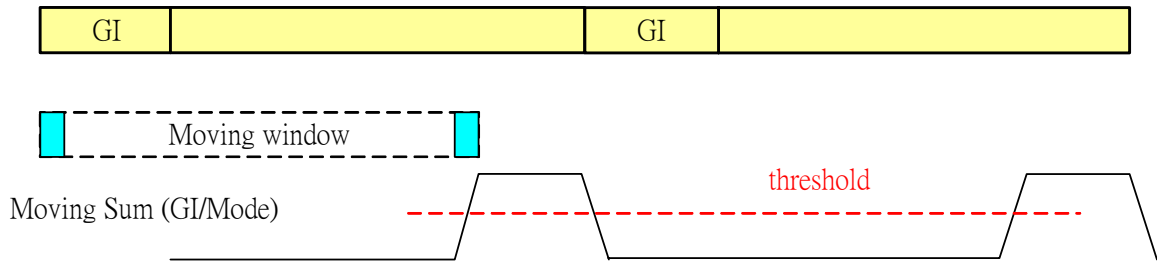


Fig 4.3 Normal Maximum Correlation algorithm for GI/Mode Detector

(2) Coarse Symbol Synchronizer

Coarse Symbol Synchronization is the first action after Mode/GI detector. The target of Coarse Symbol Synchronization is to make a one-shot decision finding symbol boundary. It must locate in the guard interval for ISI error free. We use correlation concept and choose the NMC algorithm to illustrate the moving sum curve, as shown in Fig 4.4. The equation is expressed as:

$$Moving\ sum(CoarseSym) = \frac{\left| \sum_{i=0}^{N_{gt}-1} r(k-i) \cdot r^*(k-i-N) \right|}{\left| \sum_{i=0}^{N_{gt}-1} r(k-i) \cdot r^*(k-i) \right|} \quad (4-2)$$

The moving length is the guard interval length that is the most notable different between Coarse Symbol Synchronizer and GI/Mode Detector. Hence, we can consider choosing NMC algorithm can reach the most relation and obtain the best cost saving.

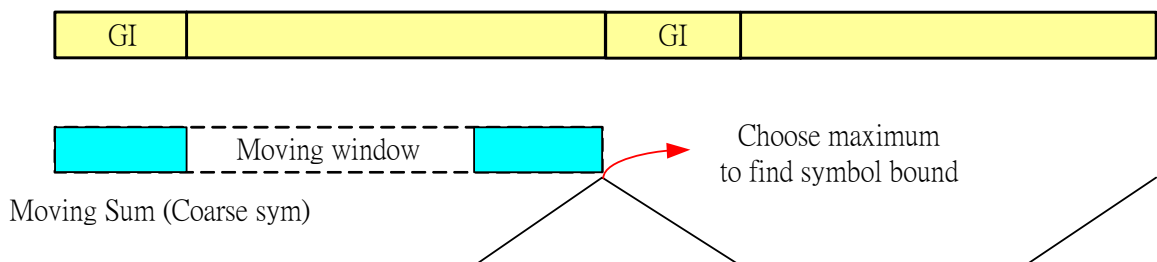


Fig 4.4 Normal Maximum Correlation algorithm for Coarse Symbol Synchronizer

(3) Fractional CFO synchronizer

From chapter 2, we can know that the phase of the received signal in time domain is rotated by CFO linearly according to the sample time instant t_n as (2-4) shows. When the difference of sample time instant between two received signals is equal to FFT length N , the phase error difference caused by CFO between them can be expressed as

$$\begin{aligned}
 \theta_l(n+N) - \theta_l(n) &= 2\pi\Delta f t_{n+N} - 2\pi\Delta f t_n \\
 &= 2\pi\epsilon(I N_s + N_g + n + N) / N - 2\pi\epsilon(I N_s + N_g + n) / N \\
 &= 2\pi\epsilon = 2\pi(\epsilon_I + \epsilon_F).
 \end{aligned} \tag{4-3}$$

The tail received sample and its cyclical prefix show the same property except for a phase rotation error which is exactly $2\pi\epsilon_F$. The estimation of fractional CFO value can be accomplished with the MLE of differential phase between guard interval and the tail of symbol [18], and can be expressed as

$$\hat{\epsilon}_F = \frac{1}{2\pi} \tan^{-1} \left[\frac{\text{Im} \sum_{n=N_s-N_g}^{N_s-1} r_{l,n-N}^* \cdot r_{l,n}}{\text{Re} \sum_{n=N_s-N_g}^{N_s-1} r_{l,n-N}^* \cdot r_{l,n}} \right] \tag{4-4}$$

(4-4) shows that the distinguishable phase error is within $\pm\pi$, so the estimation range of the fractional CFO synchronization is also limited within ± 0.5 subcarrier space. In the proposed acquisition synchronization scheme, the rough estimation of fractional CFO is calculated with the first symbol after symbol boundary is decided. And then the estimated fractional CFO value $\hat{\epsilon}_F$ will be sent to the CFO compensator before data being sent to FFT demodulator. The MLE is a correlator and a moving summation of length GI. It can be shared from NMC correlator.

(4) Scattered Pilot Mode Detection

It is known that the distribution of scattered pilots has four modes. The proposed scattered

pilot mode detection exploits the property of boosted power level scattered pilots. Since the power level of scattered pilots is 16/9 while other data subcarrier is 1, we take one OFDM symbol and divide the subcarriers into 4 groups. Afterward, we accumulate the power of subcarrier belong to each group respectively as shown in (4-5)

$$SP = \arg \left\{ \max_k \left[\sum_{i=0}^{N/12-1} z(3 \cdot k + 12 \cdot i) \cdot z^*(3 \cdot k + 12 \cdot i) \right] \right\} \quad k = 0, 1, 2, 3 \quad (4-5)$$

Although the power of each subcarrier is possible larger than 16/9 such as maximum power level of 7/3 in non-hierarchical 64-QAM, many times of accumulations make the false detection rate almost reduce to zero. This correlator can be shared from NMC correlator.

(5) Integer CFO synchronizer

In order to utilize the advantage of lower computational complexity and to improve the performance in critical channel condition, in [19], it proposes a new guard band power detection based algorithm but not continual pilot based algorithm. By deciding the CFO is positive or negative, the search range of integer CFO can be reduced effectively and more OFDM symbols can be utilized to improve the acquisition performance. Thus, the guard band power detection based algorithm still keeps the moving window scheme and calculates the summation of signal power within three successive OFDM symbols, and can be expressed as

$$\hat{\mathcal{E}}_I = \min_i \left\{ \sum_{k=K_{\min}-w_2}^{K_{\min}-1} \left[|R_{l,k+i}|^2 + |R_{l-1,k+i}|^2 + |R_{l-2,k+i}|^2 \right] + \sum_{k=K_{\max}+w_2}^{K_{\max}+1} \left[|R_{l,k+i}|^2 + |R_{l-1,k+i}|^2 + |R_{l-2,k+i}|^2 \right] \right\} \quad (4-6)$$

where w_2 is the width of the moving window at both sides of the guard band, $-m \leq i \leq w_1$ while negative value estimated by the first stage, and $-w_1 \leq i \leq m$ while positive value, respectively. As Fig 4.10 shows, by the use of summation within three successive OFDM symbols, the distortion induced by noise in severe environment can be decreased effectively. And w_1 is 5, w_2 is chosen as 10, and search range m is 60. Hence, the correlator can also be

exploited from NMC algorithms.

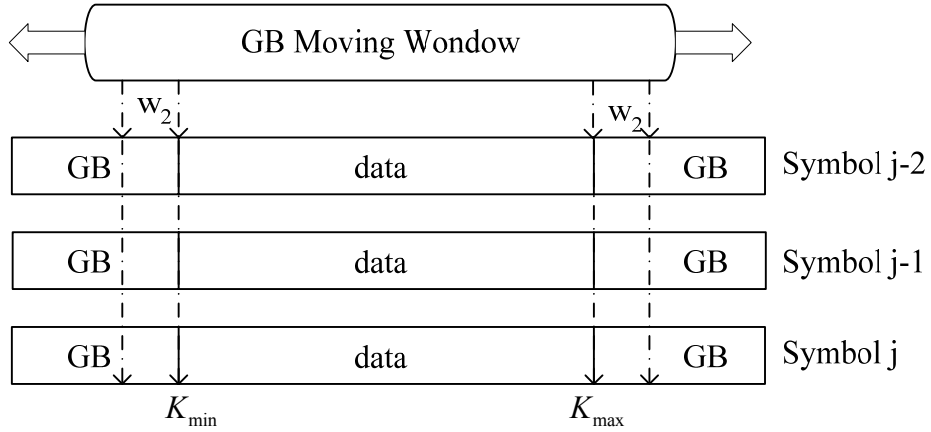


Fig 4.5 The proposed guard band power detection based approach

4.2 Tracking

Tracking system concludes three parts, one is fine symbol synchronization and the others are residual CFO and SCO tracking. The CFO tracking and SCO estimation algorithm and tracking loop are similar to each other. In this paper, we use conclusion of section 2.4: SP based algorithm and feedback forward tracking loop to determine the SCO and residual CFO synchronization. SCO equation is expressed in (2-30) and architecture is shown in Fig 2.29. The CFO estimation can be expressed as:

$$\hat{\zeta} = \frac{1}{2\pi(1 + N_g/N) \cdot 4} \cdot \sum_{k=-N/2}^{N/2-1} D_{1,x} \cdot y_{w,x},$$

$$y_{w,x} = \text{Arg} [z_{w,x} \cdot z_{w-1,x}^*]$$

$$D = (C^T C)^{-1} C^T$$

$$C = \begin{bmatrix} 1 & x_1 \\ 1 & x_2 \\ \vdots & \vdots \\ 1 & x_N \end{bmatrix} \mid x_i \in SP$$

and the tracking loop architecture is shown in Fig 4.6. And timing diagram is shown in Fig 4.7.

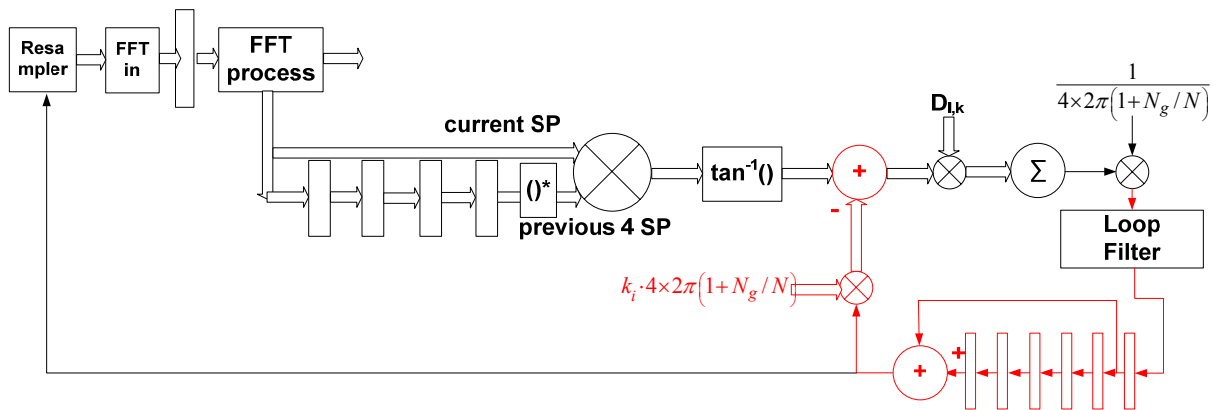


Fig 4.6 the architecture of proposed residual CFO tracking loop with SP method

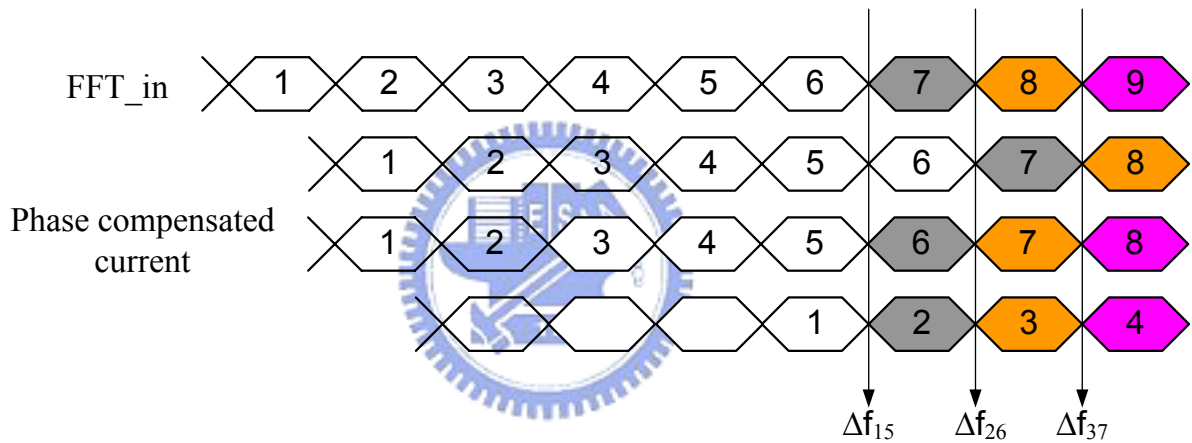


Fig 4.7 timing diagram of proposed residual CFO tracking loop architecture with SP method

From the tracking loop architecture and estimation algorithm, we can see the residual CFO and SCO is only different in one coefficient $D_{1,k}$ and $D_{2,k}$. Hence, the reuse of their hardware is applied.

4.3 Integration Result

The hardware analysis reference is from [1] proposed in ISSCC2006, and is listed in Table 4-1. In Table 4-1, It shows the synchronization function and the relative gate count.

Table 4-1 the hardware gate count of synchronization function in [1]

Function	Gate count
GI/Mode detector	7861
Coarse symbol Sync.	8590
SP mode detection	2963
Fractional CFO Sync.	8219
Integer CFO Sync.	12224
SCO tracking	11006
Residual CFO tracking	11686
Total	62549

The proposed hardware integration result is listed in Table 4-2, in Table 4-2, it shows the gate count of proposed synchronization function and the reused part, moving correlation core and tracking core.



Table 4-2 the hardware gate count of synchronization function for the proposed design

Function	Gate count
GI/Mode detector	784
Coarse symbol Sync.	1535
SP mode detection	329
Fractional CFO Sync.	1117
Integer CFO Sync.	5020
Moving correlation core	7268
SCO tracking	1195
Residual CFO tracking	1399
Tracking core	10156

Total	28803
-------	-------

In Table 4-1 and Table 4-2, we can calculate the proposed design hardware integration. The hardware decreases from 62549 to 28803, and the saving of hardware reaches 46% than conventional design [1] in ISSCC2006.



Chapter 5 .

Conclusion and Future Work

The synchronization system for DVB-T/H standard is completed in this paper. In this paper, we propose three synchronization designs: carrier phase alignment, sampling clock synchronization and fast synchronization. First, Carrier phase alignment solves worst channel in the mobile environment. At SCO 20ppm and Doppler frequency 70Hz in Rayleigh multipath with SNR 34dB, our DVB-T/H system still reaches Quasi Error Free (QEF) criterion. Second, sampling clock synchronization separates into two parts: SCO estimation and SCO tracking. The target is different for these two parts. Target of SCO estimation is estimation accuracy and targets of SCO tracking are tracking convergence and convergent time. In this paper, the proposed design improves the SCO estimation accuracy 2~5 times and reduces the SCO tracking time 3 times. Third, in fast synchronization discussion, our proposed design can decrease the synchronization time 2~4.5 times. It also means that, in timing slicing architecture for DVB-H standard, we can save power consumption 65%~95% and reduce receiver buffers 1Mbits~3Mbits. Finally, the overall system performance of the proposed synchronization system loses below 0.31dB for all kinds of channels, including static and mobile environments.

In this paper, we also integrate the hardware of synchronization schemes. We proposed to reuse the similar part of the synchronization architecture. The proposed hardware integration method decreases 46% gate counts than the conventional design [] proposed in ISSCC2006.

In the future, we plan to integrate the proposed designs, including the 3 proposed synchronization designs and proposed hardware integration, with the DVB-T/H system in [1].

Bibliography

- [1] Lei-Fone Chen, Yuan Chen, Lu-Chung Chien, Ying-Hao Ma, Chia-Hao Lee, Yu-Wei Lin, Chien-Ching Lin, Hsuan-Yu Liu, Terng-Yin Hsu, and Chen-Yi Lee, "A 1.8V 250mW COFDM Baseband Receiver for DVB-T/H Applications," *IEEE ISSCC2006*, pp.262-263, pp.652, Feb. 2006.
- [2] M. Speth, S. Fechtel, G. Fock, and H. Meyr, "Optimum Receiver Design for OFDM-Based Broadband Transmission-Part II: A Case Study", *IEEE Trans. Comm.*, Vol. 49, No. 4, pp. 571-578, Apr. 2001.
- [3] ESTI EN 300 744 V1.5.1, "Digital Video Broadcasting (DVB); Framing Structure, Channel Coding and Modulation for Digital Terrestrial Television," Nov. 2004.
- [4] ETSI EN 301 192 V1.4.1, "Digital Video Broadcasting (DVB); DVB specification for data broadcasting" May 2003.
- [5] M.H. Hsieh and C.H. Wei, "Channel Estimation for OFDM Systems Based on Comb-Type Pilot Arrangement in Frequency Selective Fading Channel," *IEEE Trans. Consumer Electronics*, vol. 44, No. 1, pp.217-225, Feb. 1998.
- [6] ESTI EN 302 304 V1.1.1, "Digital Video Broadcasting (DVB); Transmission System for Handheld Terminals (DVB-H)," Nov. 2004.
- [7] IEEE 802.11a IEEE Standards for Wireless LAN Medium Access Control and Physical Layer Specifications, Nov. 1999.
- [8] T.A. Lin, and C.Y. Lee, "Predictive Equalizer Design for Dvb-T System," *ISCAS2005*, pp. 940-943, May 2005.
- [9] S. Liu and J. Chong, "A Study of Joint Tracking Algorithms of Carrier Frequency Offset and Sampling Clock Offset for OFDM-based WLANs," *IEEE International Conf. Communications, Circuits and Systems and West Sino Expositions*, vol. 1, July. 2002.

- [10] Cheng-Wei Kuang, "Timing Synchronization for DVB-T System," *MS Thesis, NCTU*, Sep. 2004.
- [11] T. Schmidl and D. Cox, "Robust frequency and timing synchronization for OFDM," *IEEE Trans. Commun.*, vol. 45, Dec. 1997.
- [12] S. Bug, C. Wengerter, I. Gaspard and R. Jakoby, "WSSUS-Channel Models for Broadband Mobile Communication Systems," *Vehicular Technology Conf.*, vol. 2, May. 2002.
- [13] P. Robertson and S. Kaiser, "The Effects of Doppler Spreads in OFDM(A) Mobile Radio Systems," *IEEE Vehicular Technology Conf.*, Vol. 1, pp. 329-333, Sep. 1999.
- [14] L. Litwin, "Matched Filtering and Timing Recovery in Digital Receivers," *RF design*, pp.32-48, Sept. 2001.
- [15] H. Meyr, M Moeneclaey, and S. Fechtel, "Digital Communication Receivers," Wiley Interscience, 1997.
- [16] Y.J Ryu and D.S Han "Timing phase estimator overcoming Rayleigh fading for OFDM systems" *IEEE Trans. Consumer Electronics*, vol. 47, No. 3, Aug. 2001.
- [17] M. Speth, S. Fechtel, G. Fock, and H. Meyr, "Optimum Receiver Design for Wireless Broad-Band Systems Using OFDM-Part I", *IEEE Trans. Comm.*, Vol. 47, No. 11, pp. 1668-1677, Nov. 1999.
- [18] J. J. van de Beek, et al., "A Time and Frequency Synchronization Scheme for Multiuser OFDM," *IEEE J. Select. Areas Comm.*, Vol. 17, No. 11, pp. 1900-1914, Nov. 1999.
- [19] Lu-Chung Chien, "Low Complexity Carrier Frequency Synchronization for DVB-T/H System" *MS Thesis, NCTU*, July. 2005.
- [20] B. Yang, K.B. Letaief, R.S. and Cheng, Z. Cao, "Timing recovery for OFDM transmission," *IEEE Journal Selected Areas in Commun.*, vol. 18, No. 11, pp.2278-2291, Nov. 2000.
- [21] Y.J Kim, D.S Han and K.B Kim "A new fast symbol timing recovery algorithm for

- OFDM systems" IEEE Trans. Consumer Electronics, vol. 44, No. 3, Aug. 1998.
- [22] Ludwig Schwoerer, and Jussi Vesma "Fast Scattered Pilot Synchronization for DVB-T and DVB-H" Proc. 8th International OFDM Workshop, Hamburg, Germany, Sept. 24./25. 2003.
- [23] W. C. Jakes, "Microwave Mobile Communications," *John Wiley & Sons Inc.*, 1974.
- [24] Hsuan-Yu Liu, Yi-Hsin Yu, Chien-Jen Hung, Terng-Yin Hsu, Chen-Yi Lee "Combining Adaptive Smoothing and Decision-Directed Channel Estimation Schemes for OFDM WLAN Systems", *ISCAS*, 2003.
- [25] Yi-Hsin Yu, "A Channel Equalizer for OFDM-based Wireless Access Systems," *MS Thesis, NCTU*, Jun. 2004.



作者簡歷

姓名：李家豪

出生地：台灣省台南市

出生日期：1982. 8. 22

學歷：1989. 9 ~ 1994. 6 台南市立永華國民小學

1994. 9 ~ 1997. 6 台南市立新興國民中學

1997. 9 ~ 2000. 6 國立台南第一高級中學

2000. 9 ~ 2004. 6 國立暨南國際大學 電機工程學系 學士

2004. 9 ~ 2006. 7 國立交通大學 電子研究所 系統組 碩士

